NERC Scientific Facilities and Technology Ion Microprobe Facility

**University of Edinburgh
NERC Ion Microprobe Facility**

Annual Science Report

Ion Microprobe Facility
School of Geosciences
Kings Buildings
West Mains Road
Edinburgh
EH9 3JW

http://www.geos.ed.ac.uk/facilities/

Contents

Ion Microprobe Projects

Climate variability in the Southern tropical Pacific

N. Allison, A.W. Tudhope

School of Geography and Geosciences, University of St. Andrews, St. Andrews KY16 9AL, UK

Introduction

Accurately reconstructing the past sea surface temperatures (SSTs) of the tropical Pacific Ocean is fundamental for understanding global palaeoclimate and predicting future climate change. IODP Expedition 325 drilled a succession of fossil reef structures, on the shelf edge of the modern day Great Barrier Reef. Dating indicates that the reefs span the last glacial maximum and postglacial sequence. The majority of fossil corals recovered from the cores are from the genus *Isopora*. These are shallow water species, closely related to *Acropora* and widespread in the modern Indo-Pacific. We are working, as part of a larger project (funded by the Australian Research Council), to derive climate estimates from the geochemistry (Sr/Ca and $\delta^{18}O$) of these fossil coral specimens.

We were awarded SIMS beamtime for the analysis of Sr/Ca in modern Isoporan specimens. Our aim was twofold: i) to characterise the skeletal Sr/Ca distribution in the primary coral aragonite, and ii) to confirm a relationship between skeletal Sr/Ca and seawater temperature in this coral genus. SIMS indicates that the skeletal Sr/Ca of the primary coral structures in other modern coral genera e.g. *Porites*, is dominated by weekly-monthly oscillations, which exceed the magnitude of seasonal variations observed in drilled samples [1]. These short term oscillations do not reflect SST but probably reflect variations in biological processes in the coral tissue. In spite of this, credible SST records can be obtained from Porites spp. coral skeletons by smoothing multiple SIMS analyses at ~2 monthly resolution and minimizing the effects of short-period high frequency biological noise [2,3]. Similar short term Sr/Ca oscillations have been observed in some Porites spp. fossil corals, analysed by SIMS. The preservation of these oscillations in the geochemistry of the primary coral structures suggest that they are diagenetically unaltered [3] and lends weight to climate estimates derived from their analysis.

Analytical

Analyses were made on the Cameca 4f. Positive secondary ions were produced by a 5nA, 10.72 kV, $^{16}O^-$ primary beam. Primary aperture = 1, field aperture =1. The primary beam was focussed to elongate and was ~20 x 30 μm. Secondary ions were measured by electron multiplier by sequential stepping of the magnetic field through a cycle of relative atomic mass. Singly-charged cations were collected at masses ^{11}B (5 seconds), ^{26}Mg (3s), ^{44}Ca (2s), ^{88}Sr (4s) and ^{138}Ba (20s). A pre-analysis sputter time of 60 s in spot mode was used to remove surface contamination. External Sr/Ca reproducibility was calculated from the standard deviation (σ) of 10 replicate analyses on the carbonate standards Haxby ($\sigma/(\sqrt{10})$) and was <0.1‰. Analyses from the outermost 1 mm of skeleton, occupied by the coral tissue, at the time of sampling and potentially contaminated by remnant organics materials, have not been included in the dataset.

Results

We analysed a modern (living at the time of collection) *Isopora cuneata* specimen, collected from Myrmidon Reef, GBR in December 1981. Bulk $\delta^{18}O$ analyses of this specimen indicate that annual extension rate in this coral is ~15-20 mm year^{-1}. We observed significant variations in Sr/Ca of ~0.6 mmol mol^{-1}, over short skeletal distances, nominally equivalent to periods of ~18-35 days (Figure 1). These oscillations do not reflect SST or seawater chemistry but indicate the importance of other, biologically induced, cyclical factors on skeletal geochemistry. The cause of these oscillations is currently unresolved. The oscillations are similar in magnitude and duration to the Sr/Ca heterogeneity observed in *Porites* spp. skeletons [1,2]. Smoothing the SIMS data with an ~2 monthly running mean highligths a seasonal variation in Sr/Ca which is in agreement with SST variations at the study site. The smoothed Sr/Ca data ranges from ~8.4-8.8 mmol mol^{-1} while mean SST ranges from 23.5-28.5°C, implying a Sr/Ca temperature sensitivity of ~ 0.08 mmol mol^{-1} °C. This is similar to the temperature sensitivity observed in smoothed SIMS data in *Porites lobata* corals [2].
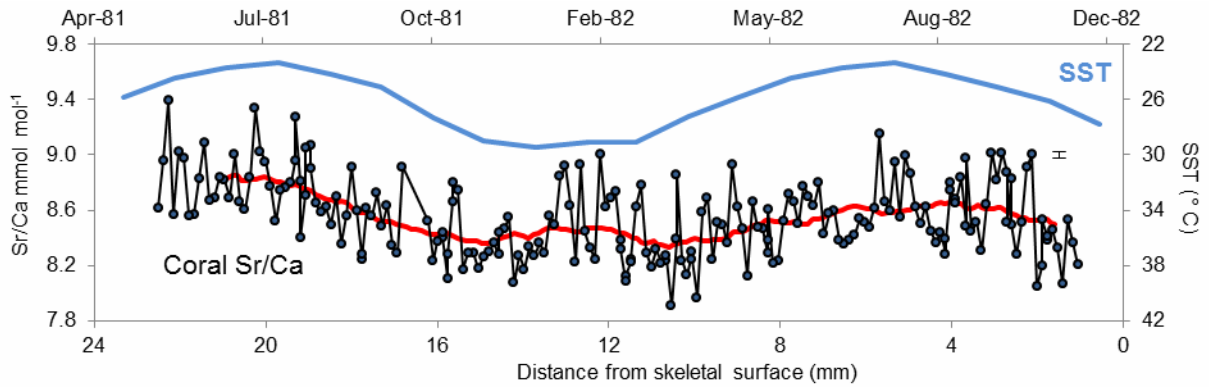
Figure 1. SIMS Sr/Ca measurements across a transect of *Isopora cuneata* skeleton. Error bars indicate precision (2σ) of individual analyses. A smoothed, ~2 month running mean is shown by the red line. IGOSS SST data for the study site is illustrated by the blue line. IGOSS data were unavailable for May – October 1981 and these data have been calculated from the mean monthly SST observed at the study site in subsequent years.

Our preliminary dataset is short but suggests that the Sr/Ca of Isoporan corals is similarly distributed to that of *Porites* corals. A credible SST trend can be resolved by smoothing multiple SIMS analyses.

References
[1] N. Allison et al., (2010) Geochim. Cosmochim. Acta, **74**, 1790-1800
[2] N. Allison and A.A. Finch (2004) G-cubed**, 5**, Q05001, doi 10.1029/2004GC000696
[3] N. Allison et al., (2005) Geophys. Res. Lett., **32**, L17609, doi: 10.1029/2005GL023183

The impact of transcellular Ca transport on the δ^{44}Ca of coral skeletons

N. Allison, A.A. Finch

School of Geography and Geosciences, University of St. Andrews, St. Andrews KY16 9AL, UK

Introduction

Preliminary data indicate that the δ^{44}Ca of coral aragonite is temperature dependent [1] and the δ^{44}Ca of fossil corals may provide estimates of past sea surface temperatures. However the processes controlling δ^{44}Ca in biogenic carbonates are poorly understood and the δ^{44}Ca of coral aragonite is offset from inorganic aragonite by about +0.5‰ [1]. This offset may reflect fractionation during trans-cellular Ca transport or storage. Coral skeletons precipitate from an extracellular calcifying fluid enclosed in a semi-isolated space between the skeleton and the aboral ectoderm (the tissue layer at the base of the coral organism). Seawater diffuses directly to the calcification site [2] and the calcification fluid has a composition derived from that of seawater but modified by other transport processes. In zooxanthellate corals, Ca^{2+} is also transported trans-cellularly i.e. across cell membranes, to the calcification site, by both calcium channels and by the carrier protein Ca-ATPase [3].

To test the hypothesis that transcellular Ca transport mechanisms across biological tissues cause calcium isotopic fractionation in coral, we cultured a suite of corals (*Pocillopora damicornis*) under constant temperature, salinity and pH. We used the biochemical inhibitors ruthenium red and verapamil hydrochloride to decrease the activity of the enzyme Ca-ATPase and to block Ca ion transport channels respectively. We proposed to use SIMS to characterise the δ^{44}Ca composition of the skeleton deposited in the presence of each inhibitor to identify if these transcellular Ca transport mechanisms cause fractionation of Ca isotopes.

Analytical

To ensure that the skeleton analysed by SIMS, at the outermost surface of the coral skeleton was deposited during the culture period, we added a stable isotope tracer (^{42}Ca, added as ^{42}CaCO$_3$) to the seawater at the same time as the biochemical inhibitors. ^{42}Ca has an isotopic abundance of ~0.6% and hence doubling ^{42}Ca of the seawater results in a small (0.6%) increase in the total seawater Ca concentration. Skeleton deposited during the culture period has a significantly higher ^{42}Ca/^{44}Ca than that deposited in unlabelled seawater.

δ^{44}Ca analyses were made on the Cameca 1270. Positive secondary ions were produced by a 7.7nA, 10 kV, ^{16}O$^-$ primary beam and a mass resolution of ~2400. Primary mass filter aperture = 4, final primary aperture = 2, entrance slit = fully open, imaged field = 60 μm. The primary beam was focussed to ~20 x 25 μm. Singly-charged Ca isotopes were measured simultaneously for 20 cycles of 5 s each by faraday cups as follows: ^{40}Ca (L'2), ^{42}Ca (H1), ^{44}Ca (H'2). Typical count rates on the *Porites* M93 standard were ~6.5 x 10^8, 4 x 10^6 and 1.3 x10^7 cps respectively. A pre-analysis sputter time of 60 s in spot mode was used to remove surface contamination.

Internal ^{40}Ca/^{44}Ca reproducibility (the precision at a single point) was calculated from the standard deviation (σ) of the 20 cycles in each coral analysis ($\sigma/(\sqrt{20})$) and was typically 0.05‰. External ^{40}Ca/^{44}Ca reproducibility was calculated from the standard deviation (σ) of 10 replicate analyses on the carbonate standards ($\sigma/(\sqrt{10})$) and was typically 0.14‰.

Results

δ^{44}Ca could not be analysed with the required precision in the samples or carbonate standards to test the hypothesis i.e. to resolve a difference of 0.5‰. Groups of 10 analyses were made on 3 standards: M93 *Porites* coral, Haxby coral and Iceland Spar. Groups of analyses had typical precision ($\sigma/\sqrt{10}$) of ±0.14‰ but significant drift (often >1‰) occurred between many batches of analyses (Figure 1). ^{44}Ca/^{40}Ca was correlated with ^{40}Ca count rate, between individual SIMS analyses (Figure 2) and between batches of 10 analyses (Figure 3). This suggests an instrumental mass fractionation effect which could not be resolved in the current session.
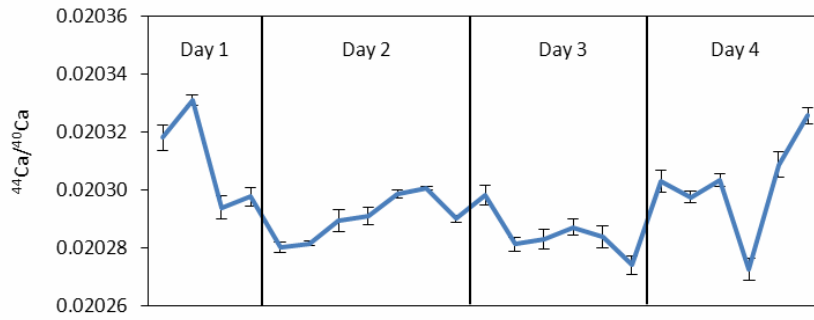
Figure 1. Mean $^{44}Ca/^{40}Ca$ in the *Porites* coral standard M93 (laser block) over 4 days (Tuesday-Friday). Each point is the mean of 10 analyses and error bars indicate precision ($\sigma/\sqrt{10}$).

Figure 2. The relationship between ^{40}Ca count rate and $^{44}Ca/^{40}Ca$ of individual SIMS analyses in 4 batches of analyses made under the same conditions on the M93 standard on Day 4. All analyses were made using a double transfer scan (i.e. a first transfer scan with the field aperture fully open followed by a second scan with a smaller aperture).
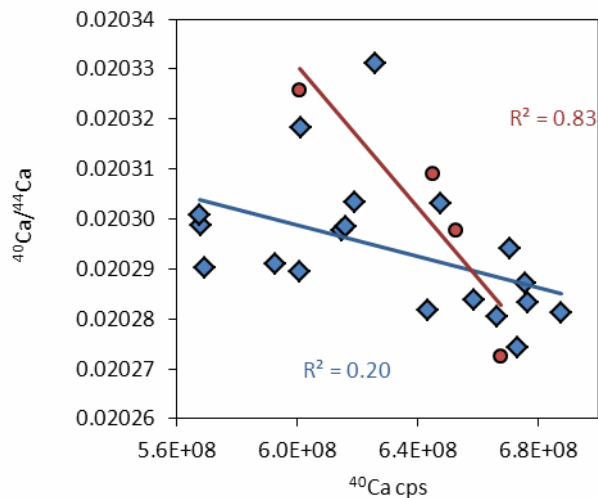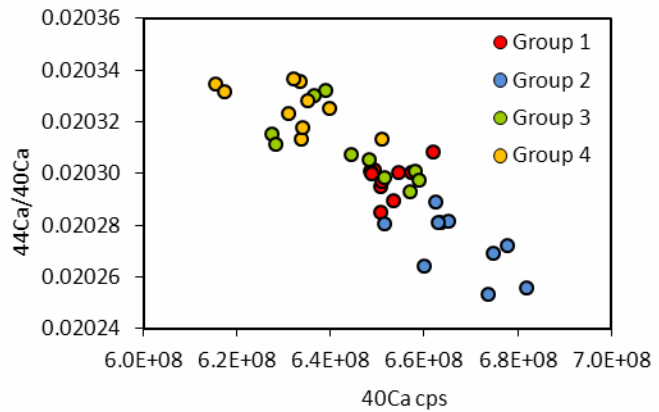
Figure 3. The relationship between ^{40}Ca count rate and $^{44}Ca/^{40}Ca$ in all the batches of analyses illustrated in Figure 1. Each point is the mean of 10 SIMS analyses (1 batch). Blue symbols illustrate batches which used a single transfer scan while red symbols indicate analyses made using a double transfer scan.

References
[1] F. Bohm et al., (2006) Geochim. Cosmochim. Acta 70 4452-4462.
[2] J. Erez, A. Braun (2007) Geochim. Cosmochim. Acta, 71, SA260.
[3] A.T. Marshall (1996) Science, 271, 637-639.

The impact of biological processes on the δ^{11}B of coral skeletons and their significance for palaeo-pH records

N. Allison, A.A. Finch

School of Geography and Geosciences, University of St. Andrews, St. Andrews KY16 9AL, UK

Introduction

The δ^{11}B of coral aragonite indicates potential as an indicator of seawater pH [1]. However a high resolution SIMS study indicates that skeletal δ^{11}B is dominated by large cyclical oscillations which are deposited over short skeletal distances, nominally equivalent to periods of 20-30 days [2]. This geochemical heterogeneity does not reflect changes in seawater composition but likely indicates variations in the composition of the extracellular calcification fluid (ECF) used during skeletal precipitation. The ECF is largely derived from seawater which diffuses to the calcification site through the overlying coral tissue. Photosynthesis (utilising CO_2) and respiration (producing CO_2) in the coral tissue and calcification (utilising CO_3^{2-}), may affect the pH of the ECF. In addition, the enzyme Ca^{2+}-ATPase pumps H^+ out of the calcification site, increasing the pH of the ECF.

To investigate the relationship between Ca-ATPase activity and skeletal δ^{11}B, we cultured a suite of *Pocillopora damicornis* corals under stringently controlled temperature, light and pH conditions. We used a biochemical inhibitor (ruthenium red) to decrease the activity of the enzyme Ca-ATPase in some corals. The photosynthesis, respiration and calcification rates of all colonies were monitored throughout the experiment. We identified and analysed the skeleton deposited in the presence of the inhibitor using secondary ion mass spectrometry (SIMS) and we compare the geochemistry of the skeletons deposited in each of the treatments.

Analytical

δ^{11}B analyses were made on the Cameca 1270 using a mass resolution of ~2400. Secondary ions were measured by electron multiplier by sequential stepping of the magnetic field through a cycle of relative atomic mass. Singly-charged cations were collected at masses ^{10}B (11 seconds) and ^{11}B (3s). Typical count rates were ~1400 and 5300 cps respectively. Each analysis is the sum of 60 cycles. To ensure that the skeleton analysed by SIMS, at the outermost surface of the coral skeleton was deposited during the culture period, we added a stable isotope tracer (^{42}Ca, added as ^{42}CaCO$_3$) to the seawater at the same time as the biochemical inhibitors. ^{42}Ca has an isotopic abundance of ~0.6% and hence doubling ^{42}Ca of the seawater results in a small (0.6%) increase in the total seawater Ca concentration. Skeleton deposited during the culture period has a significantly higher ^{42}Ca/^{44}Ca than that deposited in unlabelled seawater. Doubly charged cations were collected at masses 14 (^{28}Si/2, 1s), 21 (^{42}Ca/2, 2s) and 22 (^{44}Ca/2, 1s) to confirm that the analysed skeleton was deposited in the presence of the inhibitors. A pre-analysis sputter time of 30s in spot mode was used to remove surface contamination. Internal reproducibility (the precision at a single point) was calculated from the standard deviation (σ) of the 60 cycles in each coral analysis ($\sigma/(\sqrt{60})$) and was typically 1.6‰. The primary beam was focussed to elongate and was ~15 x 35 μm. δ^{11}B was estimated by normalising the ^{11}B/^{10}B ratios of the coral sample to the mean ratio (3.769 ± 0.35‰ (1σ), n=12) obtained from multiple SIMS analyses of a *Porites* sp. coral standard (M93-TB-FC-1). TIMS and MC-ICP-MS measurements of fragments of the same coral standard yield δ^{11}B = 24.8 ± 0.4 ‰, 2σ, (Kasemann et al., 2009) and this error encompasses the uncertainty of the reference material used for bulk analysis. Daily variations in instrument stability were assessed by performing multiple analyses within a small area of this section and were insignificant (within analytical precision). External reproducibility (the precision of 12 SIMS δ^{11}B estimates on the coral standard) was ± 1.5‰.

Results

Skeletal δ^{11}B was significantly lower in the corals cultured in the highest concentration of ruthenium red compared to both sets of controls (ANOVA, p=0.05).We estimate the pH (total scale) of the ECF from skeletal δ^{11}B using the empirically-determined $^{11-10}K_B$ [3], the theoretical equation of B speciation in seawater with boric acid pK_B = 8.5687 (at salinity = 40.6 and T = 25ºC [4]) and assuming that the δ^{11}B of the calcification fluid is the same as seawater (39.5‰). Estimated ECF pH (Figure 1)

was significantly lower in the corals cultured in 5.3 μM ruthenium red compared to both sets of controls. The ECF pH in these treated corals is essentially the same as ambient seawater. ECF pH in the control corals is ~0.25-0.3 units higher than ambient seawater.

Calcification and gross and net photosynthetic rates (Figure 2) were significantly reduced in the ruthenium red treatments compared to the controls but respiration rates were not affected [5]. The reduction in ECF pH is consistent with the suppression of Ca-ATPase but may also reflect the decrease in photosynthesis. Notwithstanding, the observed ECF pH decrease is consistent with a reduction in Ca transport of 11% (assuming that Ca-ATPase exchanges $2H^+$ for each Ca^{2+} transported into the calcification site), in the corals cultured in ruthenium red 5.3 μM, compared to the DMSO controls. Assuming that Ba^{2+} does not substitute for Ca^{2+} during Ca-ATPase transport and that Ca-ATPase activity effectively dilutes the Ba/Ca of the ECF, then this figure is in agreement (within error) with the observed increase in skeletal Ba/Ca between the control and inhibited corals (~18%) suggesting that the pH decrease directs reflects the influence of Ca-ATPase.
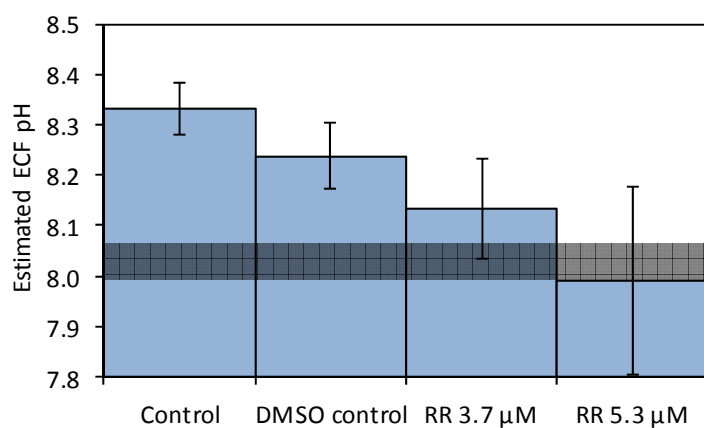
Figure 1. Estimated ECF pH (from skeletal $\delta^{11}B$) in the different coral treatments. Error bars indicate 95% confidence limits. The pH of seawater used during culturing was 7.99-8.06 and is indicated by the dark grey horizontal band. All inhibitors were dissolved in dimethyl sulfoxide solution (DMSO) to a final concentration of 0.1% and both DMSO and seawater only controls were tested. RR = ruthenium red.

Figure 2. Mean net photosynthesis rates of duplicate corals in each treatment. Rates are shown on a proportional scale and are calculated from the mean of observations on days 2–5 (e.g. in the presence of the inhibitors, if used) relative to the rate observed on day 1 (before inhibitor addition). Error bars indicate one standard deviation. RR = ruthenium red.
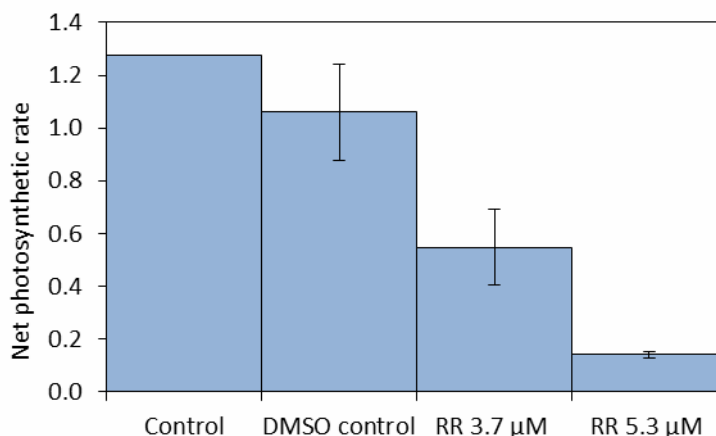
References
[1] B. Honisch et al. (2004) Geochim. Cosmochim. Acta., **68**, 3675-3685
[2] N. Allison et al., (2010) Geochim. Cosmochim. Acta, **74**, 1790-1800
[3] K. Klochko et al. (2006) Earth Planet. Sci. Lett., **248**, 276-285
[4] DOE (1994) Handbook of Methods for the Analysis of the various parameters of the CO_2 system in seawater. A.G. Dickson & C. Goyet, eds. ORNL/CDIAC-74, Version 2.
[5] N. Allison et al., (2011) Geochim. Cosmochim. Acta, **75**, 6350-6360

Ti-in-quartz in low pressure hydrothermal systems

A.K Barker[1], L.A. Coogan[2] & H. Annersten[1]

Centre of Experimental Mineralogy, Petrology and Geochemistry (CEMPEG), Department of Earth Sciences, Villavägen 16, Uppsala University, Uppsala SE-752 36, Sweden.
[2]School of Earth, Ocean and atmospheric sciences, University of Victoria, Victoria, British Columbia, Canada.

The concentration of titanium in quartz has been shown to vary as a function of temperature[1]. This has the potential to provide a thermometer for many geological applications where quartz is present, such as the production of evolved magmas or melting of the crust e.g. granites, metamorphism e.g. gneisses, and even silica saturated hydrothermal systems, such as black-smokers.

Since the initial publication of the Ti-in-quartz thermometer TITANIQ[1], there has been a study proposing pressure dependence[2]. In addition to this a suitable thermometer should not be extrapolated beyond it's calibration range, which for the TITANIQ is 600 to 1000ºC[1]. Therefore, in order to calibrate Ti-in-quartz as a thermometer for low pressure hydrothermal systems, we undertook experiments of Ti saturated silica rich systems at low pressure (0.5 kb) and temperatures of (300 to 500ºC), using the hydrothermal autoclave laboratory at CEMPEG, Uppsala University.

Accurate analytical measurement requires known, reproducible standard analyses, which has so far caused a problem for determining the analysed concentrations of Ti-in-quartz. A problem with using available NIST glasses is that they contain many other elements, the influence of which are hard to constrain. However a recent study[3] has suggested a correction factor for matrix effects based on 3 NIST standards (NIST 610, 612, 614). Additionally matrix-matched standards have been produced by fusing silica precipitated from a gel, to form quartz, producing a standard suite with known Ti concentrations (2 ppm, 5 ppm, 10 ppm), which have been characterised by LA-ICP-MS[4].

Unfortunately analyses of the matrix-matched standards at the spatial resolution offered by the SIMS, showed them to be heterogeneous and therefore unreliable as standards. However, it was possible to analyse Ti in quartz with respect to NIST 612, which is one of the standards used for matrix corrections in [3]. Furthermore analyses of the experimental products proved heterogeneous perhaps due to surface contamination, proximity to the Ti-bearing phase rutile, or heterogeneity of the experimental sample. The study continues to determine the influencing factors in the heterogeneity of the experiments. This preliminary study requires adapting the synthetic production of standards and the experimental procedure to produce reliable homogeneous standards and samples in order to facilitate calibration of Ti-in-quartz as a thermometer for low pressure hydrothermal systems.

References

[1] D.A. Wark and E.B. Watson (2006) Contrib Mineral Petrol **152**, 743-754. Doi: 10.1007/s00410-006-0132-1
[2] J.B. Thomas et al. (2010) Contrib Mineral Petrol Doi: 10.1007/s00410-010-0505-3
[3] W.M. Behr et al. (2011) American Mineralogist **96**, 1100-1106 doi: 10.2138/am.2011.3702
[4] A.K. Barker et al. (2010) Geology **38**, 39-382. Doi: 10.1130/G30542

Water in kimberlites as deduced from olivine from Igwisi Hills Volcano, Tanzania

I. Buisman[1], R.S.J. Sparks[2] & M. J. Walter[2]

[1]Department of Earth Sciences, University of Cambridge, Downing Street, Cambridge, CB2 3EQ, U.K.
[2]Department of Earth Sciences, University of Bristol, Will's Memorial Building, Bristol, BS8 1RJ, U.K.

Introduction

Kimberlites are ultramafic rocks formed from small-volume melts that originate from the lithospheric mantle- or deeper [1,2]. They are thought to erupt rapidly and violently due to their high volatile content [3]. The importance of CO_2 in kimberlites is well documented through phase relation studies in CO_2-bearing peridotite as well as the presence of primary calcite [4,5]. Water is thought to play an important role in reducing the melting temperatures during the formation of kimberlite melt allowing for low estimated kimberlite eruption temperatures [6].

Kimberlites are generally highly altered rocks that contain abundant serpentine minerals making it impossible to quantify the primary water content [5]. Deducing the primary water content of kimberlite magmas may best be achieved by looking at the water content of nominally anhydrous minerals (NAMs), such as olivine. Olivine in kimberlites occurs as both xenocrysts and phenocrysts, and because it will have crystallized at depth olivine may preserve a record of the primary magmatic water content.

The aim of this project is to quantify the water content of olivine in natural kimberlite samples, and to thereby establish the role of water in kimberlites magma-genesis. The natural samples were selected from an exceptionally young (Holocene) kimberlite of the Igwisi Hills Volcano, Tanzania (Figure 1). The olivine in this kimberlite is remarkably fresh and uniquely occurs in both lavas and pyroclastic deposits, allowing for a comparison of olivine water content in two different cooling regimes.
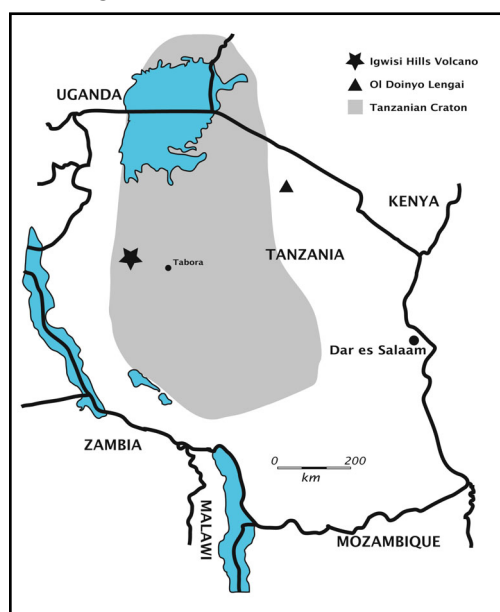
Figure 1. Location of the Igwisi Hills Volcano on the western edge of the Tanzanian Craton.

Results

We measured the water concentrations in xenocrystic olivine grains from both the lava and pyroclastics deposits. These xenocrysts have rim compositions that are similar to the phenocrysts, which we interpret as reflecting olivine crystallising from the kimberlite host magma. However, xenocryst cores show a clear mantle signature (high NiO content and Cr-spinel inclusions). The xenocrysts are also zoned in terms of trace elements (NiO, MnO and CaO; Figure 2).
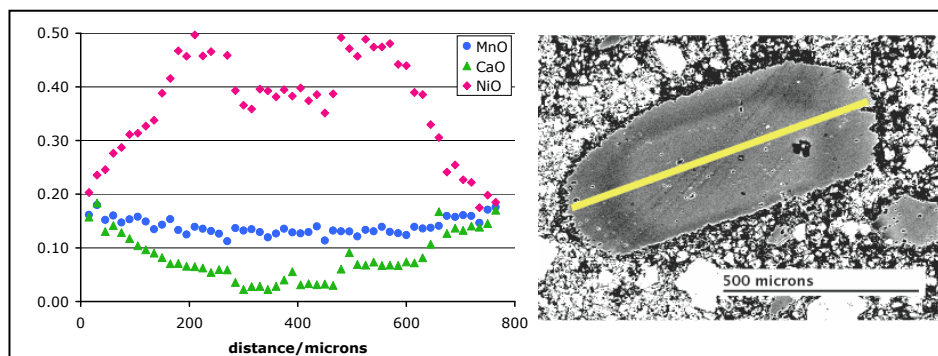
Figure 2. Back Scattered Electron (BSE) image of a xenocrystic olivine showing clear zonation between the rim and core due to differing Fo-content. NiO, CaO and MnO profiles illustrate minor element zonation in this olivine.

Water concentrations measured by SIMS illustrated some stark differences between the overall water content in the olivine recovered from the lava and pyroclastics deposits. Olivine crystals from pyroclastic deposits show relatively homogenous water content of ~35 ppm. In contrast, olivine xenocrysts in lava show a large water variation, with some cores containing up to 230 ppm and decreasing markedly to around 20-30 ppm (Figure 3). The concentration of water at the rims of these olivine grains zoned in water content is remarkably consistent from one olivine crystal to the next. The high water content of the cores shows that water must have diffused out from the cores. This suggests that the magma disrupts the mantle to mix in with xenocrystal olivine, which is dry, and mixes in these xenocrysts/microxenocrysts thoroughly for a period of time. This scenario is supported by work done on minor element chemistry (NiO, MnO, Cr_2O_3, CaO and P) of Igwisi olivine [7].
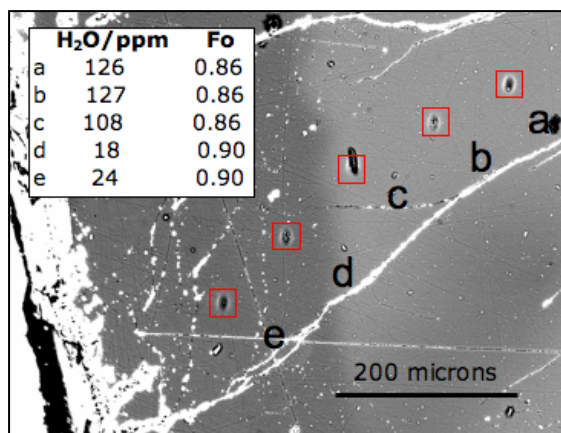
	H_2O/ppm	Fo
a	126	0.86
b	127	0.86
c	108	0.86
d	18	0.90
e	24	0.90

200 microns

Figure 3. BSE image of an olivine xenocryst that has an overgrowth rim collected from a lava sample. Water concentrations (ppm) as measured by SIMS are included.

The change in the water concentration appears to be closely related to the change in olivine chemistry. FTIR performed on some crystals measured by SIMS demonstrate how the water content depends on the mechanism of H incorporation into the olivine structure, which is likely dependent on the chemistry of the olivine (Figure 4). Although the quantification of FTIR spectra appears to produce different absolute values of water to those obtained through SIMS, these results illustrate, like SIMS, that the cores of the olivine xenocrysts from the lava contain very high water contents and decreases towards the rim.

The SIMS data was used as part of a PhD thesis [8] and this data together with FTIR data will form part of a manuscript currently being put together for submission. This SIMS data formed part of a poster presented at the 10th International Kimberlite Conference 2012, Bangalore, India [9].

Figure 4. FTIR for an olivine crystal from a lava rock illustrating the changing mechanism of H incorporation into the olivine structure.
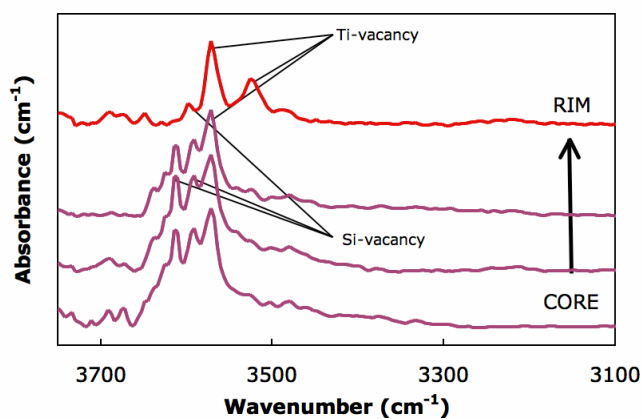
References
[1] R.H. Mitchell (1986) Kimberlites: Mineralogy, geochemistry and petrology. Plenum Press, New York
[2] J.B. Dawson (1980) Kimberlites and their xenoliths. Springer-Verlag, New York
[3] R.S.J. Sparks et al. (2006) Journal of Volcanology and Geothermal Research **155**, 18-48
[4] J. A. Dalton and D. C. Presnall (1998) Journal of Petrology **39**, 1953-1964
[5] R.S.J. Sparks et al. (2009) Lithos **112**, 429-438
[6] Y. Fedortchouk and D. Canil (2004) Journal of Petrology, **45**, 1725–1745
[7] I. Buisman (in review) Olivine chemistry of exceptionally young (Holocene) kimberlite of the Igwisi Hills Volcano, Tanzania. Contributions to Mineralogy and Petrology
[8] I. Buisman (2012) The origin and evolution of kimberlitic melts: an experimental and petrological approach. University of Bristol.
[9] I. Buisman (2012) Olivine chemistry of exceptionally young (holocene) kimberlite of the Igwisi Hills Volcano, Tanzania. Poster at the 10th International kimberlite conference, Bangalore, India.

Dehydration of biotite during anatexis: constraints from microstructure-assisted SIMS analysis of hydrogen

S. Meli[1], B. Cesare[2], G. Cruciani[3], M. Silvestri[3], L. Valeriani[1], J.C.M. de Hoog[4]

[1]Earth Sciences Department, University of Parma, Italy
[2]Geosciences Department, University of Padova, Italy
[3]Earth Sciences Department, University of Ferrara, Italy
[4]Edinburgh Ion Microprobe Facility, University of Edinburgh, UK

Introduction

The SIMS-based study of Ti-H relationships in biotite during the prograde and retrograde phases of HT metamorphism and anatexis [1] has been expanded with the addition of three new case studies, which help providing a coherent scenario for metapelitic rocks. Two of the three studied sample suites are enclaves or xenocrysts in lavas, which have been demonstrated to be the ideal setting for the preservation of the primary composition of biotite from high-grade anatectic metapelites [3]. During the SIMS session in 2011 we focussed our attention on biotite crystals which are contained in garnet xenocrysts (Fig. 1) and in Grt-bearing enclaves occurring in the Crd-bearing lavas from Lipari (Aeolian arc, Italy; [3]).
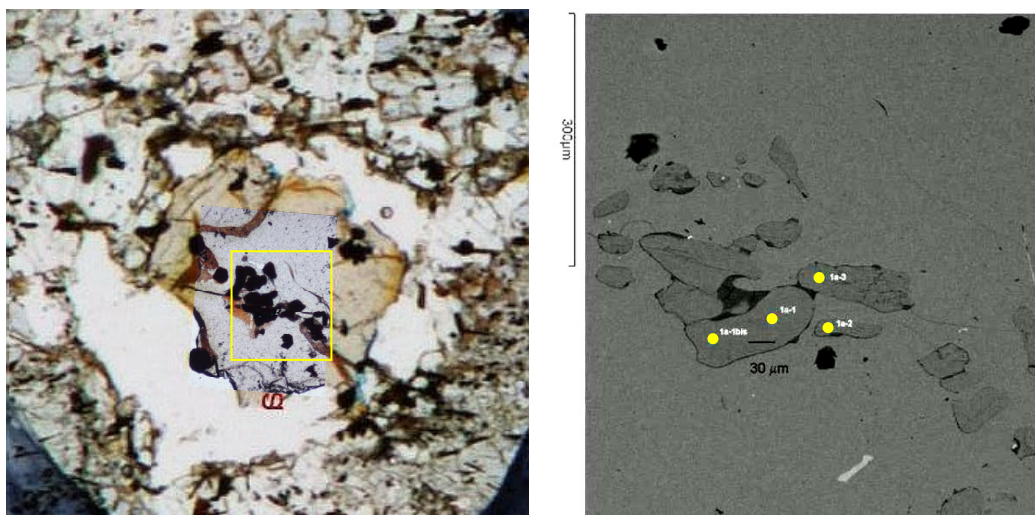
Figure 1. Left: peritectic garnet with biotite inclusions (plain polarised light). Right: Detail of biotite inclusions with analysis spots (backscatter electron image)

Analytical

We analyzed four elements (H, Si, Ti, K); the two latter were mainly monitored to check contamination by the host crystal during ion sputtering as some inclusions were very small (<20 μm width, Fig. 1). As a whole, 52 inclusions were measured. NBS30, a natural biotite standard, was used for calibration. As this fine-grained standard is slightly heterogeneous from grain to grain, the results for ten analyses on different grains were averaged to obtain the calibration line.

While evaluating the data, some discrepancies between TiO_2 and K_2O analysed both by EPMA and SIMS became apparent (Fig. 2). Low values by SIMS can be attributed to overlap of the ion beam with the host crystal during analysis of the small inclusions. As this overlap will also affect
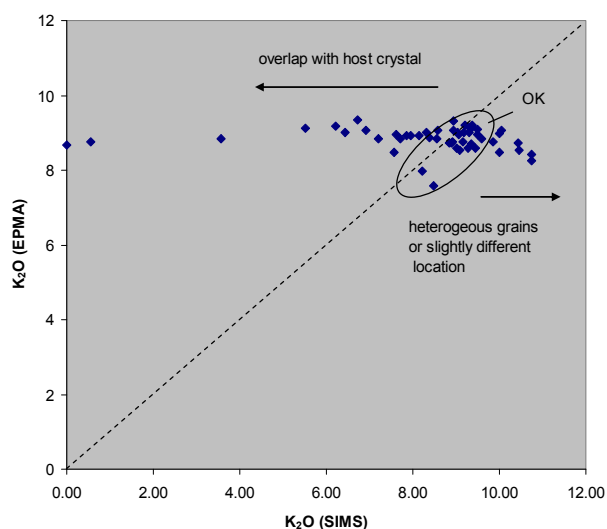
Figure 2. Comparison between K analyses performed by both EPMA and SIMS.

TiO_2 and H_2O these elements were normalized to the K_2O content of the inclusion as measured by EPMA. In a few cases K_2O was higher, which we attribute to heterogeneity of the grains or a possible crystal orientation effect.

Results

The main result is the find of nearly anhydrous biotite crystals, which are hosted within a peritectic garnet and show microstructural evidence of prograde reaction within the xenolith, that gave rise to melt and the host garnet. In the biotite crystals hosted in the enclaves, the range of Ti contents (5 to 11 wt% TiO_2), detected previously by EPMA but also confirmed by SIMS, includes the highest values reported in the literature, whereas analyzed H contents include the lowest (from 1.7 down to 0.3 wt.% H_2O). These data extend the occurrence of Ti-oxy exchange $[(Mg,Fe)^{2+} + 2OH^- = Ti^{4+} + 2O^{2-}]$ to TiO_2 contents not previously investigated. In addition, they suggest that the (OH+F+Cl) content of extremely Ti-rich biotites may decrease to almost zero (Fig. 3).
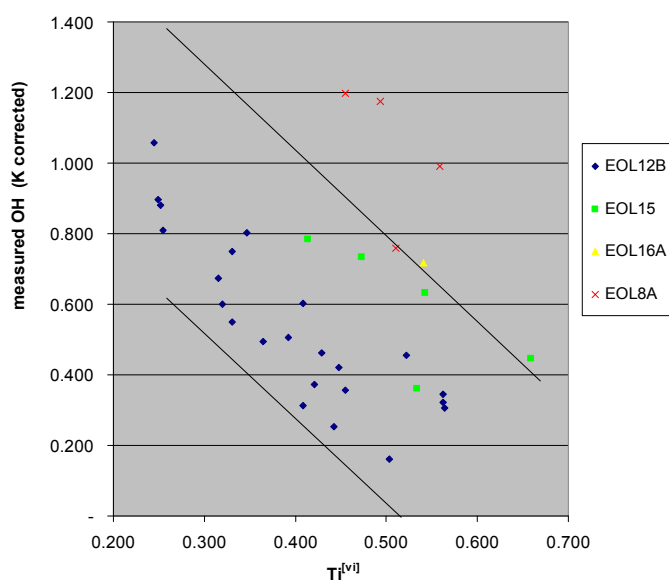
Figure 3. OH vs. $Ti^{[vi]}$ of selected (on the basis of SIMS and EPMA agreement) biotite inclusions. Slanted lines show slope of the Ti-oxy vector at different bulk TiO_2 contents.

Conclusions and Future Work

The new data solidify previous findings showing that:
1. Ti-oxy is the dominant exchange mechanism over the entire TiO_2 range so far investigated in biotite from metapelitic rocks;
2. During prograde heating and continuous melting biotite is progressively dehydroxylated via Ti uptake, until it may eventually become OH-free.

At the present we are looking to perform in-situ microanalysis of Fe^{3+} on biotite to obtain better constrained crystal chemical formulas as to better distinguish between Ti-oxy, Ti-vacancy, Fe-oxy and Fe-vacancy substitution mechanisms.

The SIMS results have been already presented at several conferences [4, 5] and a manuscript for submission to *American Mineralogist* is in preparation.

References
[1] Cesare et al. (2008) American Mineralogist, 93, 327-338.
[2] Cesare et al. (2003) American Mineralogist, 88, 583-595.
[3] Di Martino et al. (2011) Contributions to Mineralogy and Petrology, 1011-1030.
[4] Cesare et al. (2011) Epitome, 4: 208.
[5] Cesare et al. (2011) Mineralogia, Special Paper, 38: 43-44.

Diffusion of Si and O in silicate melts and glasses

S. Chakraborty[1] & P. Sengupta[1,2]

[1]Institut für Geologie, Mineralogie und Geophysik, Ruhr Universität Bochum, D-44780 Bochum, Germany
[2]BARC, Trombay, 400085 Mumbai, India.

The Problem

Diffusion rates of Si and O in silicate melts and glasses have been measured by many authors over the past decades, including some pioneering measurements from high pressure experiments that have come out of the Edinburgh Ion Microprobe facility. These data have established beyond doubt that diffusion rates of Si and/or O can be related to viscosity of silicate melts via the Eyring relation. This relationship has then been exploited to study various aspects of melt structure and dynamics. The "and/or" in the preceding statement arises from the fact that these rates are always close to each other when a global dataset is considered (e.g. within an order of magnitude of each other), and differences are subtle and relevant only for detailed models of specific compositions. However, several key questions remain unanswered, even for the broad behavior, in spite of this large body of work. Some of these are:

1. Viscosity of silicate melts changes non-linearly at the glass transition, and the nature and extent of this non-linearity depends on the composition / structure of the glass. The logarithm of viscosity changes more non-linearly as a function of temperature [1] for so called fragile glasses (e.g. diopside) than for strong glasses (e.g. SiO_2), as shown in the figure below. Viscosity is proportional to diffusivity of Si and/or O, following the Eyring relation, in the liquid state for all of these compositions.
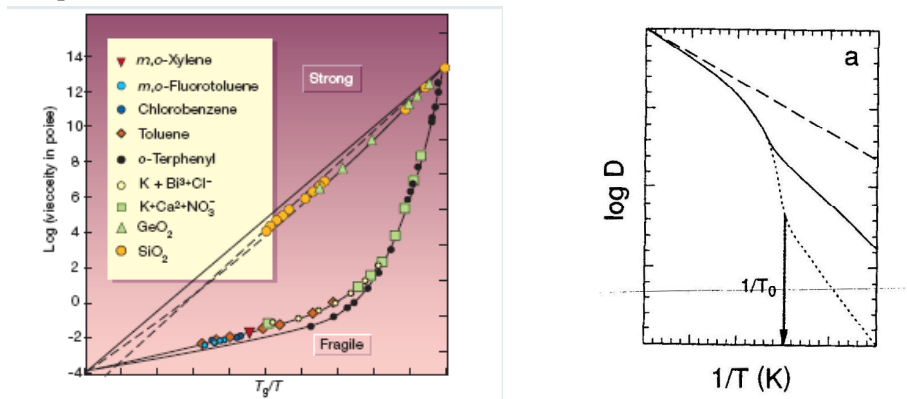
Figure: Left panel is from Ref. [1], right panel is from Ref. [2]

However, it has not been explored what happens below the glass transition. Does the Eyring relation break down? Or do the diffusion rates of Si / O track the non-linear behavior of viscosity, and the Eyring relation continues to be maintained at these lower temperatures. Answers to this question are extremely important for developing predictive tools for the viscous and diffusive behavior in glasses. But the limited data (older, and hence of a quality lower than what is achievable today) available so far suggests that diffusion rates and viscous flow follow different kinds of behavior [2] across the glass transition (left and right panels in the figure above, respectively). We are carrying out controlled experiments to characterize this behavior and address this important general question.

2. Diffusion of O in various glasses has been found to be dependent on oxygen fugacity. If the Eyring (or any other similar) relation connects viscosity to diffusivity of oxygen, then it would imply that viscosity would be a function of oxygen fugacity, which would be an extremely interesting result for Materials Sciences. Alternately, the diffusion behavior of Si and O could become decoupled, and viscosity may become unrelated to the diffusion of O, unlike in the liquid state. Some of our experiments are carried out at controlled oxygen fugacities to test this behavior.

The Experiments

We have synthesized glasses in the system CaO-Al$_2$O$_3$-SiO$_2$, where a large body of experimental data on diffusion rates and viscosity are already available. What has not been available is glasses with very high SiO$_2$ contents (~ 80%). We have produced bubble-free material of such glasses at the laboratory of Prof. D. Dingwell in Münich. Subsequently, we have used these glasses for several kinds of measurements: (i) Simultaneous measurement of Si and O diffusion rates using the pulsed laser thin film deposition technique available in our laboratory in Bochum, (ii) chemical diffusion coefficients of Ca, Al and Si in these melts (iii) measurement of viscosity of these compositions in the high temperature liquid state, and (iv) measurement of viscosity of these compositions at low temperature glassy states. Measurements (iii) and (iv) were carried out at the laboratories of Prof. Dingwell in Münich. After the diffusion anneals, concentration profiles of isotopically enriched Si and O were measured at the Ion Microprobe facility in Edinburgh.

Results

One of the challenges in carrying out these experiments was to anneal glasses below the glass transition temperatures for sufficiently long durations to induce measurable diffusion profiles, but short enough that no crystallization occurred. We have succeeded in doing this after some trials and now we have diffusion profiles from samples annealed at temperatures between 700 – 1000 °C. Preliminary analysis shows that Si and O diffusion do get decoupled at these conditions i.e. their diffusion rates are not as close as at high temperatures. Comparison with direct measurement of viscosity at these conditions indicates that there is no straightforward relationship between diffusivity and viscosity, as at higher temperatures. More analysis of measured profiles and experiments are underway to complete the characterization.

References

[1] Debenedetti, P. and Stillinger, F.H. (2001) Supercooled Liquids and the Glass Transition, Nature 410, 259 – 267.
[2] Chakraborty, S. [1995] Diffusion in Silicate Melts, in *Structure, Dynamics and Properties of Silicate Melts*, Reviews in Mineralogy, vol. 32, Mineralogical Society of America, Washington D.C.

The role of volatiles in crystal transfer during magma mingling

S.J. Collins[1], J.P. Davidson[1], D.J. Morgan[2] & E.W. Llewellin[1]

[1]Department of Earth Sciences, Durham University, Durham DH1 3LE, UK
[2]School of Earth and Environment, University of Leeds, Leeds LST 9JT, UK

Introduction

Observations from Chaos Crags, Lassen Peak National Park (Figure 1) indicate that enclave formation is an important stage in the magma mingling process. There is general agreement that enclave formation is related to vesiculation and the generation of density instabilities as a more mafic magma comes into contact with a cooler, more differentiated magma in a magma reservoir[2]. In addition the evidence for exchange of crystals during mingling in these systems is overwhelming. At Chaos Crags, mafic enclaves in a dacite host contain crystals of biotite and sodic plagioclase which clearly originated in the dacite. In addition microlites which originated in both the host and the inclusion and which crystallized in response to quenching and volatile exsolution have been exchanged

Figure 1: Location map of the 6 volcanic domes which make up Chaos Crags within the Lassen Peak national park, California. Modified from Tepley et al., 1999[1]

between the magmas prior to ascent and eruption. Less clear is how the crystals are transferred before and/or during the enclave formation process and how this relates to the vesiculation process. Consequently, quantifying the volatile contents of the magmas involved during magma mingling is a vital step towards generating a physical model for how crystal transfer occurs.

We have quantified major element, trace element and H_2O and CO_2 contents of the magmas involved during magma mingling using EMP and SIMS analysis of olivine, feldspar, amphibole and quartz hosted melt inclusions as well as matrix glass in both the host lava and enclave.

Objectives

The objectives of these analyses are as follows:

1. Analysis of melt inclusions will quantify the volatile content of both the host magma and the intruding mafic magma prior to mingling.

2. Analysis of H_2O from the rim to the core of the enclave will determine the mechanism and timing of volatile exsolution during quenching of the mafic magma on contact with host.

3. Analysis of trace elements will underpin quantitative modelling of degassing during magmatic evolution, including crystallisation and magma mixing.

4. Li is semi-volatile and diffuses rapidly in melts. Analysis of Li in the glasses will provide an extra constraint on the gas transfer mechanisms which occur during vesiculation.

Samples and Approach

During a recent field trip to Chaos Crags (Figure 1) we collected a suite of samples of mafic enclaves hosted within rhyodacite dome rock. The enclaves vary in texture from complex with a fine grained but vesiculated core, a coarse grained centre and a quenched fine-grained rim (Group 2, domes C-F) to homogenous in texture with no obvious vesiculation and a simple quenched rim (Group 1, domes A-B) (Figure 2). All enclaves and their host lavas contain crystals which have been

Figure 2: Examples of a complex and more simple and homogenous enclave texture.

transferred between magmas and which host melt inclusions. These samples provide an excellent opportunity to determine how the volatile content varies between the host magma and that of the enclave. The melt inclusions will provide estimations of parental volatile contents and the matrix glass will help determine the amount of gas lost within the enclave on quenching.

Results and Initial Interpretation
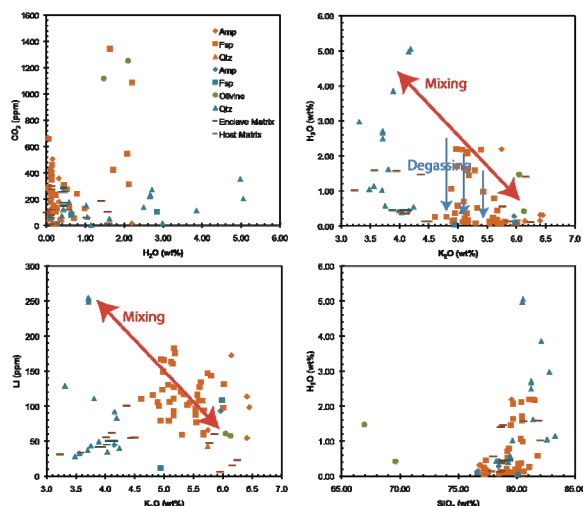
Figure 3: Volatile contents for melt inclusions and matrix glass. See text for details.

Difficulty arose with understanding what the melt inclusions represented in terms of whether they are pre- or post-mingling. Initial interpretations are as follows. The quartz hosted melt inclusions have highly variable H_2O contents (0-5.6wt% H_2O) and low CO_2 contents <300ppm, we interpret these to represent the rhyodacite host end member of the mingling process. Compositionally these lie within a group of high Sr and low K_2O melt inclusions (coloured blue in Figure 3). High H_2O and low CO_2 contents may have evolved from crystallisation of a H_2O undersaturated but CO_2 saturated magma. Feldspar hosted melt inclusions were typically only found in those feldspar, which had been resorbed after being transferred from the rhyodacite to the mixed and homogenised enclave. These inclusions are typically open and linked however they are not chemically similar to either the enclave or host matrix glass composition (instead they are compositionally distinct with low Sr and higher K_2O). It is possible that these represent the mixed magma and show variable amounts of degassing and mixing. Olivine hosted melt inclusions were rare, those that were analysed had highly anomalous compositions and were not in equilibrium with the host crystal (H_2O <2.1wt%, CO_2 ~1200ppm).

Matrix glass H_2O contents (Figure 4) are generally lower than the melt inclusions representing the degassed nature of the glass, however the concentrations do relate to the textural nature of the enclaves. In the complex enclaves (typically from group 2 domes) which have variably quenched rims and interiors H_2O contents do vary from 0-1.6wt%, however in those more simple enclaves (typically from group 1 domes) water contents are split between low H_2O contents (0-0.1wt%) which represent the degassed interiors and high H_2O (1.4wt%) which represents the quenched rims. In comparison the host lavas have very restricted water concentrations of 0.4wt% H_2O.

Figure 4: Matrix glass H_2O contents from simple enclaves from the group 1 domes to more complex textures of the group 2 domes.

Summary

Volatile and trace element concentrations in melt inclusions can constrain end-member compositions and we have begun to use these compositions to link crystallisation and degassing processes which occur as a consequence of magma mingling. In addition H_2O contents of matrix glass relate to textural observations such as the degree of quenching and vesiculation.

References

[1] Tepley FJIII, Davidson JP, Clynne, MA, 1999, Magmatic interactions as recorded in plagioclase phenocrysts of Chaos Crags, Lassen volcanic center, California. J. Petrol., 40, 787-806

[2] Sparks RSJ, Sigurdsson H, Wilson L, 1977. Magma mixing: a mechanism for triggering acid explosive eruptions. Nature 267

In situ dating of low-temperature alteration of the upper oceanic crust: a new approach using ^{40}K-^{40}Ca dating on adularia

L.A. Coogan[1] & R.H. Hinton[2]

[1]School of Earth and Ocean Sciences, University of Victoria, B.C., Canada,
[2]School of GeoSciences, University of Edinburgh, Edinburgh EH9 3JW, UK

Introduction

The composition of seawater impacts many aspects of the Earth System, and the record of past changes in ocean chemistry provide information about how the Earth System has changed through time in response to various forcings. Low-temperature, off-axis, hydrothermal systems may play an important role in controlling ocean chemistry (e.g. extracting large amounts of alkali elements and carbon through "reverse weathering") but currently the fluxes are poorly constrained. One of the key problems in accessing the importance of low-temperature, off-axis, hydrothermal circulation in ocean chemistry has been determining the timing of alteration. This is critical to address whether differences in the extent of alteration between crustal sites of different ages reflect: (i) differences in seawater composition with time; (ii) progressive (age dependent) alteration of the ocean crust; or (iii) local conditions.

In situ K-Ca dating of hydrothermal adularia by ion microprobe

One of the more important elemental fluxes during low-temperature alteration of the oceanic crust is the up-take of alkalis into clays and secondary alkali feldspar (adularia). Previous dating of this alkali uptake has concentrated on two approaches: (i) Rb-Sr idsochron ages from separates of multiple different clay minerals [e.g. 1] and (ii) K-Ar dating of celadonitic clays [e.g. 2]. The precision of the former ages is suspect due to the lack of justification of the assumption that different clay minerals, with different Rb/Sr, should have formed at the same time. The latter ages are also potentially problematic because of the possibility for Ar loss. The ideal dating approach would be an *in situ* method to date individual mineral grains.

As part of a broader program of dating secondary minerals formed during low-temperature alteration of the oceanic crust we have explored the potential of ^{40}K-^{40}Ca dating of adularia (90% of ^{40}K decays to ^{40}Ca with only 10% decaying to the more commonly discussed daughter product ^{40}Ar). The approach broadly follows the methodology of Harrison et al. [3] in using doubly charged ions to suppress isobaric interference of ^{40}K on ^{40}Ca due to the orders of magnitude lower ion yields for doubly charge alkalis than for Ca [4]. Because there is very little oceanic crust older than Cretaceous in age this approach is analytically challenging due to the limited radiogenic Ca production. A key to successful dating using this approach is to analyse material with low unradiogenic Ca contents.

500 μm
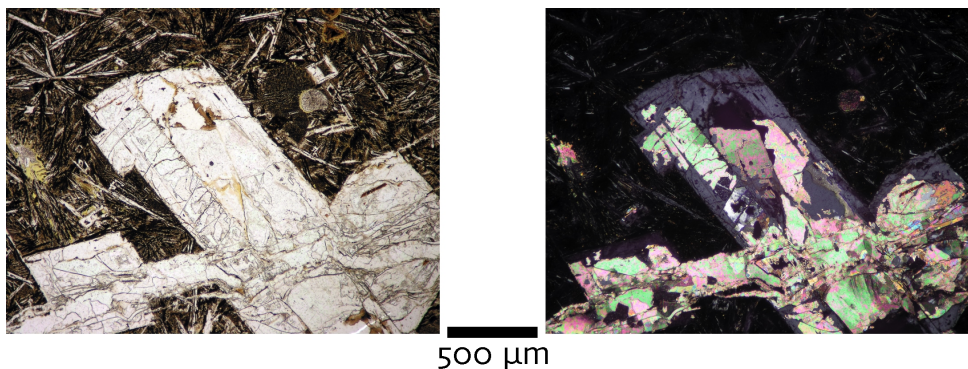
Fig. 1. Typical texture for adularia in altered oceanic lavas. Adularia and calcite replace both phenocrysts and microlites of plagioclase. Adularia is the low birefringence phase.

A typical texture for adularia in altered oceanic lavas is shown in Fig. 1. Adularia most commonly forms pseudomorphs after plagioclase commonly intergrown with calcite. Mineral separation for bulk analysis is near impossible but *in situ* analysis is possible and would allow direct dating of the timing of K-metasomatism.

Results

We have measured adularia Ca contents down to ~5 ppm (by ion microprobe) and Na contents to ~0.1 wt% (by electron microprobe) indicating that this is very near the pure potassium end-member feldspar. This high purity is consistent with formation at very low temperatures. K-Ca "isochrons" show that adularia formed within <40 Myr of crustal accretion (Fig. 2) in both locations studied (DSDP Sites 417 and 543). Measured analytical precision approximately matches expected precision based on counting statistics. The scatter in the data may represent adularia (re)crystallization at different times. The intercepts represent the planetary $^{40}Ca/^{44}Ca$. These ages are consistent with new U-Pb ages for carbonates from the same samples (LAM-MC-ICP-MS; R. Parrish Pers. Com.).
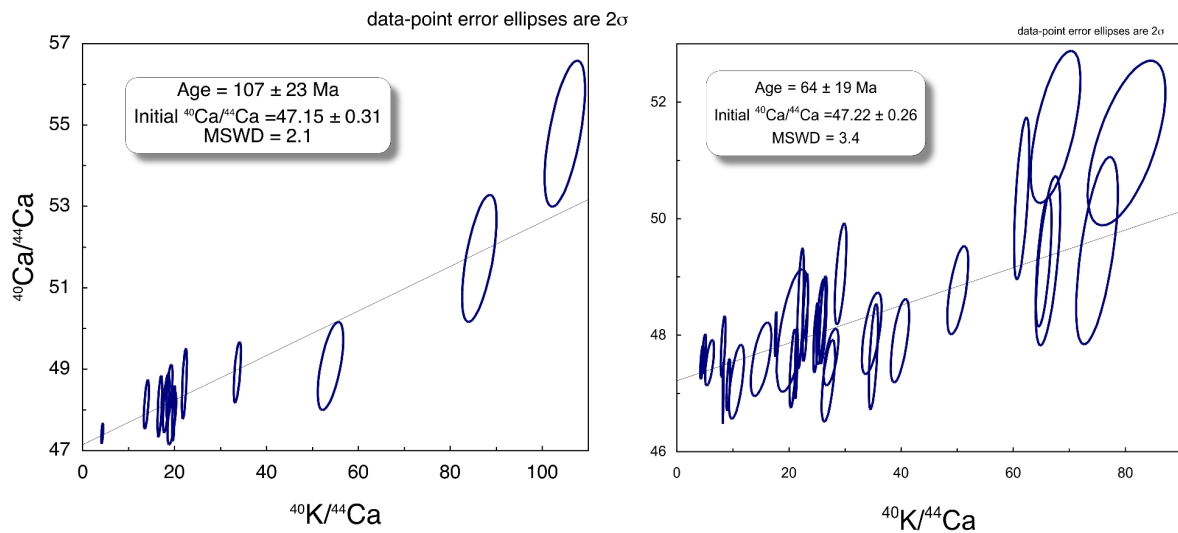
Fig. 2 "isochron" diagrams for adularia K-Ca data from two samples. Crustal ages are 120 Myr and 80 Myr indicating in both cases that adularia formed within <40 Myr of crustal accretion.

References
[1] S.R. Hart and H. Staudigel H. (1986) *Geochim. Cosmochim. Acta* **50**, 2751-2761.
[2] W.E. Gallahan and R.A. Duncan R. A. (1994) Journal of Geophysical Research. **99**, 3147-3161
[3] T.M. Harrison et al., (2010) Earth and Planetary Science Letters **299** 426-433
[4] R.W. Hinton, (1990) Chemical Geology **83**, 11-25

Disentangling biological, ontogenetic and environmental influences on oxygen isotope composition of brachiopod and bivalve shells

M. Cusack[1]

[1]School of Geographical & Earth Sciences, University of Glasgow G12 8QQ, UK

Introduction

Marine biomineral carbonates record environmental information such as ambient seawater temperature that can be interpreted using proxies such as oxygen isotope composition or Sr/Ca or Mg/Ca ratios. These carbonates are not passive recorders of such environmental data since they are produced under exquisite biological control that determines mineral type, polymorph, structure and crystallography. To ensure accurate interpretation of environmental data, it is imperative to gain a detailed understanding of how biological control influences environmental data. This project uses the NERC Ion Probe facility to measure stable oxygen isotope ($\delta^{18}O$) composition of brachiopods.
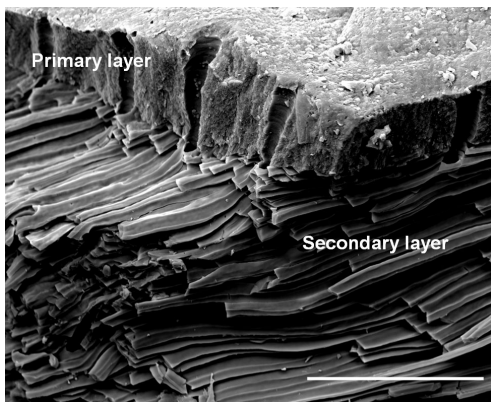
Figure 1. Secondary electron image of a fracture section of *T. retusa* shell. Scale bar=10 μm.

There is a sharp transition between the outer (primary) layer and inner (secondary) layer of Rhynchonelliform brachiopods which have low Mg-calcite shells (Figure 1). The secondary layer is in oxygen isotopic equilibrium with seawater [1-2]. Auclair et al [3] used micro-sampling to demonstrate that, in *Terebratalia transversa*, there is no switch to isotopic equilibrium concomitant with the sharp transition from the primary to secondary layer. Instead there is a progression towards oxygen isotope equilibrium towards the innermost shell. This has important implications for the use of brachiopods as seawater temperature proxies since it implies that, not only is it essential to sample secondary layer calcite but also to measure the isotopic composition of shells that have reached sufficient maturity that the inner calcite has achieved isotopic equilibrium with ambient seawater. This project used SIMS analyses to determine the consistency of this trend in *T. transversa* and *Terebratulina retusa*.

Original Results

Oxygen isotope composition of both *T. transversa* and *T. retusa* becomes heavier from outer to inner shell (Figure 2).
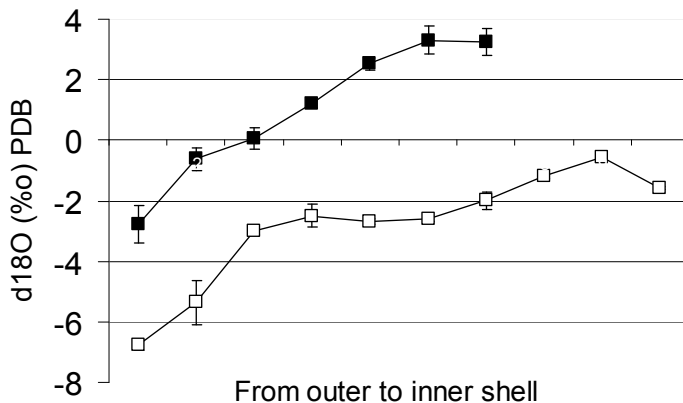
Figure 2. Oxygen isotope composition ($\delta^{18}O$) ‰ PDB from the outer (left) to innermost (right) secondary layer of the ventral valve of *T. retusa* (filled squares) and *T. transversa* (open squares). Mean vales and standard deviations from three transects.

Supplementary work

The recent analyses were supplementary to **IIMP 284/1006** in which the δ^{18}O measurements were obtained from two species of brachiopod, *T. retusa* and *T. transversa* and reported on in March 2008. While writing up the results for publication, it became obvious that it was not possible to determine the extent to which the phenomenon was widespread, by only analysing two species of brachiopod. A third species, *Notosaria nigricans* was analysed. Thus, the full survey included three species of brachiopod from two Orders and two sub-orders. An additional contrasting feature is that *N. nigricans* lacks punctae while *T. retusa* and *T. transversa* are punctate (Figure 3).

Overall Results

Secondary ion mass spectrometry (SIMS) analyses reveal that this trend of oxygen isotope equilibrium, being attained towards the innermost shell rather than being a feature throughout the secondary layer, occurs in brachiopods from two Orders and two sub-orders (Figure 3). This suggests a general pattern among brachiopods with low magnesium-calcite shells and leads to the recommendation that only the innermost fibres of mature valves be included in proxy calculations of seawater temperature. Although the trend is common in the three species studied here, the extent of the isotopic range is much less marked in the species that lacks punctae. The range of δ^{18}O values (grey box) and measured temperatures at the locations are indicated in Figure 3. Temperatures in red text indicate the increase from mean temperature that would be calculated were the δ^{18}O values of the first formed calcite fibres included in calculations of temperature.
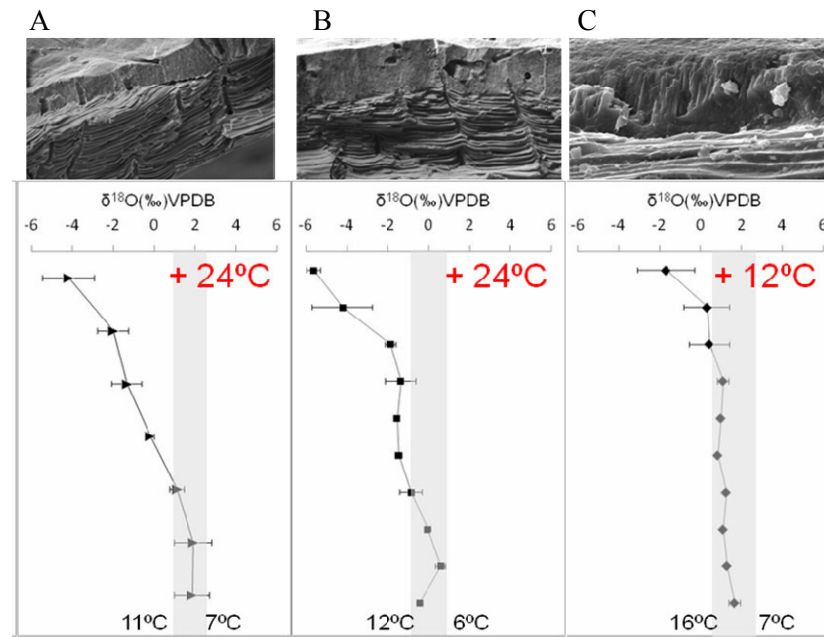
Figure. 3. Shell structure and oxygen isotope composition of three brachiopod species.
(A) *T. retusa*, (B) *T. transversa* and (C) *N. nigricans*
Top: Secondary electron images of fractured sections.
Bottom: Isotopic composition from outer (top) to innermost (bottom) fibres of secondary layer. Mean values and standard deviation for mean of three values across neighbouring parallel transects for (A) *T. retusa* (triangles), (B) *T. transversa* (squares) and (C) *N. nigricans* (diamonds) determined by secondary ion mass spectrometry (SIMS). Grey box indicates region of equilibrium δ^{18}O values for each locality delineating a temperature range of (A) 7.4°C to 11.4°C for *T. transvera* from Friday Harbor, USA, (B) 6.2°C and 12.3°C for *T. retusa* from the Firth of Lorn in Scotland and 7.0°C to 16.0°C for *N. nigricans* from Otago Shelf, South Island, New Zealand [2].

This work has been submitted to *Chemical Geology* and has been presented at the Oceans Science 2012 Meeting in Feb in Salt Lake City USA and will be presented at the Goldschmidt Conference in Montreal in June 2012.

References
[1] Carpenter, S.J.& Lohmann, K.C. (1995) *Geochimica et Cosmochimica Acta*. **59**, 3749-3764.
[2] Parkinson, D*., et al.* (2005) *Chemical Geology*. **219**, 193-235.
[3] Auclair, A.C*., et al.* (2003) *Chemical Geology*. **202**, 59-78

The record of magma generation during early stages of Earth's evolution

B. Dhuime[1,2], C.J. Hawkesworth[1] & P.A. Cawood[1]

[1] Department of Earth Sciences, University of St. Andrews, North Street, St. Andrews KY16 9AL, UK
[2] Department of Earth Sciences, University of Bristol, Wills Memorial Building, Bristol BS8 1RJ, UK

Crust generation and reworking: Archaean versus post-Archaean conditions

The timing, rates and the geodynamical conditions of continental crust generation, destruction and reworking remain a topic of considerable debate. Around 7% of the present-day exposed crust consists of rocks of Archaean age, yet ~75% of the present-day volume of the continental crust may have formed by the end of the Archaean [1]. Recently we identified systematic variations in Hf and O isotopes in detrital zircons with a large range of crystallisation ages [1]. When combined with large U-Pb and Hf isotopes data sets representative of the crust, these variations can be used to calculate the balance between the generation of new crust and the reworking of old crust with time throughout Earth's history. The continental crust appears to have been generated continuously, but with a marked decrease in the continental growth rate at ~3 Ga [1]. The Meso-Archaean inflexion in the continental growth curve at ~3 Ga indicates a change in the way the crust was generated and preserved. This change may be linked to the onset of subduction-driven plate tectonics and discrete subduction zones as observed at the present day [2-4].

Pre- 2.5 Ga record of magma generation: The Northern Pilbara Craton case study

The Meso-Archaean therefore represents a key period during which fundamental changes in the processes of crust generation, preservation, and reworking, may have occurred. Preserved igneous and sedimentary rocks from this period are scarce on the Earth's surface scale, and yet they are widespread in the Northern Pilbara Craton (NPC), Western Australia [5]. Eight sedimentary rocks with deposition ages ranging between ca. 2.6 and 3.4 Ga have been sampled across the NPC, and the zircons separated from these rocks were analysed for U-Pb isotopes (Fig. 1).
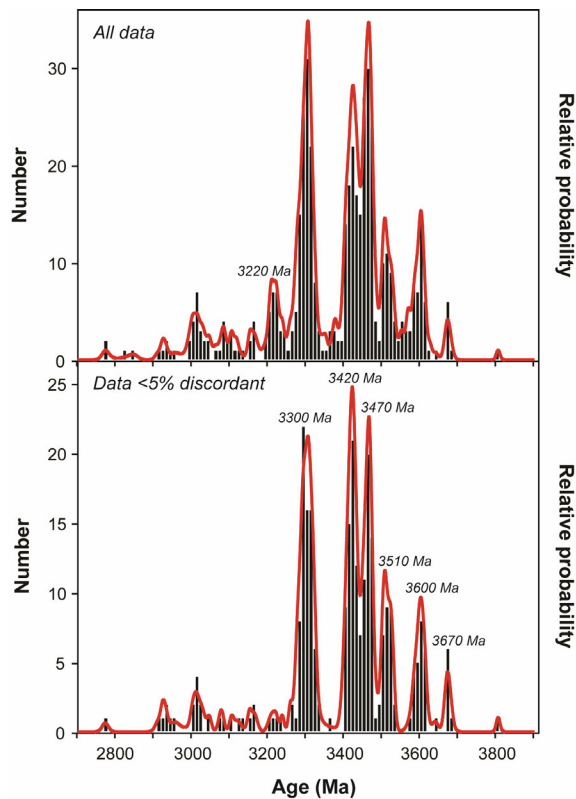
Figure 1. Distribution of ^{207}Pb/^{206}Pb ages in zircons from sediments sampled across the North Pilbara Craton, with deposition ages ranging between ca. 2.6 and 3.4 Ga. The ages of the main crystallisation peaks are highlighted.

The crystallisation ages of the detrital zircons cover a large Meso/Palaeo-Archaean time span, ranging ~2.8–3.8 Ga. Six well-defined ages peaks are present at ~3670, 3600, 3510, 3470, 3420 and 3300 Ma. A seventh peak occurs at ~3220 Ma, though it is not observed in the distribution filtered from

discordant analyses (Fig. 1, lower panel). The ~2.8–3.25 Ga period is characterised by no distinct age peak and a lesser number of crystallisation ages. These may be in part due to the large range of deposition ages for the sediments analysed (~2.6-3.4 Ga), which overlap this period.

Crystallisation age peaks are a common feature in the zircon record, at least in samples less than 2.9 Ga in age [e.g. 6]. Recent studies suggest that the post-Archaean record is biased by the supercontinent cycles, and that periods of enhanced preservation result in age peaks in the continental record [7-8]. However both the preservation of magmatic rocks and any bias of the rock record that might have been occurred in response to tectonic processes (such as the development of supercontinents) may have been low before the onset of plate tectonics at ~3 Ga [8]. The crystallisation age peaks sampled by the NPC sediments may therefore reflect the 'true', unbiased record of geological processes that occurred during early stages of Earth's evolution in this particular terrain. Geodynamical processes that might have dominated before ~3 Ga include shallow subduction and delamination [9] or 'intra-plate' lithospheric extension/mantle upwelling [10]. Given the relatively continuous nature of subduction-related magmatism, the latter case scenario may better explain the ca. 100 Ma periodicity of the Palaeo-Archaean age peaks in NPC sediments.

References

[1] B. Dhuime et al. (2012) A Change in the Geodynamics of Continental Growth 3 Billion Years Ago. Science 335 no. 6074 pp. 1334-1336. [2] P.A. Cawood et al. (2006) GSA Today 16, 4-11. [3] S.B. Shirey and S.H. Richardson (2011) Science 333, 434-436. [4] M.J. Van Kranendonk (2011) Science 333, 413-414. [5] A.H. Hickman (1983) Geol. Survey of Western Australia Bull. 127, 268p. [6] K.C. Condie et al. (2009) Gondwana Research Today 15, 228-242. [7] C.J. Hawkesworth et al. (2009) Science 323, 49-50. [8] C.J. Hawkesworth et al. (2010) J. Geol. Soc. London 167, 229-248. [9] S.F. Foley et al. (2003) Nature 421, 249-252. [10] M.J. Van Kranendonk (2010) American Journal of Science 310, 1187-1209. [11] M. Wiedenbeck et al. (1995) Geostandards Newletter 19, 1-23. [12] J.S. Stacey and J.D. Kramers (1975) EPSL 6, 15-25. [13] L.P. Black et al. (2004) Chemical Geology 205, 115-140.

Appendix

The U-Pb isotope data were measured with a Cameca ims 1270 at the EIMF. 10 analytical cycles were acquired for each analysis. U/Pb ratios were normalised to the zircon 91500 Geostandard [11], embedded into grain mounts. This standard was analysed to bracket every ~6 measurements on the unknown samples. Correction for in situ common Pb was made using measured ^{204}Pb counts and using the present-day composition of common Pb of Ref. [12]. Changes in beam density or energy were monitored and corrected using the variation between Pb/UO$_2$ and UO$_2$/UO ratios. The zircon Temora 2 [13] were periodically analysed as a monitor on data quality. The weighted average ^{206}Pb/^{238}U age measured was 417.6±1.2 Ma (2σ, *n*=57). These values are similar to the 416.8±1.3 Ma ID-TIMS value of Ref. [13].

An ion microprobe study of trace-minor elements in cold-water coral *Lophelia pertusa* skeleton

M. Douarin, M. Elliot, A. Sadekov

School of GeoSciences, University of Edinburgh, Edinburgh EH9 3JW, UK

Introduction

Coral have great potential for high-resolution ocean chemistry and temperature reconstructions. However, limited understanding of cold-water coral processes of bio-mineralization poses a significant challenge for their use for palaeo-environmental reconstructions. Coral has two main types of microstructure: (1) the early mineralization zones (EMZ) surrounded by (2) the sclerodermites. (1) and (2) are assumed to result from two distinct processes of calcification [1] (Figure a). "Grey and white" bands within the sclerodermites were related to band of growth based on the analogy with the tropical corals [2], this is however debated and some authors refer to "EMZ-like" bands as they exhibit isotopic and trace element values similar to the EMZ. In this study we aimed to document 1) the reproducibility of trace/minor element ratios variability within the coral skeleton and 2) to make accurate correspondence between coral's ultra-structures and trace/minor ratios composition.

Analysis

Four profiles perpendicular to the growth axis were performed on 1 cross section of *Lophelia sp.* skeleton at 10 µm spatial scale with ion microprobe technique (Figure a). The 4 profiles elemental Mn, Ba, Sr, B, Mg and Li (relative to Ca) variability were plotted using *Analyseries* following the microstructures to test the reproducibility of the element variability within a same coral skeleton (Figure b).

Results and preliminarily interpretations

Our results show that the Li/Ca, Mg/Ca, B/Ca, Sr/Ca, Ba/Ca and Mn/Ca ratios within coral microstructures are of 7-19.6 µmol/mol, 1.4-5.2 mmol/mol, 0.5-1.8 µmol/mol, 8.6-11.2 mmol/mol, 1.1-4.3 µmol/mol, 0.1-0.4 µmol/mol, respectively, which is coherent with the literature. For each ratio the 4 profiles exhibit relatively similar patterns, but for B/Ca and Li/Ca for instance, distinct ranges of value are measured.

There is a hyperbolic correlation between the Mg/Ca and Li/Ca ratio (Figure c). The EMZ and EMZ-like (white and porous area) are enriched in Mg/Ca and Li/Ca relative to the sclerodermites (darker).

It has been proposed that changes to aragonite crystals size, shape compaction would result in difference trace element incorporation partly due to growth rate changes [3]. In addition the mixing of two end-members (Mg-Li-low vs. Mg-Li-high) would result in a hyperbolic relationship. The EMZ (white and porous) which are Mg-Li rich and the sclerodermites (darker) which are Mg-Li depleted would constitute these two end-members. Every other area, including the EMZ-like would be a mixture of the 2 end-members. This would imply that the variably in those ratios reflect more the frequency of the internal structure rather than being driven by environmentally driven changes in the chemistry of the corals.

References

[1] Lazier, A.V., Smith, J.E., Risk, M.J. and Schwarcz, H.P. (1999) The skeletal structure of Desmophyllum cristugulli: the use of deepwater corals in sclerochronology. Lethaia **32**: 119-130.
[2] Cohen, A.L., and Gaetani, G.A., Lundälv, T., B.H., C. and George, R.Y. (2006) Compositional variability in a cold-water scleractinian, Lophelia pertusa: New insights into ''vital effects''. Geochemistry Geophysics Geosystems **7**: 1525
[3] Sinclair, D.J. (2005) Correlated trace element "vital effects" in tropical corals: A new geochemical tool for probing biomineralization. Geochimica et Cosmochimica Acta **69**: 3265-3284.
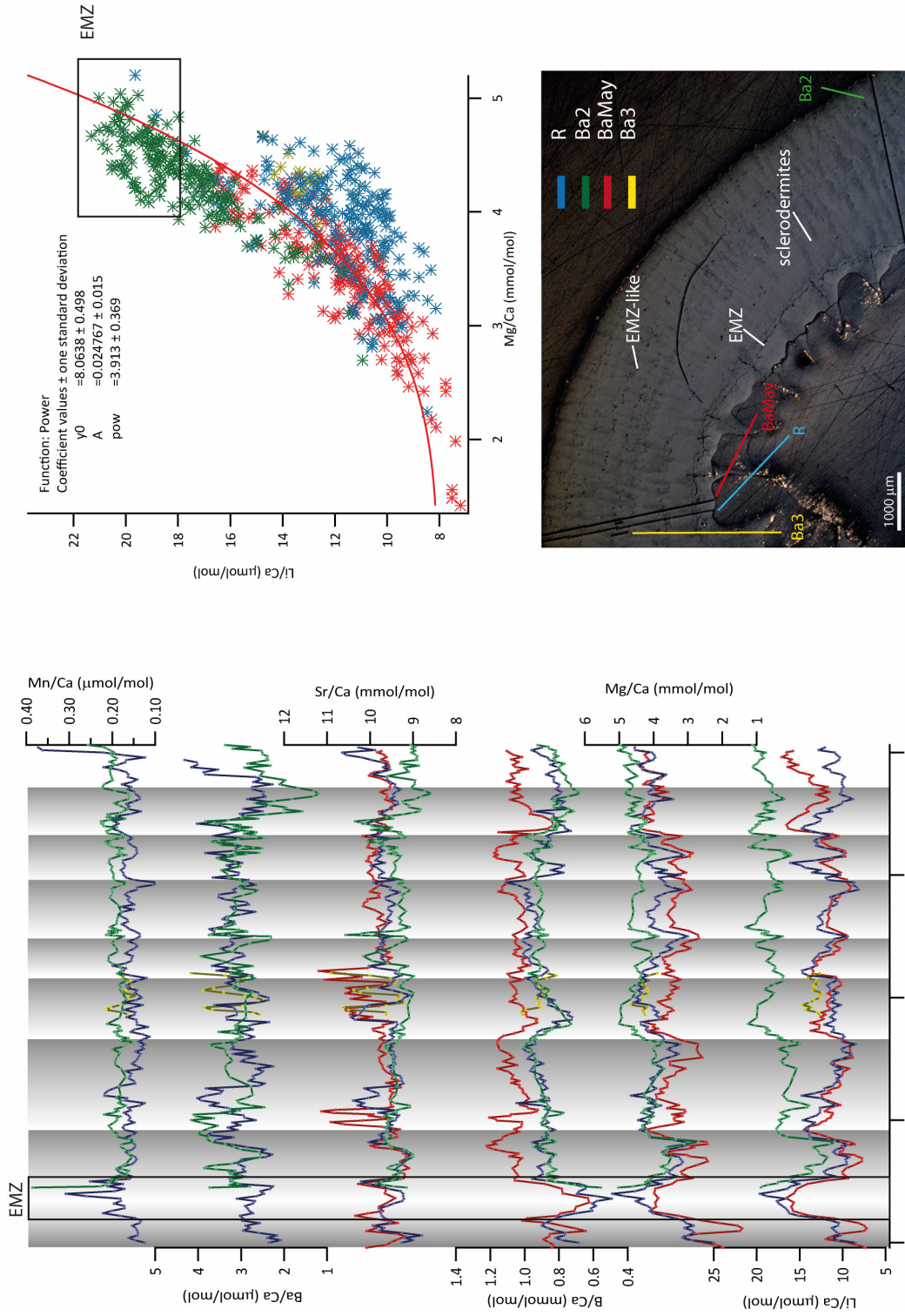
Figure: a. Cross section of a L. pertusa polyp showing the internal stuctures (1) Early Mineralisation Zone (EMZ), (2) EMZ-like, (3) sclerodermites. Are also reported the ion microprobe tracks.

b. Mn/Ca, Ba/Ca, Sr/Ca, B/Ca, Mg/Ca profiles from tracks R (blue), Ba2 (Green), BaMay (Red), Ba3 (Yellow).

c. Li/Ca vs. Mg/Ca correlation for all profiles.

Surface ocean productivity through the Eocene/Oligocene transition using the Sr/Ca composition of coccolith calcite

Tom Dunkley Jones[1], Katy Prentice[2]

[1]School of Geography, Earth and Environmental Sciences, University of Birmingham, B15 2TT, UK
[2]Department of Earth Science and Engineering, Imperial College, London, SW7 2AZ, UK

Rationale

The Eocene/Oligocene transition (E/OT; ~34 Ma) is the largest climate transition of the past 65 million years. In less than 500 kyr Antarctic ice sheets grew to continental extent for the first time in the Cenozoic. This climate transition had major impacts on the marine carbon cycle, patterns of surface ocean nutrient distribution and biological productivity, which may, in turn, have lead to a series of extinctions in the calcareous phyto- and zooplankton. Although these events are well documented at the gross scale, their relative timing and spatial distribution are still poorly defined. In particular, both the cause of extinction in the tropical microplankton and the response of low-latitude productivity zones to high-latitude cooling are largely unknown.

Here, we used a novel geochemical approach, the measurement of Sr/Ca ratios of fossil coccoliths using Secondary Ionization Mass Spectroscopy (SIMS), as a direct means of quantifying changes in surface-water nutrient availability at the time of coccolith formation. As long as there are coccoliths present in the sediment, this technique is not affected by changing rates of pre-burial carbonate dissolution. This study focused on coccolith material recovered through the E/OT from Integrated Ocean Drilling Program (IODP) Expedition 320 in the equatorial Pacific. This region has been an upwelling zone of planetary importance throughout the Cenozoic and has yielded the most detailed climate records of the E/OT available to date.

Methods

Samples were taken from IODP Expedition 320 (March-May 2009) across the E/OT from IODP Site U1334 (present location 8.0ºN 132.0ºW), across the interval ~305 to 290m CCSF-A, equivalent in time to ~34.6 to 33.4 Ma. This site is reconstructed to be at ~1ºN during the E/OT, beneath or close to the zone of peak equatorial upwelling.

Prior to SIMS analysis, samples were prepared using the microfiltration technique. Once prepared, sub-samples of the coccolith size-fractions were taken for SEM and light microscope observation to assess their taxonomic composition at the species level. Appropriate size splits were then chosen for SIMS analysis, diluted in distilled water and flooded onto indium coated ion probe stubs. Stubs were then gold coated and subjected to SEM examination to locate, identify and image individual nannofossil specimens suitable for SIMS analysis. Microprobe analyses were undertaken during November 2011 at the NERC Ion Microprobe Facility at Edinburgh University. Analyses targeted four key species (*Coccolithus pelagicus, Discoaster tanii, Reticulofenestra bisecta* and *Reticulofenestra dictyoda*) with between 5 and 15 individual coccoliths analyzed from within each sample interval. Trace element distributions, especially Mg and Al, were monitored on and around the specimen during analysis to check for clay contamination.

Results

Coccolith Sr/Ca data from IODP Exp. 320 Site U1334, the first ever coccolith Sr/Ca dataset from across the E/OT, are shown in Figure 1. The first, and most striking result, is a consistent and marked increase in Sr/Ca ratios across all four species at ~34.4 Ma. This is most apparent in the discoaster record, which increases by ~1000 ppm across a very short interval of ~20 kyr. It is remarkable that this event exactly coincides with the latest Eocene extinction of the oligotrophic, blue-water, multirayed discoaster, *D. saipanensis* at this site. Sr/Ca ratios of all taxa remain elevated from this *D. saipanensis* extinction up to the first positive step in oxygen isotopes at the start of the E/OT glaciation event. The presence of a persistent positive anomaly in coccolith Sr/Ca during this period is a completely novel result; further analyses would allow a full documentation of the magnitude, timing and duration of this anomaly.
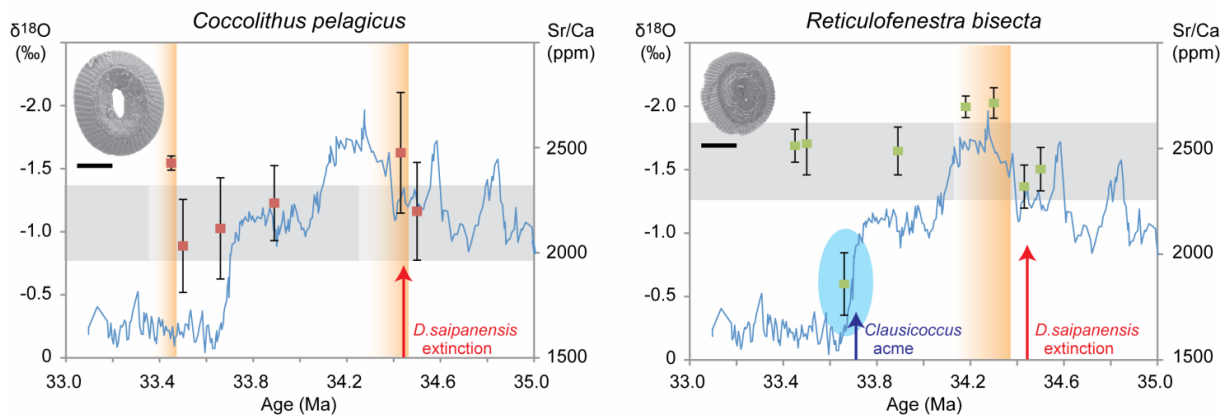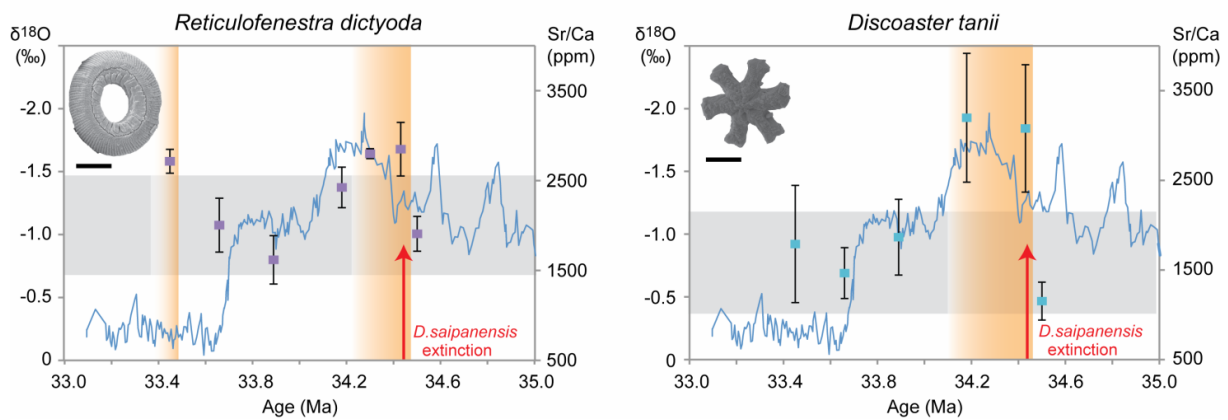
Figure 2: Pilot SIMS analyses of fossil coccolith Sr/Ca ratios across the E/OT from Site U1334, together with bulk oxygen isotope data (blue curve; Wilson et al. in prep). Sr/Ca data for each species are shown as the mean values, and standard errors, of multiple single specimen analyses at each sample level. Grey horizontal bars are an interpretation of the "normal" range of Sr/Ca recorded for each species across the whole interval; orange vertical bars indicate regions of significantly increased Sr/Ca concentrations. The anomalously low values recorded in *R. bisecta* at ~33.7 Ma are highlighted by the blue ellipse.

During the characteristic E/OT two-step increase in δ^{18}O (~34.1 to ~33.6 Ma), Sr/Ca ratios of all taxa tend to return to more 'normal' values for the entire interval analysed. The notable exception to this is a very large but transient reduction in the Sr/Ca ratio of *R. bisecta* towards the end of the second step in δ^{18}O (~33.7 Ma). Again this interval is coincident with a major coccolithophore marker event, especially in the tropical Pacific, the start of an abundance acme in the species *Clausicoccus subdistichus*. Above this event, in the earliest Oligocene, there is a hint of a further increase in Sr/Ca ratio in both *C. pelagicus* and *R. dictyoda* at around 33.4 Ma.

Further Work

Based on the promising results collected to date, further work is being undertaken to determine a higher resolution coccolith Sr/Ca record based on microfiltered size splits. It is hoped these, together with the SIMS data produced to date, will be supported by additional SIMS analyses, in order to more fully delineate the patterns of coccolith Sr/Ca variability across the E/OT. Once achieved this record will be integrated with both other palaeoproductivity proxy data and high resolution biotic records of microplankton change across the E/OT.

The onset of modern plate tectonics from the perspective of rutile

F. Enea[1], C. Storey[1] & H. Marschall[2]

[1]School of Earth and Environmental Sciences, University of Portsmouth, Portsmouth PO1 3QL, UK
[2]Woods Hole Oceanographic Institution, Department of Geology and Geophysics, Woods Hole, 02543 MA, USA

Abstract

The occurrence of rutile is concentrated in rocks involved in major plate-tectonic processes, such as subduction of oceanic and continental crust or crustal thickening in the course of continental collision. Rocks formed in modern subduction zones, i.e. blueschists and ultrahigh-pressure rocks, are notoriously difficult to preserve, as they are highly metastable. Robust minerals, such as rutile, from within these rocks, however have a much larger preservation potential where they are eroded and deposited as detritus in later sediments. Rutile also forms in eclogites and high-pressure granulites, formed at higher temperatures than blueschists, within subduction and continental collision zones. The intimate link between rutile formation and tectonic processes calls for a closer investigation of rutile geochemistry and geochronology. In this study we have focussed on analysing O isotopes coupled with U-Pb geochronology within the same analytical site from detrital rutiles. Trace element analysis by LA-ICPMS will add to these data and aid in the interpretation at a later stage.

Oxygen Isotopes and U/Pb Geochronology

The closure temperature for O diffusion in rutile is high, around 650°C for a crystal with a 100 µm radius and a cooling rate of 10°C Ma^{-1} [1]. Pb has likely around the same closure temperature [2]. It holds that any low temperature, high-pressure metamorphism (<600°C, i.e. blueschist facies) would not suffer from diffusional resetting and the signatures would remain robust, unless they have subsequently suffered high temperature metamorphism. In order to try and measure primary ages and O isotopes from old detrital rutiles (i.e. prior to the oldest known blueschists and UHP rocks on Earth, c.800 Ma), two sandstone samples have been chosen as they have not suffered excessive metamorphism.

Our first target is syn-Grenvillian (c.1100 Ma) sandstone of the Grunehogna Craton of East Antarctica. These sandstones contain detrital zircons with a major mode of igneous grains at c.1.1 Ga as well as rutile and sample a major continental arc formed prior to continental collision at c.1.05 Ga. This is ideal since the rutiles will be showing the pre-collision subduction history and it is c.300 Ma older than any known low-temperature high-pressure rocks. Our second target is the Pilbara Craton of northwest Australia, where a putative arc c.3.1 Ga old is recognised [3]. Sediments deposited between c.2.9 and 3.1 Ga were sampled, which contain both detrital rutile and zircon. Hence, this is an ideal place to look for early Archaean rutile, which may have formed within a subduction zone to collisional setting and for which no evidence of high-pressure rocks exist.

The Antarctica sample shows a limited spread in $\delta^{18}O$ with values between 4.5 and 7.7 ‰ (with an average of 6 ‰ - **Figure 1a**). This suggests little re-equilibration from a mantle-like pre-cursor for the detrital rutile grains with little or no input from sediments, suggesting a MORB-like source for the protolith.

The Pilbara samples indicate a more widespread $\delta^{18}O$ range with values between -10.7 and 11.8 ‰ (**Figure 1b**) that is probably related to a range of processes, which requires further investigation.

The oxygen isotope data coupled with Zr thermometry and trace element chemistry will help assess the tectonic environment in which the source rocks formed and any subsequent metamorphic or alteration processes that may have affected the isotopic and trace element signatures.
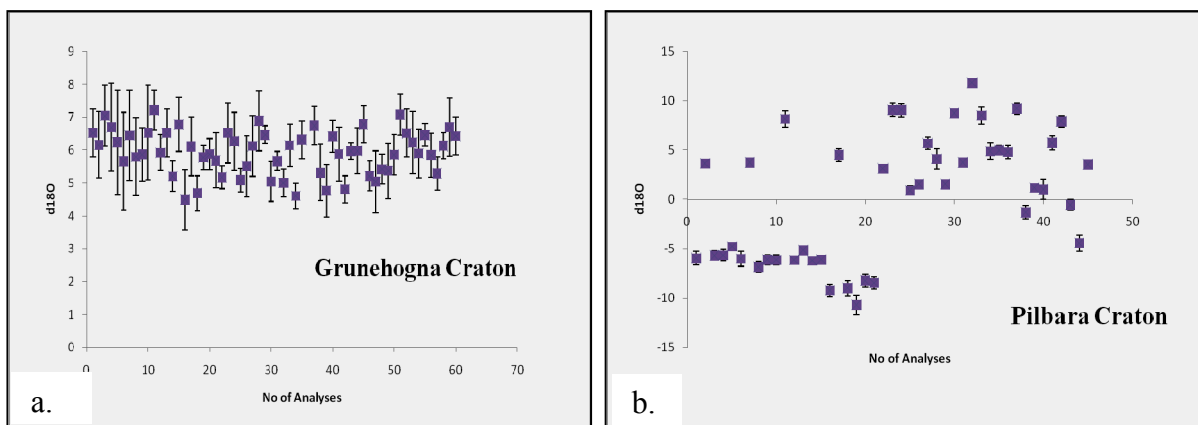
Figure 1 $\delta^{18}O$ values (including the 2σ uncertainty) for the investigated detrital rutiles: **a.** Grunehogna Craton showing mantle-like values; **b.** Pilbara Craton analyses indicating a large range of positive to negative $\delta^{18}O$ values.

The U-Pb SIMS data for the Antarctica detrital rutiles gave $^{207}Pb/^{206}Pb$ ages ranging between 1.02 and 1.16 Ga, with a U/Pb Concordia upper intercept age of 1.107 Ga (**Figure 2a**). Statistically these ages are within uncertainty and the best interpretation is that the grains come from a single source. It is therefore likely that these grains were derived from a subduction zone prior to the main collision phase of the orogeny and they can be used to infer metamorphic conditions within that subduction zone.

Detrital rutiles from Pilbara are largely concordant and between c.2.8 and 3.2 Ga (**Figure 2b**). These grains are extremely interesting and may represent material from early crustal thickening or potentially primitive subduction zones. Zr-in-rutile thermometry will further help explain the U-Pb rutile ages by assessing the temperature regimes in which these rutiles have formed. However, the oxygen isotope data will require close consideration in the case of the Pilbara samples in particular, but encouragingly many of the grains have concordant U-Pb ages.
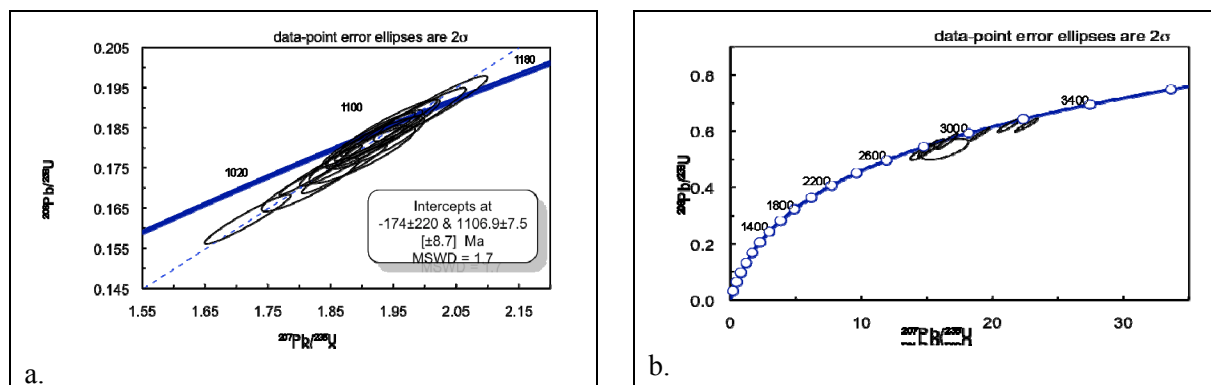
Figure 2: SIMS U/Pb ages for: **a.** Grunehogna Craton with an upper intercept age of 1107 Ma and **b.** Pilbara Craton with near concordant ages between 2.8 and 3.2 Ga.

References
[1] D. K. Moore (1998) et al. American Mineralogist **83,** 700–711
[2] D. J. Cherniak (2000) et al. Eos, Transactions, American Geophysical Union, **41**, S25
[3] R. H. Smithies (2005) et al. Earth and Planetary Science Letters, **231**, 221-237.

The 2010 eruption of Erta Ale, Afar, Ethiopia

Lorraine Field[a], Talfan Barnie[b], Jon Blundy[a], Richard A. Brooker[a], Derek Keir[c], Elias Lewi[d], Kate Saunders[a]

[a]School of Earth Sciences, University of Bristol, Queen's Road, Bristol BS8 1RJ
[b]Department of Geography, University of Cambridge, Downing Place, Cambridge CB2 3EN
[c]National Oceanography Centre Southampton, University of Southampton Waterfront Campus, European Way, Southampton SO14 3ZH
[d]Geophysical Observatory, University of Addis Ababa, Addis Ababa, Ethiopia.

Scientific Report

Erta Ale volcano, Ethiopia, erupted in November 2010, the first such eruption from the southern pit within the main crater since 1973[1], and the first eruption at this remote volcano in the modern satellite age. We were able to collect zero-age samples for analysis (fig. 1). Three samples were collected: EA01 collected from the margin of the first overflow onto the main crater floor (figs. 1 and 3a) approximately 12 hrs. after emplacement; EA02 collected from the main crater floor i.e. the flow underlying the newly erupted flows – 1973 eruption; EA03 from the last overflow observed by the field team, collected < 1 hr. after emplacement.

Figure 1. Image of the eruption in progress.

Olivine crystals within the erupted samples (EA01 and EA03) were euhedral and showed no signs of alteration. Melt inclusions were clearly visible and were rounded. Melt inclusion bearing crystals were hand-picked and petrographic observation ensured all mounted grains contained melt inclusions (fig. 2). These were examined and mapped on the SEM uncoated, under variable vacuum, to minimise carbon contamination. Any melt inclusions that showed obvious signs of post-entrapment crystallisation, fracture, or re-entrants were rejected. All melt inclusions were bubble-free. Eleven spot analyses from five separate melt inclusions were made, analysing for CO_2, H_2O and a number of trace elements by secondary ion mass spectrometry (SIMS) using a Cameca ims4f instrument at the University of Edinburgh Ion Microprobe Facility. Two analyses of matrix glass were made for CO_2 and H_2O.

The ion-probe analyses allowed us to determine that the melt inclusions were volatile-saturated, and therefore calculate depth of crystallisation – this occurred largely as a response to degassing (upper 1.5 km of the conduit). The magma was relatively dry (<0.15 wt.% H_2O) although the low volatile contents are sufficient at eruption temperature and low pressure to account for the vesicularity seen within the erupted lava. The eruption and overflow of magma from the lava lake in November 2010 facilitated almost complete magma degassing. The calculated composition of the released gas is broadly consistent with measured gas fluxes from the Erta Ale lava lake[2,3].

This work is currently in review in Bulletin of Volcanology. Field et al. (2012) Integrated field, satellite and petrological observations of the November 2010 eruption of Erta Ale.

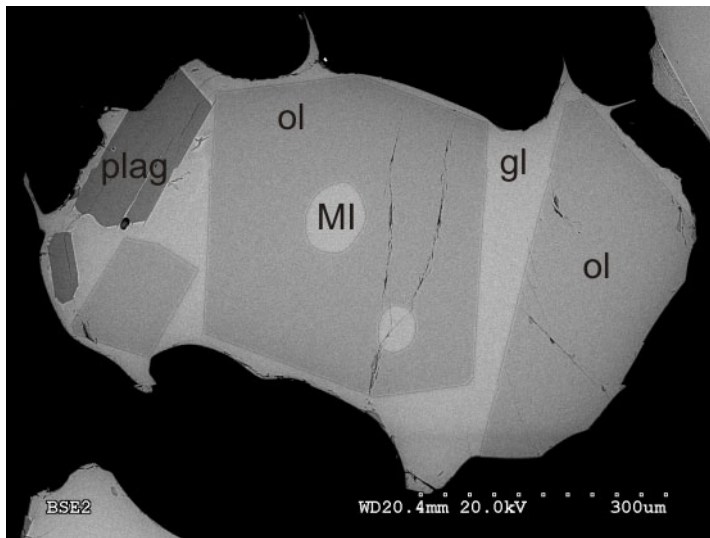

Figure 2. Typical olivine crystal from sample EA03 showing euhedral nature and rounded melt inclusions.

References
[1] Tazieff H (1973) Revue De Geographie Physique Et De Geologie Dynamique **15**(4):437-441
[2] Gerlach TM (1980) Journal of Volcanology and Geothermal Research **7**(3-4):415-441
[3] Sawyer GM, et al. (2008) Journal of Volcanology and Geothermal Research **178**(4):837-846

Past records of ocean acidification - the Palaeogene hyperthermals

L.C. Foster[1], R. W. Hinton[2], D. N. Schmidt[1], C. Coath[1], A. Ridgwell[1]

[1]Department of Earth Sciences, Will's Memorial Building, University of Bristol, Bristol, BS8 1RJ, UK
[2]School of GeoSciences, University of Edinburgh, Edinburgh, EH9 3JW, UK

Project background

The project examines four ocean acidification events during the time interval 58 and 52 Ma, namely: the Early Late Palaeocene, Paleocene-Eocene Thermal Maximum, ELMO, and 'X' events (EPLE, ETM 1,2,3). To allow palaeoenvironmental reconstructions, we are measuring boron isotopes and Mg/Ca ratios in benthic foraminifera from cores covering these time intervals obtained from a range of sites from the Atlantic, Indian and Pacific Oceans. The isotopic fractionation of B in sea water has been shown to be strongly related to pH. Mg/Ca can be used to reconstruct temperature variation.

Measurements during this year were to complete this dataset for publication. Three additional $\delta^{11}B$ measurements for Site 1135 and Site 1263 were performed to enhance the resolution of the dataset together with the associated trace element variation for those samples.

Sample Preparation

B concentrations in this species are relatively low (<10 ppm) therefore primary high beam currents (>20nA) were required to ensure sufficient B total count to achieve reasonable precision with each measurement. Unfortunately, the benthic foraminifera in these samples are very thin-walled and the beam diameters attendant on high beam currents made analysis of wall sections impractical. To ensure there was sufficient area to make multiple analyses, samples were prepared by Mike Hall at Edinburgh such that only a section through the outer wall was exposed. Samples were prepared in resin in batches of 3 individuals. Initially the individual foram's were attached to tape prior to backfilling with resin and setting under vacuum (to remove air bubbles). Latterly the samples were glued down to a Si-rubber sheet using the minimum amount of resin possible (i.e. single hair application). Samples were ground down with 1200 and 2500 grit until the first foram was exposed after which the samples were polished with 0.3μm alumina. Often on final polishing all three became exposed. After analyses were completed on exposed areas, and where deemed practical, samples were re-polished below the level of the analysis pits and re-analysed.

Measurements of $\delta^{11}B$ using 1270

The operating conditions and post processing are the same as those given in the previous year's report. O_2^- primary beam were used with a primary beam energy of 12.2 keV and secondary ion energy of 10keV, with illuminating the aperture after the primary mass filter. Surface contamination was minimised using a 30 second pre-sputter with a ~10μm² raster. The integration times for one measurement 'cycle' were optimised to 11s, 3s, 1s and 1s for ^{10}B, ^{11}B, Si^{2+} and Ca^{2+} with waiting time of 3s, 1s, and 1s respectively. Typically, a 'clean' measurement consisted of approximately 60 measurement cycles of useable data. In order to achieve at least 2‰ precision (1 σ) for a single specimen it was necessary to combine at least 20 such measurements. With standards this number of repeats was possible in a single day using the 'Chain Analysis' option and 24 hour a day operation. By measuring Ca^{2+} we were able to monitor the ionisation behaviour of the carbonate and interaction with the beam, as well as B/Ca ratio, which can used to provide information on the palaeoenvironment of the carbonate ion. Measurement of Si^{2+} allows us to determine if there is any contamination, in particular clays which potentially could have high boron content.

Post processing of data

The post-processing was the same as used in the previous datasets. Data points shown to have high Si^{2+} were removed from our analysis. A subsequent check by SEM analysis confirms the position of analysis and has shown that this method for removal is robust (i.e. any spots rejected by SEM analysis had already been rejected by using Si^{2+}). As the B secondary ion signal always decreased slowly with time, the subsequent data processing follows [1] which corrects for any systematic bias caused by the

time-varying signal intensity. In addition, this treatment, which time-interpolates then averages each isotope's intensity before taking their ratio, largely avoids the bias which occurs by averaging ratios of individual cycles which is particularly acute in cases of very low count rates.

Application of new technique- preliminary findings
We have compiled a large dataset ready for publication for submission by May 2012. In summary we have analysed foraminifers for $\delta^{11}B$ and trace elements from Walvis Ridge (1262, 1263), Shatsky Rise (1210), Central Exmouth Plateau (762), central Pacific (1221) and Kerguelen Plateau (1135). We have analysed samples from PETM, ELMO and EPLE events to quantify the changes during each of these hyperthermals and have built up a dataset of potential differences in $\delta^{11}B$ within different oceans during the PETM. Variation in $\delta^{11}B$ in the foraminifera is larger than expected and has required us to revisit some of the assumptions $\delta^{11}B$, specifically the $\delta^{11}B$ of the seawater during the Paleogene and do additional studies into preservation of foraminifera during ocean acidification events in the Paleogene.

We have done a number of additional analyses using Electron BackScatter Diffraction (EBSD), as well as Synchrotron Radiation X-ray tomographic microscopy (SRXTM) at the TOMCAT beamline at the Swiss Light source, to improve our understanding of the preservation and diagenetic alteration within these samples. This was imperative so we can build up a robust interpretation of the dataset. Some of the preservation data has just been submitted to Science (February 2012), and thus we expect to submit the manuscript containing the SIMS dataset within the next few months. We have presented this data at a number of conferences including at Goldschmidt in Prague in August 2011.

References
[1] K.J. Coakley, D.S. Simons, A.M. Leifer (2005) *Int. J. Mass Spectrom.* **240**, 107-120.

Volatile and light lithophile trace element geochemistry of the 2010 and other recent eruptions of Merapi volcano, Java, Indonesia

R. Gertisser[1], K. Preece[2], K. Berlo[3], J. Barclay[2], R. Herd[2], H. Handley[4] & M. Reagan[5]

[1]School of Physical and Geographical Sciences, Keele University, Keele, ST5 5BG, UK
[2]School School of Environmental Sciences, University of East Anglia, Norwich, NR4 7TJ, UK
[3]Department of Earth Sciences, University of Oxford, Oxford, OX1 3AN, UK
[4]GEMOC, Department of Earth and Planetary Sciences, Macquarie University, Sydney, NSW 2109, Australia
[5]Department of Geoscience, The University of Iowa, Iowa City, IA 52242, USA
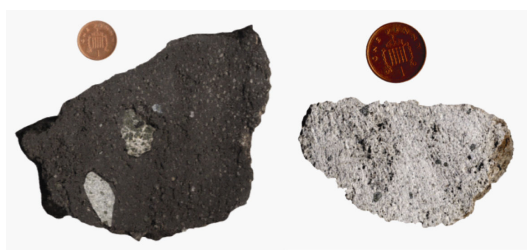
Background and rationale

The unusual, large-magnitude eruption of Merapi that started on 26 October 2010 (Fig. 1) was the volcano's biggest since 1872 and the deadliest event since 1930 [1]. Before 2010, Merapi's recent
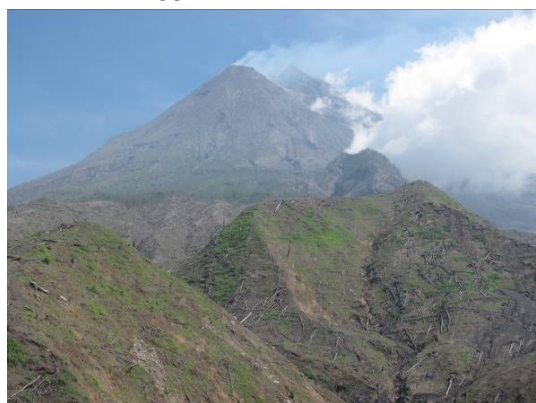
Fig. 1. View of Merapi from the south showing the destruction by surges and the deep summit scar formed during the 2010 events. Photograph taken on 3 February 2011.

eruptive activity was characterised by periods of slow basaltic andesite lava dome extrusion punctuated by gravitational dome failures, generating small-volume pyroclastic density currents (PDCs) with runout distances of typically < 10 km. By contrast, the 2010 eruption began with an explosive phase that was not preceded by a lava dome at the surface. Between 31 October and 4 November, a dark lava dome (*cf.* Fig. 2) extruded rapidly, exceeding growth rates observed at the peak of the preceding eruption in 2006 by a factor of ~ 22. During the most vigorous eruptive phase on 5 November, at least one PDC travelled more than 15 km (more than twice the distance of the largest flows in 2006) beyond the summit along the Gendol river valley on Merapi's south flank. In a late phase of the eruption, scoria- and pumice-rich PDCs were produced (*cf.* Fig. 2), forming a thin veneer on top of the deposits of the largest PDC(s) from 5 November. Provisional estimates suggest that the tephra volume deposited in 2010 was ~ 10 times higher than that of other recent eruptions and that the CO_2 output associated with the 2010 events has been the highest at Merapi since records began [2].

A NERC Urgency grant (NE/I029927/1) has been awarded to the project team to unravel the driving forces behind the unusual explosive behaviour of Merapi in 2010 through a multifaceted petrological study. The ion probe analyses contribute to several of the key objectives of the Urgency grant by determining volatile and light trace element concentrations in the 2010 and other recent eruptive products, including those of the dome-forming episode in 2006. The data obtained allow us to constrain magma storage depth(s), pre-eruptive melt compositions, magma ascent dynamics and accompanying crystallisation and

Fig. 2. Selected samples from the 2010 Merapi eruption analysed in this study: lava dome fragment with plutonic xenolith and light-coloured inclusion (left); pumice clast (right).

degassing processes, and the impact of these processes on eruption style.

Samples and analytical work programme

About 60 dacitic to rhyolitic, primarily clinopyroxene-hosted melt inclusions (MIs) and groundmass glass in basaltic andesite samples from various phases of the 2010 eruption (see above; Fig. 2) and other recent eruptions were analysed for light trace (^{7}Li, ^{9}Be, ^{11}B) and volatile (^{1}H, ^{12}C) elements by SIMS on the Cameca 4f ion microprobe at the University of Edinburgh between 28 November and 2 December 2011. The data presented here are preliminary as the ion microprobe analysis have yet to be combined and calibrated more vigorously with major element and volatile concentrations obtained on the same inclusions and groundmass glass by electron microprobe and, possibly, FTIR.

Please ensure that your Annual Report fits into the two pages and complies with the *Instructions to Authors* given below. Please remember that the Annual Reports are a requirement of NERC and are reviewed by the Steering Committee

Results and preliminary interpretation

Li, Be and B concentrations – This first compilation of light lithophile trace element analyses for Merapi suggests a moderate range in the concentration of Li (13-67 ppm) and B (34-90 ppm), and uniform Be concentrations (1-2 ppm) in MIs across all studied samples. Concentrations of these elements in groundmass glasses lie within the range observed in the inclusions. The lack of major element compositional data precludes a rigorous interpretation at this stage, although the data suggest enrichment of Li at low H_2O contents (< 1.5 wt%), possibly reflecting influx of Li-rich vapours at relatively low pH_2O.

H_2O and CO_2 concentrations – To the best of our knowledge, the data presented here are the first direct measurements of H_2O and CO_2 contents in MIs at Merapi using SIMS. H_2O concentrations in MIs in the 2010 products are variable, ranging from 0.1 to 3.9 wt% (Fig. 3a). MIs from the 2010 lava dome contain varied H_2O contents, many being relatively H_2O-poor, which may suggest some leakage from the inclusions. The highest H_2O contents are preserved in the 2010 scoria and pumice clasts. Groundmass glass in the 2010 lava dome is strongly degassed, containing 0.1 wt% H_2O. H_2O concentrations in MIs in the 2010 products are comparable to those of the preceding eruption in 2006, but lower than those of the sub-Plinian Trayem tephra [3], for which H_2O contents up to 4.8 wt% were determined (Fig. 3b). The highest CO_2 contents of ~ 1100 ppm in the 2010 eruptive products are recorded in the aforementioned pumice clasts. Again, similar CO_2 contents (up to ~ 1200 ppm) are found in the 2006 eruptive products, whilst a single MI from the (presumably) 1872 products, the only VEI-4 eruption in recorded history at Merapi [1, 2], preserves ~ 1600 ppm CO_2. Groundmass glasses are outgassed and contain low CO_2 contents of generally less than ~ 150 ppm (Fig. 3). From Fig. 3, it is apparent that a simple, single decompression-driven degassing path cannot

Fig. 3. H_2O and CO_2 contents of MIs (filled symbols) and groundmass glass (open symbols) of (a) different lithologies (and phases) of the 2010 eruption and (b) samples from the 2010 eruption compared with other Merapi eruptions. Isobars (dashed lines) and vapour isopleths (solid lines) are calculated using VolatileCalc [4].

explain the H_2O and CO_2 data. Variable H_2O contents at comparatively low CO_2 concentrations in MIs in the 2010 and other eruption products may indicate trapping at a range of pressures, consistent with shallow decompression-induced crystallisation. In such a scenario, the shift to higher dissolved CO_2 contents at intermediate H_2O contents, recorded primarily by MIs within the pumice-rich PDCs from the final eruptive stages in 2010, could reflect enrichment through CO_2 fluxing from a deeper magma reservoir or CO_2 addition from the sub-volcanic carbonate basement, as proposed previously [e.g., 5].

Outlook and future work

This project is part of a NERC-funded research initiative to understand the recent eruptive behaviour of Merapi. Ion probe data will be complemented by [210]Po-[210]Pb-[226]Ra isotopic analyses currently carried out to constrain the timescales of crystal growth and gas transfer in the weeks to decades before the 2010 (and 2006) eruption. This project also served as a probing study for in-situ measurements of $\delta^{13}C$ and $\delta^{18}O$ to better constrain magma and volatile sources as well as crustal contamination processes that may exert notable control on the volcano's erratic eruptive behaviour.

References

[1] R. Gertisser et al. (2011) Geology Today **27**, 57-62; [2] Smithsonian Institution (2011) Bulletin of the Global Volcanism Network, **36 (1)**; [3] R. Gertisser et al. (in press) Bulletin of Volcanology; [4] S. Newman and J.B. Lowenstern (2002) Computers and Geosciences **28**, 597-604; [5] F.M. Deegan et al. (2010) Journal of Petrology **51**, 1027-1051

Boron isotopes in tourmaline, prismatine and grandidierite in granulite-facies paragneisses from the Larsemann Hills, East Antarctica

JohnRyan MacGregor & Edward S. Grew

Department of Earth Sciences, University of Maine, Orono, Maine 04469 USA

Rationale for the study

Because of its relative affinity for aqueous fluids and granitic melts, boron is an excellent tracer of metamorphic and anatectic processes, and thus provides information that supplements the data obtained on other trace elements in unravelling the origin and evolution of the unique boron-rich paragneisses exposed the Larsemann Hills. Boron isotopes offer potential evidence that can help us deduce the tectonic environment of deposition of the precursors of these rocks. Inferring the isotopic signature of the precursors to the boron-enriched paragneisses must take into account the effects of metamorphism, anatexis, devolatilization and fractionation among borosilicate minerals, and consequently, we selected samples with the greatest diversity of mineral assemblages for analysis.

Scope and methodology

Twenty one samples of tourmaline quartzite, prismatine bearing leucogneiss, grandidierite-bearing borosilicate gneiss and other boron-rich rocks from the Larsemann Hills, together with 6 samples of anatectic pegmatites from this area, were selected for in situ analysis of the three borosilicate minerals with the a Cameca ims 4f ion microprobe. Generally 4-7 grains of each mineral per sample were analysed. The data were calibrated using 3 tourmaline standards, 3 prismatine standards and one grandidierite standard, three of which were from the Larsemann Hills. The full suite of standards was run at the start of the day, and a subset was run several times during the day and at its close.

Results

$\delta^{11}B$ (= {[sample$^{11}B/^{10}B$ / SRM 951$^{11}B/^{10}B$] – 1} × 1000) averaged over several grains per sample ranges from –3.0 to –14.3‰ in tourmaline (Tur), from –9.6 to –18.1 ‰ in prismatine (Prs) and from –1.9 to –8.7 ‰ in grandidierite (Gdd) (1s mostly 1-2‰ per sample). Tur in Tur quartzite is isotopically homogeneous from grain to grain in each sample and average Tur $\delta^{11}B$ varies little from sample to sample (7 samples: –5.7 to –8.7‰, Figure 1). Average leucogneiss Tur composition is lighter (3 samples, $\delta^{11}B$ = –9.6 to –14.3‰), whereas average borosilicate-gneiss Tur varies more (6 samples, $\delta^{11}B$ = –3.0 to –11.8‰). In the anatectic pegmatites, $\delta^{11}B$ ranges from –4.8 to –12.1 ‰ in Tur (4 samples), –12.5 to –14.0‰ in Prs (2 samples) and –6.6 to –6.8‰ in Gdd (2 samples). These ranges lie within the corresponding ranges in the metamorphic rocks, which suggest that melting and crystallization from melt collectively did not fractionate B isotopes when compared to host rock Tur (Fig. 1), Prs and Gdd $\delta^{11}B$.

With two exceptions, average $\delta^{11}B$ increases in a given sample Prs < Tur < Gdd with Prs B 4.8±1.6‰ (9 pairs) lighter and Gdd B 2.8±1.9‰ (6 pairs) heavier than Tur B. This regularity is consistent with the preference of ^{10}B for tetrahedral sites (Prs) and ^{11}B for trigonal sites (Tur, Gdd) and crystallization in near isotopic equilibrium. Crossed tie lines do not bear a simple relationship to microstructures (Figure 2).
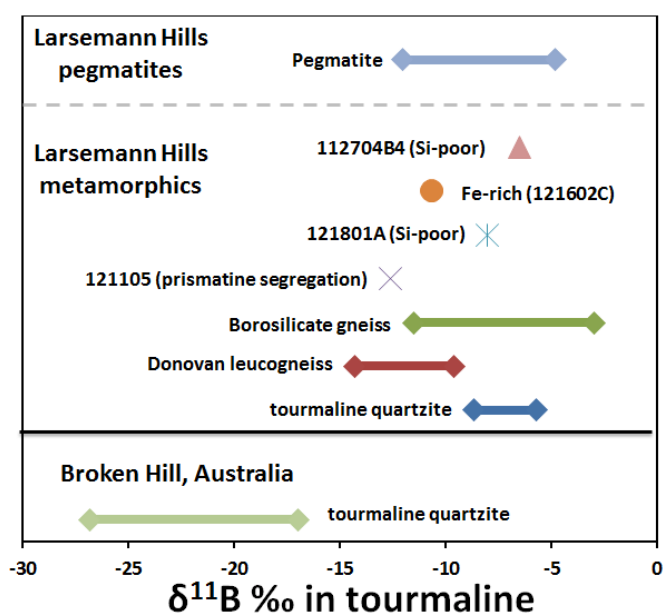
Figure 1. Isotopic compositions. Broken Hill from [1]
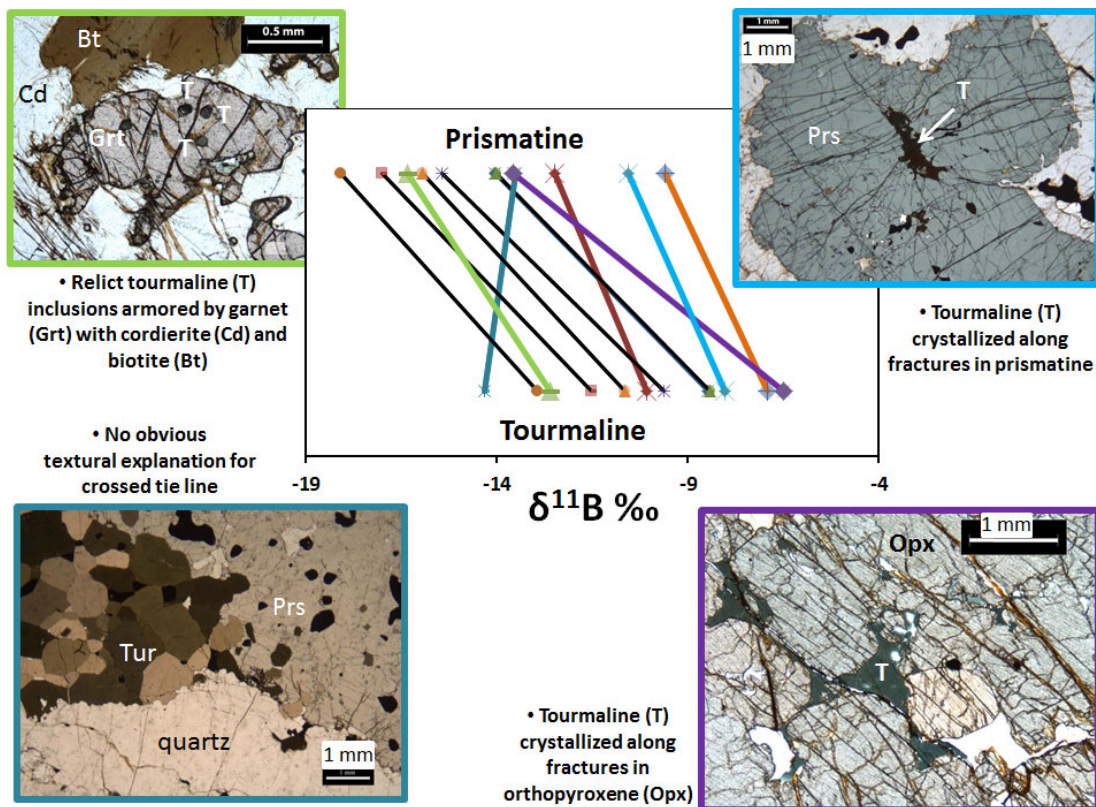
Figure 2. Boron isotope fractionation between tourmaline and prismatine. The frames of the photomicrographs have the same colours as the corresponding tie lines.

Implications

The precursor of the boron-rich rock least changed by metamorphism, Tur quartzite, is interpreted to be a product of pre-metamorphic, hydrothermal boron-metasomatism of clastic sediments. If there had been no $\delta^{11}B$ decrease from devolatization during metamorphism, quartzite Tur $\delta^{11}B$ (–8.7 to –5.7‰) constrains $\delta^{11}B$ of pre-metamorphic fluid to be –3 to 0‰ (Tur-fluid $\Delta^{11}B$ for 200 °C from [2]), consistent with a scenario whereby the hydrothermal fluids had mobilized boron from non-marine evaporitic borate, as was proposed for the very light boron in tourmaline from Broken Hill, Australia [1]. However, more likely devolatization decreased Tur $\delta^{11}B$, and $\delta^{11}B > 0‰$ in the pre-metamorphic fluid, so an alternative precursor, such as marine evaporite, or even mud volcanoes, should be considered.

Presentations

Our abstract [3] has been accepted for oral presentation by JohnRyan MacGregor at the Northeastern Section of the Geological Society of America on March 20, and a second abstract has been submitted for presentation at the 34th International Geological Congress in August, 2012.

References
[1] J. Slack et al. (1993) Economic Geology **88**, 505-541
[2] C. Meyer et al. (2008) Contributions to Mineralogy and Petrology **156**, 259-267
[3] J. MacGregor et al. (2012) Geological Society of America Abstracts with Programs **44**, No. 2, p. 102.

Using δ^{18}O to assess the migratory route of Scottish two sea-winter wild Atlantic salmon

N.N. Hanson[1] & C.D. Todd[1]

[1]Scottish Oceans Institute, University of St. Andrews, St. Andrews KY16 8LB, UK

Background

Despite increased marine mortality and declines in growth condition of wild Atlantic salmon [1-3], the details of their marine migration remain largely unknown. Strong concordance between time series of growth condition for one sea-winter (1SW) and two sea-winter (2SW) Scottish salmon suggest that both groups occupy the same ocean area during their final months at sea. However, present migratory models place 2SW fish in the warm North Atlantic Current during return migration [4]. Electronic tagging of salmon to monitor details of their entire marine migration i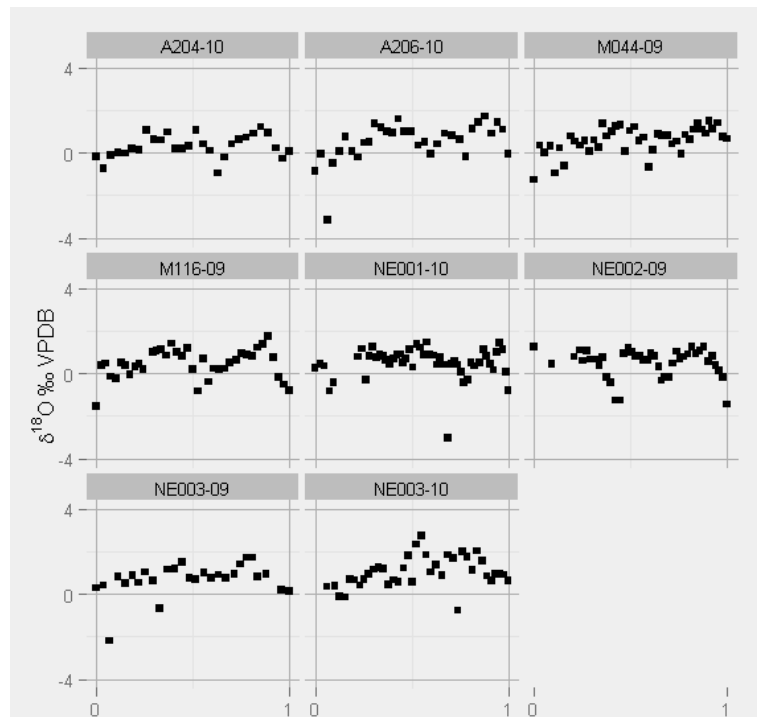s currently unfeasible but otoliths, the tiny calcium carbonate 'bones' in the fish ear, can be used as retrospective 'natural tags'. δ^{18}O values of otolith aragonite are deposited at or near equilibrium with the ambient water and the temperature during otolith deposition can be estimated provided that δ^{18}O values of ambient water are known. We sought to use high resolution SIMS profiles of otolith δ^{18}O values from 2SW salmon to infer latitudinal migration paths and test our hypothesis of shared residency in the Norwegian Sea with 1SW fish.

Results & Discussion

Between 27 and 50 δ^{18}O analyses per otolith were obtained (n = 8 individuals, 148 separate analyses). All profiles (Fig. 1) were scaled such that x=0 refers to the freshwater/marine emigration transition and 1 refers to the otolith edge (i.e. time nearest to capture). For all salmon, δ^{18}O profiles were characterised by two periods of increased values at δ^{18}O ~0.7 – 0.9‰ in the first instance and ~1-1.1‰ in the second. These rises correspond to the two winters (at lower temperatures) spent at sea, as described below. The overall mean δ^{18}O was 0.57(±0.18) ‰ and there were significant differences in mean δ^{18}O values between fish – most notably, NE003-10 had a mean value of 0.72‰. However, the majority of the variation in δ^{18}O values occurred within individual profiles (~94% variance; linear mixed effects model).

Figure 1: Intra-otolith δ^{18}O values from eight individual wild Atlantic salmon. Standard error on measurements determined by repeat analyses of a known standard (see Appendix) was 0.19‰. The x-axis is scaled such that 0 = smolt emigration to saltwater and 1 = capture (~2 years after emigration).

δ^{18}O values of otolith aragonite are inversely related to water temperature. Several 'otolith thermometry' equations have been developed empirically; here, we use an equation derived from previous SIMS work described in [5]. Four of the eight individuals were captured off the north coast of Scotland in summer 2009 and four were caught in the same location during the summer 2010 netting season. These represent two separate cohorts of 2SW salmon, but for simplicity their results are grouped in Figure 2.

[4] suggest that from December to May of the second winter, 2SW salmon of southern European origin (incl. Scotland) follow the currents

of the Labrador Sea eastward to the North Atlantic Current and onwards to the North Atlantic sub-polar gyre. If this were true, salmon migrating in these waters would have encountered markedly higher sea surface temperatures (SST) corresponding to $\delta^{18}O$ values approximately 1-2‰ (or 4-8°C) higher than in the previous winter. However, the thermal conditions experienced by salmon during each winter period were similar and varied by only ~1°C, suggesting that these fish did not migrate within the North Atlantic Current on their return migration.

When compared with thermal profiles estimated from eight 1SW salmon, the present profiles show that salmon returning after two winters at sea consistently occupied significantly lower water temperatures than those returning after only one year. This suggests that while any shared residency between age cohorts is accompanied by active thermal selection and occupation of rather different waters within the broader Norwegian Sea area known to be exploited by salmon.
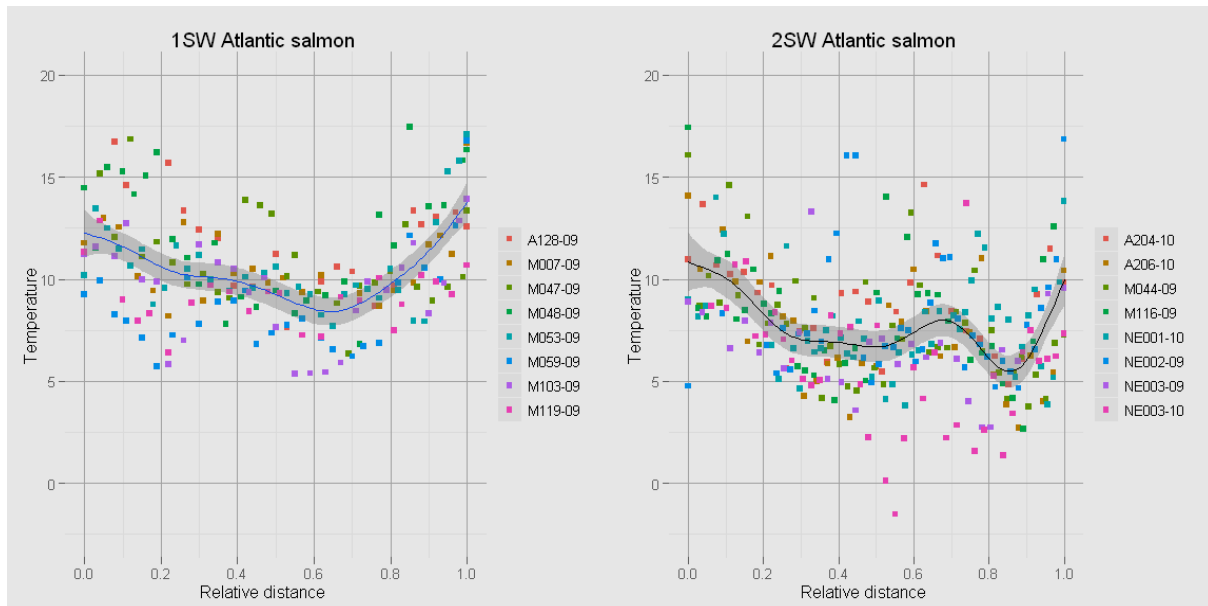
Figure 2: Estimated temperatures and GAM smooths of 1SW and 2SW wild Atlantic salmon caught in north Scotland. Temperatures were estimated using an equation derived for 1SW fish from [5], although it is the relative, rather than absolute, temperatures which are of interest here.

References

1. ICES, "Report of the Working Group on North Atlantic Salmon (WGNAS)" (2010).
2. C. D. Todd *et al.*, *Global Change Biol.* **14**, 958 (2008).
3. P. J. Bacon *et al.*, *ICES J. Mar. Sci.* **66**, 844 (2009).
4. M. J. Dadswell, A. D. Spares, J. M. Reader, M. J. W. Stokesbury, *J. Fish Biol.* **77**, 435 (2010).
5. N. Hanson, PhD, University of St Andrews (2012).

Diffusion of Volatiles in Earth's Mantle – Is it all about Grain Boundaries?

M. Hiscock & G. Bromiley

School of GeoSciences, University of Edinburgh, Edinburgh EH9 3JW, UK

Abstract
Earth's mantle contains a considerable volume of 'water' stored as interstitial H defects in mantle minerals. To constrain the important influence that H has on mantle properties and processes we need to assess the mobility of H within the mantle and between different mantle reservoirs. To date, experiments have been designed to measure lattice diffusion (H mobility through mineral structures). However, under certain conditions grain boundary diffusion of H may be the dominant mechanism as it potentially offers a low energy, quick pathway for diffusing species. Here, SIMS analysis of H abundance in olivine grains as part of a novel experimental design was used to provide the first data on grain boundary diffusion of H under mantle conditions. Initial findings indicate that grain boundary diffusion of H operates at a broadly similar rate to lattice diffusion of H in single crystals of olivine but is perhaps slightly more important at lower temperatures.

Grain boundary Diffusion of H under Mantle Conditions

Diffusion of atomic species in Earth's mantle can occur via one of two mechanisms: (1) Through mineral grains; *lattice diffusion* or (2) Along the boundaries between grains; *grain boundary diffusion*. Research in materials science and solid-state chemistry has demonstrated that grain boundary diffusion may be the dominant process under certain conditions. However, to date the relative importance of grain boundary diffusion under high-PT conditions of Earth's deep interior remains poorly constrained. Grain boundary diffusion has been suggested to play an important role in mobilising highly incompatible elements in the mantle, for example in providing an efficient mechanism for mixing highly siderophile elements from the core into the lower mantle [1]. It has previously been assumed (without any real justification!) that lattice diffusion of H is dominant, although the relative efficiency of grain boundary diffusion of H under high PT conditions of the mantle remains unknown. Here we used a novel experimental design and SIMS analysis to provide the first assessment of the grain boundary diffusion of hydrogen under mantle conditions.

Grain boundary diffusion coefficients for H under mantle conditions were determined from experiments conducted at high temperature (800-1600°C) and pressure (3GPa) using a novel capsule de sign (Figure 1). The experimental design ensured only grain boundary diffusion would be measured by utilising stoichiometric Mg-spinel as a matrix mineral. Mg-spinel is unable to accept any water into its structure [2]; thus, water (or more specifically H) released from the pyrophyllite (our source) as it decomposed during heating would be forced to move along grain boundaries until it reached an olivine sink grain. By measuring H contents of the olivine grains and determining their distance from the interface of the spinel and pyrophyllite (by subsequent SEM analysis) a grain boundary diffusion coefficient could be determined.

Figure 1.
Capsule design.

A grain size of approx. 100μm was used to ensure that the sectioned capsule presented grains of a suitably large area for analysis with a beam size of approx. 20 x 25μm (the actual section and so individual grains which are exposed when the capsule is cut in half is essentially random) (Figure 2). A 5nA beam current was used and H, Li, Si & Al contents were measured. The measurement of Li was a useful indicator of any potential irregularities within a grain.

Compiled results (see Figure 3 for example data) indicate that grain boundary diffusion coefficients of H under mantle conditions are of a similar magnitude to those obtained from single crystal diffusion of H in olivine [3] but grain boundary diffusion may be slightly more important at lower temperatures (Figure 4).
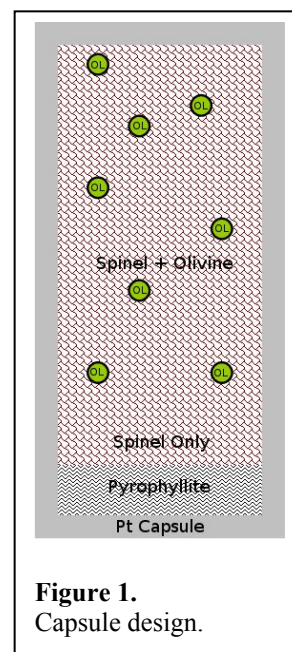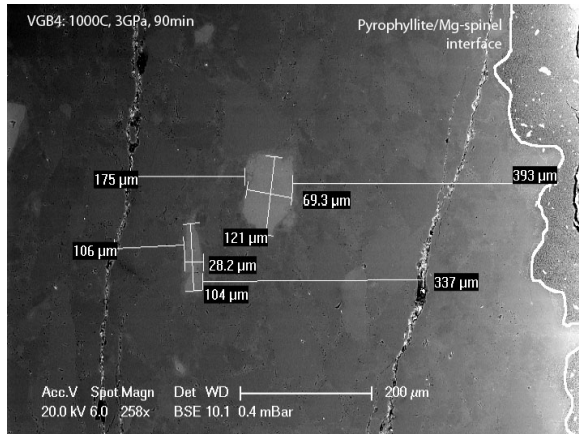
Figure 2.
SEM image of sectioned capsule. Large grain sizes allow for the easy positioning of an ion probe beam on the sample. Distances for the calculation of diffusion coefficients are subsequently measured using an SEM.
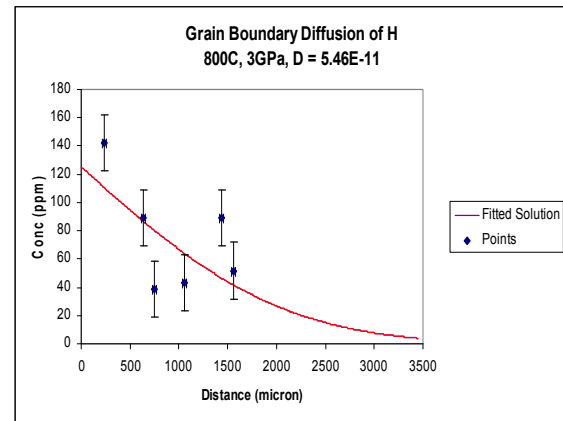
Figure 3.
Example diffusion law fit from experiment analysed by SIMS this year.
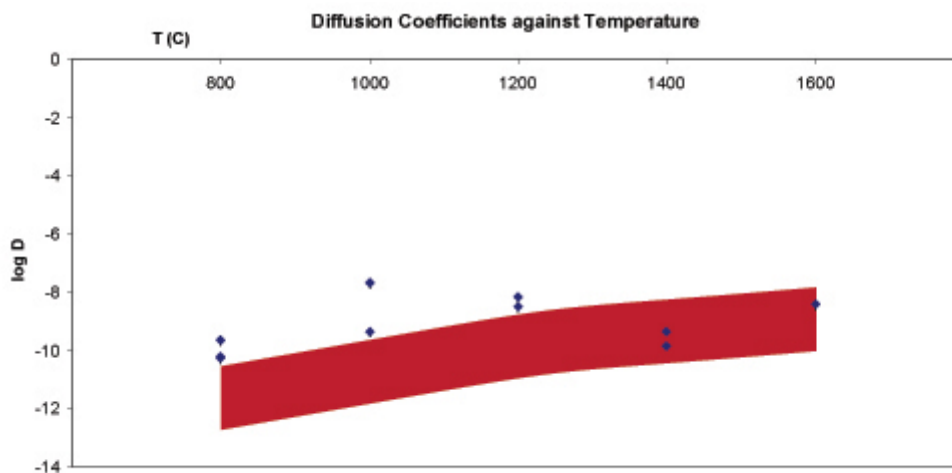
Figure 4.
Graph of logarithms of measured diffusion coefficients (points) against temperature for the experiments conducted and analysed by SIMS to date (multiple points per temperature are repeat experiments). Error in measurements is approximately the same size as datapoints. Coloured block shows variation in diffusion coefficients for H diffusion in single crystal olivine in orthogonal crystallographic directions.

References

[1]   L. A. Hayden and E. B. Watson, "A diffusion mechanism for core-mantle interaction," *Nature*, vol. 450, no. 7170, pp. 709–711, Nov. 2007.
[2]   G. D. Bromiley, F. Nestola, S. A. T. Redfern, and M. Zhang, "Water incorporation in synthetic and natural MgAl2O4 spinel," *Geochimica et Cosmochimica Acta*, vol. 74, no. 2, pp. 705–718, Jan. 2010.
[3]   S. J. Mackwell and D. L. Kohlstedt, "Diffusion of Hydrogen in Olivine: Implications for Water in the Mantle," *J. Geophys. Res.*, vol. 95, no. B4, pp. PP. 5079–5088, 1990.

Understanding basaltic crystal mush differentiation

M.C.S. Humphreys[1], O. Namur[2] & M. Holness[2]

[1]Department of Earth Sciences, University of Oxford, South Parks Road, Oxford, OX1 3AN, UK
[2]Department of Earth Sciences, University of Cambridge, Downing Street, Cambridge, CB2 3EQ, UK

1. Introduction

As a magma body cools, a layer of crystal mush (crystals + liquid) develops on its margins and solidifies, forming cumulate rocks and resulting in fractional crystallisation of the magma body. During solidification, the interstitial liquid between the crystals may be expelled from the mush by processes including physical compaction or compositional convection. The extent to which this occurs ultimately controls the efficiency of crystal-liquid fractionation and hence the geochemical evolution of liquids in the main magma chamber. If the interstitial liquid is not fully expelled from the mush, progressive *in situ* crystallisation results in localised nucleation of new mineral phases and zoned overgrowth of existing grains. This chemical zonation can be used to track the changes in interstitial liquid composition that occur during solidification [1,2]. We analysed zoned overgrowths of clinopyroxene and plagioclase in cumulate rocks from the Skaergaard intrusion, east Greenland, which preserves a record of silicate liquid immiscibility [2,3]. Our aim was to increase understanding of the porosity and permeability of a crystal mush during solidification, and give clues on the mechanisms of intercumulus liquid migration within the crystal mush [4,5], specifically:

(1) To track the evolving porosity by determining the relative timing of saturation of accessory mineral phases in the interstitial liquid;
(2) To estimate 2D porosity by determining plagioclase and pyroxene compositional profiles;
(3) To quantify the spatial distribution of immiscible pockets in the solid cumulates.
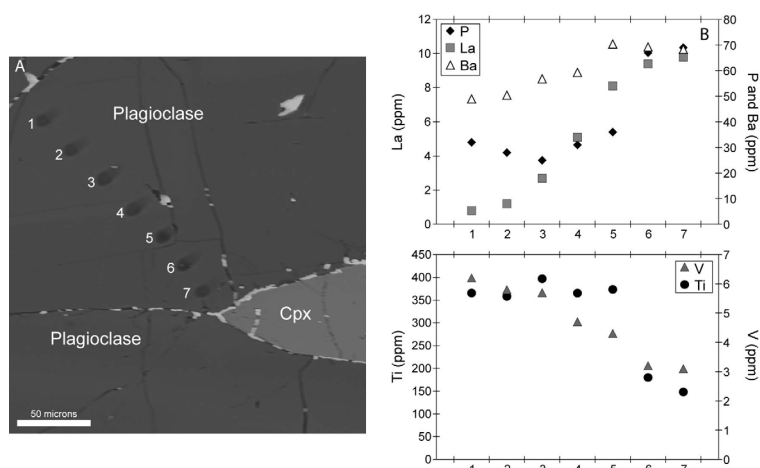
Fig. 1A – plagioclase compositions in LZa
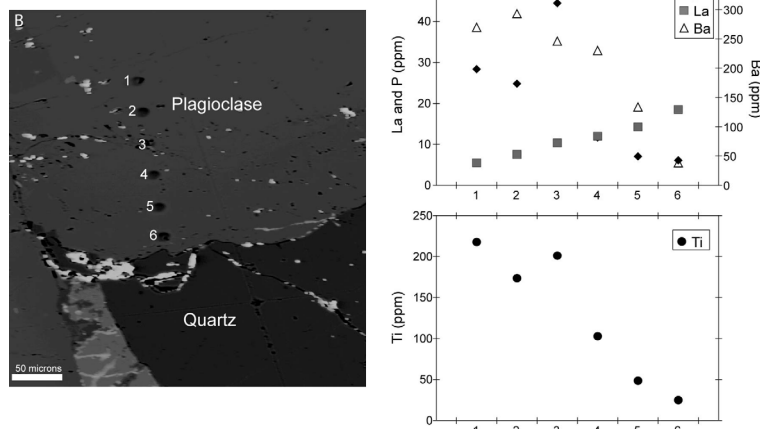
Fig. 1B – plagioclase compositions in UZb

2. Preliminary results and data interpretation

Ion probe analyses were performed using the Cameca ims-4f facility during November 2011. Six samples were selected from the lowest to the highest stratigraphic levels of the Skaergaard Marginal Border Series (crystallization against the walls of the magma chamber) and similarly for the Skaergaard Layered Series (crystallization at the floor).

Core-rim variations

As anticipated, core-rim compositional variations were observed in all samples (Figs. 1, 2). For example, near the base of the stratigraphy P, La and Ba increase adjacent to an evolved pocket of crystallised residual liquid, while Ti and V decrease (Fig. 1a). This indicates saturation of Fe-Ti oxide minerals in the interstitial liquid, but the plagioclase rim has not recorded apatite or zircon saturation in the interstitial melt.

This could result from expulsion of interstitial liquid before saturation of these phases, or simply the absence of compositional data for the last few μm on the plagioclase rim. In comparison, near the top of the stratigraphy, only La continued to increase adjacent to the margin of an evolved pocket (Fig. 1b); Ba, P and Ti decreased. This indicates that the residual liquid had already become saturated with Fe-Ti oxides and apatite by the time the plagioclase rims crystallised. The continued increase in La may indicate that the *bulk* partition coefficient for La was still <1 even when there was localised apatite crystallisation within the mush. The compositional profiles observed in plagioclase and pyroxene offer the potential to quantify the amount of interstitial liquid in the cumulate rocks, its distribution within the rock, and its chemical and physical evolution.

Efficiency of crystal-liquid separation at Skaergaard

Our data show a wide range of trace element contents in the most primitive cumulate rocks (HZ, LZa), confirming that these rocks contain abundant crystallized interstitial liquid (Fig. 2). In contrast, compositional variation is very low in rocks containing cumulus Fe-Ti oxides (MZ, UZa), indicating that crystal-liquid separation became more efficient after saturation of oxides in the main magma body. Unexpectedly, our data also reveal very wide compositional variation in the most evolved cumulate rocks of the Layered Series (UZb; Fig. 2). This is in direct contrast to studies of whole-rock concentrations of highly incompatible elements (e.g. P, Rb [6]), which suggest that the final 'trapped liquid' porosity of these rocks was very low – about 10% of that in LZa. However, our data are in agreement with the presence of large granophyre pockets in these rocks. Detailed petrography together with our new SIMS data thus indicate the presence of a significant amount of trapped liquid at the top of the Layered Series, and hence that the efficiency of crystal-liquid separation became very low during the later stages of solidification. One preliminary explanation for this observation is a significant change of the thermal regime of the magma chamber [7] or the crystal mush becoming too thin to allow compaction or compositional convection to operate [8].

Fig. 2. *Compositional variation of plagioclase and clinopyroxene in the Skaergaard layered Series. A. Range of plagioclase X_{An} as a function of stratigraphic position (data from [2, 7, 8 and unpublished data]). B and C. Compositional ranges of La in plagioclase and clinopyroxene as a function of stratigraphic position.*

3. Next steps

(1) Additional geochemical analyses. We plan to follow up the unexpected recognition of wide trace element variability in UZb with analyses in additional samples (LZc, UZa, UZb), to bring a more accurate view on the evolution of trapped liquid content in cumulate rocks.

(2) Combine the SIMS zoning profiles with SEM mapping to quantify the distribution of interstitial liquid in the network of cumulus crystals. We will compare the compositions of plagioclase and pyroxene rims adjacent to Si-rich and Fe-rich liquid pockets to determine the effect of silicate liquid immiscibility, and hence estimate the liquid lines of descent of the two immiscible liquids.

(3) Produce models of interstitial liquid evolution for Skaergaard, to understand how crystallization influences the chemical and physical evolution of the liquid. Understand how intercumulus liquid is expelled from the mush, and hence interpret the causes of the high variability in UZb.

4. References
[1] Humphreys (2009) J. Petrol. **50**, 127-145 [2] Humphreys (2011) J. Petrol. **52**, 147-174 [3] Holness et al. (2011) J. Petrol. **52**, 175-222 [4] Toplis et al. (2008) Contrib. Mineral. Petrol. **155**, 329-240 [5] Namur and Charlier (2012) Contrib. Mineral. Petrol. (in press) [6] Tegner et al. (2009). J. Petrol. **50**, 813-840 [7] Morse (2012). J. Petrol. (in press) [8] Holness et al. (2007). J. Petrol. **48**, 2359-2377

Cenozoic arc magmatism along the active Andean margin – a role for denudation?

R.Jones[1], L.Kirstein[1], R.Hinton[1], S.Kasemann[2], & T.Elliott[3]

[1]School of GeoSciences, University of Edinburgh, Edinburgh, EH9 3JW, UK
[2] Department of Geosciences, University of Bremen, Germany
[3]Department of Earth Sciences, University of Bristol, BS8 1RJ, UK

Introduction

Subduction zones, such as the active Andean margin, form large recycling systems and are the main producers of new continental crust. The subduction of continental material either through the subduction of terrigenous sediment or subduction erosion is an important consideration when estimating the mass flux through an active margin over time. The overall aim of this research project is to explore potential links between surface (erosion and exhumation) and mantle processes by using the geochemical record preserved in arc magmatic rocks from the active Andean margin. The specific aims of this study were; (i) to accurately constrain the timing of arc magmatism in the southern Central Andes (~28-33ºS) and; (ii) to determine the source and evolution of the melt.

The onset and duration of magmatic activity in the southern Central Andes is poorly constrained due to the limited number of reliable age determinations. Field relationships and the current available age data suggest a hiatus in magmatic activity between ~39 and ~26 Ma (eg. [1, 2]). In order to better constrain the timing of southern Central Andean arc magmatism and to verify the existence of a period of reduced arc magmatism in-situ U-Pb dating was carried out on zircons, separated from series of strategically collected samples, using the Cameca ims 1270. Zircon is particularly suitable for U-Pb dating as it is both chemically and mechanically robust and it readily incorporates U and Th, but not Pb, as it crystallises [3].

In order to critically evaluate the source of the Andean arc melt and how it may have evolved, oxygen isotope ratios have been measured on the dated zircons, using the Cameca ims 1270. These results have been combined with Hf isotope ratios (measured by LA-ICPMS at the University of Bristol) in order to asses the varying roles of crustal and mantle components in the magmatic evolution of the southern Central Andes. Unlike other minerals, in which the oxygen isotope values can be reset by high grade metamorphism or hydrothermal alteration, zircon retains its oxygen isotope composition from the time of crystallisation when it was in equilibrium with the melt [4]. The fractionation of oxygen isotopes increases with decreasing temperature, therefore near surface processes, such as sedimentary recycling, lead to elevated $\delta^{18}O$ values relative to the mantle [3, 4].

Results

U-Pb dating and oxygen isotope analysis has been carried out on ~250 zircons (see fig. 1) obtained from 23 samples, which range in composition from basaltic-andesites to rhyolites and granites. The U-Pb crystallisation ages obtained range from 274.0 ± 3.9 Ma to 3.7 ± 0.1 Ma. The average U-Pb crystallisation ages obtained for the 23 samples appear to cluster in the Permian, the Late Cretaceous – Late Paleocene and the Late Oligocene (see fig. 2).
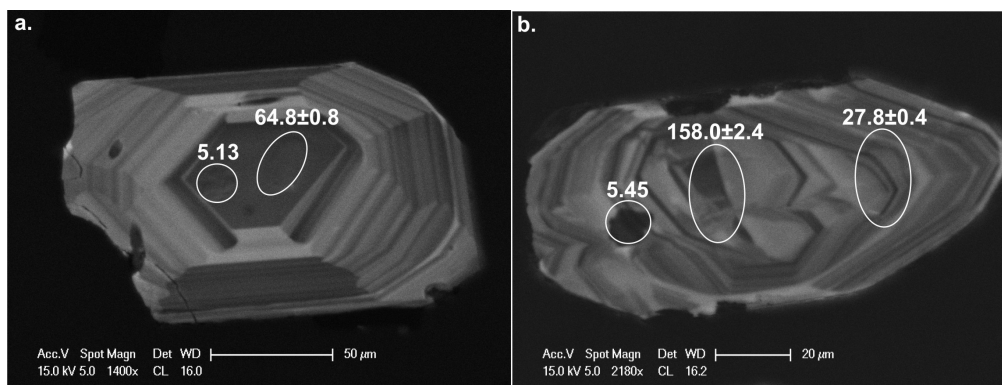
Figure 1. SEM images of zircon crystals taken in CL mode. a) An oscillatory zoned zircon extracted from sample AM0806 (granodiorite) showing a U-Pb crystallisation age of 64.8 ± 0.8 in the core and a $\delta^{18}O$ value of 5.13 ± 0.21 ‰. b) A complexly zoned zircon extracted from AM0846 (rhyolite) showing an inherited Jurassic core (158.0 ± 2.4 Ma) and a younger rim (27.8 ± 0.4 Ma).

All the zircons analysed (excluding inherited cores) were found to have $\delta^{18}O_{(VSMOW)}$ values ranging between 3.37‰ and 6.43‰ (±0.21 (1σ of the standard)). The average $\delta^{18}O$ values obtained for each of the 23 samples show either mantle (5.7 ± 0.3‰) or below mantle values (see fig. 2). Zircons from several of the rhyolitic/dacitic samples were found to have cores with Permian to Jurassic crystallisation ages and rims with Late Oligocene crystallisation ages. These inherited cores also generally yielded higher $\delta^{18}O$ values (see fig. 1). Excluding the inherited cores, the results show no consistent core to rim variations in $\delta^{18}O$ values.
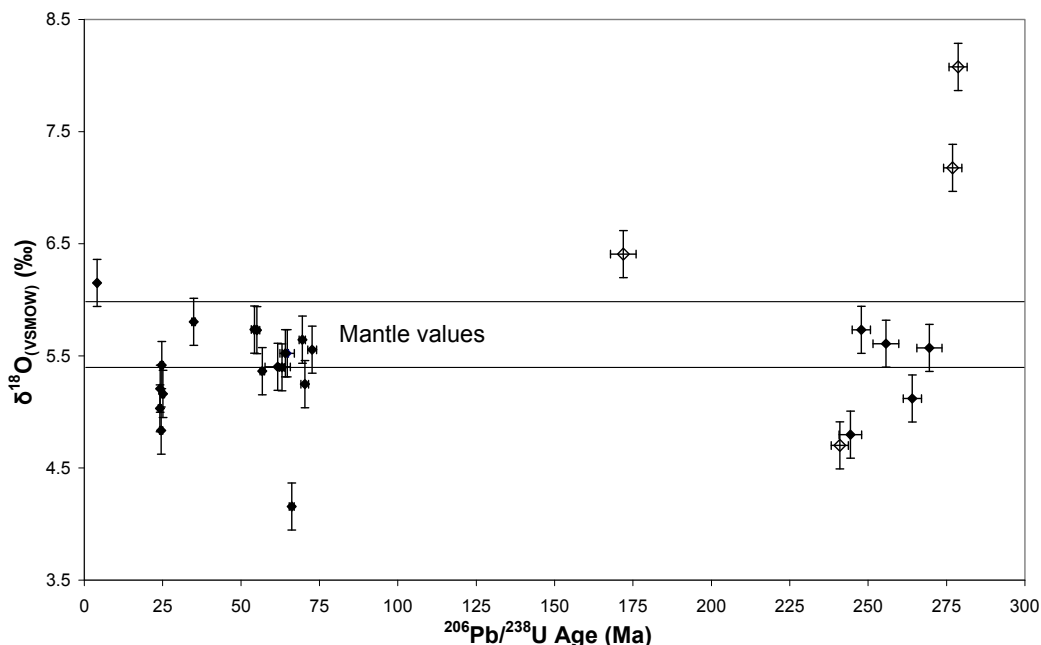
Figure 2. A plot of average $\delta^{18}O_{(VSMOW)}$ against $^{206}Pb/^{238}U$ age (Ma) for each of the 23 samples analysed. Inherited zircon grains and cores are shown separately (open diamonds). Mantle $\delta^{18}O$ values (5.7 ± 0.3‰) are shown.

Preliminary interpretations

The results of the U-Pb dating place further constraints on the presence of a widespread period of reduced arc magmatism in the southern Central Andes during the late Eocene to late Oligocene (~35 - ~28 Ma). The clustering of U-Pb crystallisation ages in the Permian, the Late Cretaceous to Late Paleocene and the Late Oligocene suggests significant arc magmatism during these time intervals. The results of the $\delta^{18}O$ analysis show a relatively restricted range of $\delta^{18}O$ values which are close to those obtained for mantle derived zircons (5.7 ± 0.3‰). This indicates that the majority of the zircons analysed are magmatic in origin and formed in high temperature isotopic equilibrium with mantle oxygen. Those zircons with below mantle values might be indicative of the interaction of hydrothermally altered crust and/or hydrothermal fluids, with the melt, prior to the crystallisation of zircon.

Further work

Additional $\delta^{18}O$ analyses, U-Pb dating (SIMS, EMMAC) and Hf isotope analyses (LA-ICPMS, University of Bristol) are currently being carried out on zircons separated from additional samples collected from the southern Central Andes in 2011. The authors intend the results presented here, combined with these new data sets, to of to form at least one publication and one conference abstract.

References

[1] Parada, M.A., et al., *Andean Magmatism*, in *The Geology of Chile*, T. Moreno and W. Gibbons, Editors. 2007, The Geological Society: London. p. 115 - 146.

[2] Parada, M.A., et al., (1988) Journal of South American Earth Sciences, **1**(3): p. 249 - 260.

[3] Harley, S.L. and N.M. Kelly, (2007) Elements, **3**: p. 13 - 18.

[4] Valley, J.W., *Oxygen isotopes in zircon*, in *Zircons*, J.M. Hanchar and P.W.O. Hoskin, Editors. 2003, Reviews in Mineralogy and Geochemistry, Mineralogical Society of America: Chantilly, Virginia. p. 343 - 386.

Volatile contents of historical eruptions at Mt. Ruapehu, New Zealand

G. Kilgour[1,2], J. Blundy[2], K. Cashman[2], H.M. Mader[2]

[1]Wairakei Research Centre. GNS Science, Taupo, New Zealand
[2]School of Earth Sciences, University of Bristol, Bristol BS8 1RJ, UK

Introduction

Mt. Ruapehu is a large, andesite stratovolcano located at the southern end of the Taupo Volcanic Zone (TVZ), North Island, New Zealand. Eruptions are common, with short repose periods (months to years) making Ruapehu one of the most active volcanoes in New Zealand. Most of the eruptions recorded since 1945 involved very small volumes of magma ($<< 0.1$ km^3) and the warning period before each eruption was short; in some cases as little as 9 min [1].

We used the volatile contents (H_2O, CO_2, F, Li, B, Be, Cl) from both melt inclusions and groundmass glasses to determine the magma storage conditions and degassing history at Ruapehu from scoria erupted in 1945, 1969, 1971, 1977, 1995, and 1996. These samples allowed us to investigate whether the magmatic system has changed over a fifty year period. These are the first volatile data obtained from Ruapehu or from any other andesite in the TVZ.
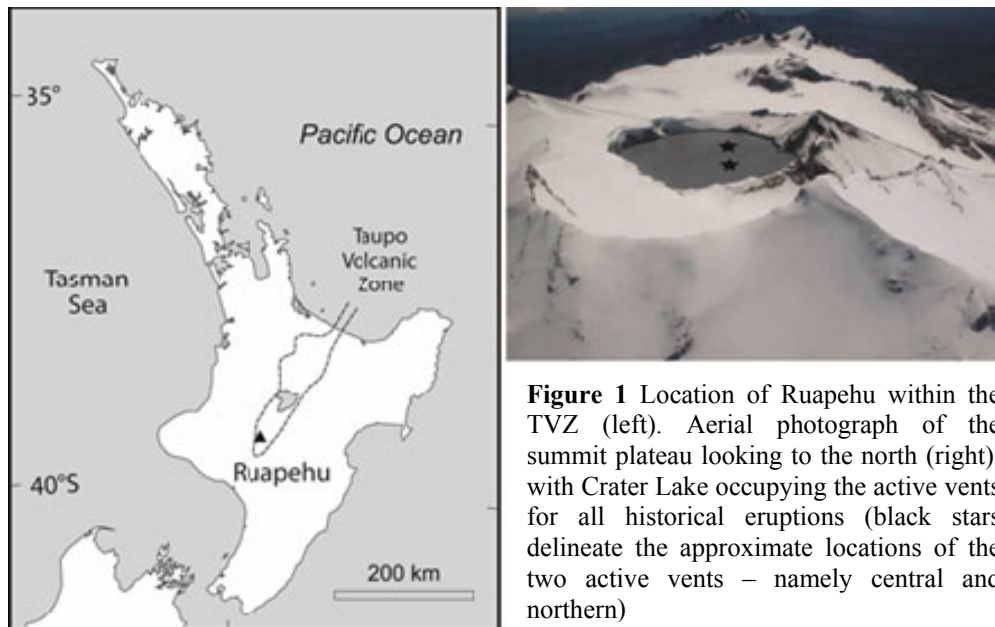
Figure 1 Location of Ruapehu within the TVZ (left). Aerial photograph of the summit plateau looking to the north (right), with Crater Lake occupying the active vents for all historical eruptions (black stars delineate the approximate locations of the two active vents – namely central and northern)

Methods

We prepared crystal separate thin sections of the historical scoria for SIMS analysis, which minimized the carbon background from excess epoxy. We followed the procedure of [2], by analysing glass standards with known H_2O and CO_2 contents, and by building working curves of $^1H/^{30}Si$ vs. H_2O and $^{12}C/^{30}Si$ vs. CO_2. A total of nine glass standards were run, covering a range of 0.15-4.1wt % H_2O and 0-2860 ppm CO_2. Standards were run at three periods during each day to account for any drift in the analyses. EPMA on the melt inclusions was completed after SIMS, for major element chemistry.

Results

A total of ~130 analyses (melt inclusion and groundmass glass) were completed over two separate weeks on the SIMS. Melt inclusions in orthopyroxene, clinopyroxene and plagioclase were analysed. Ruapehu melt inclusions are relatively H_2O-poor and CO_2-rich compared to andesites and dacites in other arc settings [3]. Melt inclusions contain ~1.5 wt % H_2O and between 30 and 1000 ppm CO_2, with no discernible differences between eruptions. Of the other elements analysed in the melt inclusions, F (up to 2000 ppm) and Cl (up to 1300 ppm) are marginally higher than other arc andesites. A maximum pressure of ~2 kb is calculated using [4], equating to ~6 km depth. This agrees well with magnetotelluric [5] and seismic tomography [6] surveys, which both show a low resistivity anomaly and low velocity zone from ~6 to ~10 km depth, marginally east of Crater Lake.

In combination with the SIMS data, major element chemistry of groundmass glasses show distinct clusters in most binary chemistry plots. Although some overlap exists, each eruption was possibly fed by a distinct magma batch. For the melt inclusions, a significant proportion of the inclusions appear to be distinct from the groundmass glass. This suggests that some of the inclusions and therefore phenocrysts are antecrysts.
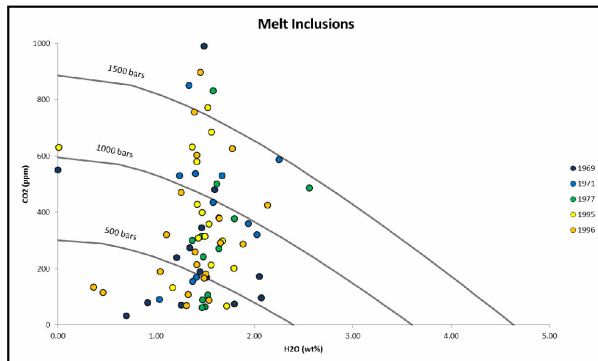
Figure 2 H_2O vs CO_2 contents of clinopyroxene-hosted melt inclusions from a range of eruptions at Ruapehu. Isobars are drawn using [4] based on a magmatic temperature of 950 ˚C and 1.5 wt % H_2O.

Discussion

Historical eruptions at Ruapehu were fed by distinct magma batches that had occupied a similar depth range. This suggests that a series of sills existed (and still exist) at ~ 6 to 10 km depth, which would account for the geophysical anomalies at this depth. These separate and small volume magmas interacted with crystal mush zone/s at depth, periodically entraining foreign crystals into the ascending magma. The small magma volumes that are often erupted at Ruapehu provide a very sensitive record of magma mixing and crystal mush interaction that may otherwise be masked in larger magmas. These data will significantly aid in producing a realistic magmatic-hydrothermal system model for the volcano.

Figure 3 Major element chemistry plots of the groundmass glass from Ruapehu scoria. Note the distinction between each eruption. This implies that a separate magma fed each event.

References

[1] G.N. Kilgour et al. (2010) Journal of Volcanology and Geothermal Research **191**, 1-14
[2] J. Blundy and K. Cashman (2008) Reviews in Mineralogy and Geochemistry **69**, 179-239
[3] P. Wallace (2005) Journal of Volcanology and Geothermal Research **140**, 217-240
[4] S. Newman, J.B. Lowenstern (2002) Computers and Geoscience **28**,597-604
[5] M.R. Ingham et al. (2009) Geophysical Journal International **179**, 887-904
[6] D.P. Rowlands et al. (2005) Geophysical Journal International **163**, 1180–1194

How Deep is the Nisyros Magma Chamber?

H.S. Kinvig and J.D. Blundy

School of Earth Sciences, University of Bristol, Bristol, BS8 1RJ, UK

Introduction

Nisyros Island (Greece) is a Quaternary strato-volcano in the eastern South Aegean Volcanic Arc. Nisyros hosts a well developed central caldera, associated with two large explosive rhyolitic eruptions: the Lower Pumice and Upper Pumice. Post-caldera rhyo-dacitic lava domes today fill the western portion of the caldera. The relationship between these eruptions, their magmatic storage conditions and the contribution of the explosive events to caldera formation, are all currently uncertain. Petrologically, the Lower Pumice and Upper Pumice are almost identical with each hosting a common phenocryst assemblage including plagioclase feldspar, amphibole and pyroxenes. Bulk compositions show considerable overlap between the units. Co-magmatic gabbroic xenoliths, representing crystal mush, are contained as plutonic nodules within the pyroclastic deposits of the Lower Pumice. These are basaltic in bulk composition and comprise olivine, pyroxenes, amphibole, plagioclase feldspar and spinel within a more evolved glassy groundmass.

Ongoing uplift and ground deformation in the north-west of Nisyros, and recent volcano-seismic unrest, have been interpreted to be a response to fresh magmatic intrusions and inflation of a magma chamber located just north-west of the island [1, 2, 3]. Despite the potential volcanic hazard, the plumbing system and depth evolution of Nisyros' magmas is largely unknown. Identifying the temporal evolution of magma storage conditions and understanding pre-eruption processes behind the caldera forming events is essential for hazard planning and monitoring of the volcano, particularly in-light of the contemporary local magmatic inflation. SIMS is the only technique able to provide reliable analysis of dissolved volatiles (H_2O and CO_2) in volcanic glasses, which are necessary to allow estimation of magma storage pressures [4] and in turn unambiguously ascertaining the source-depth evolution of Nisyros volcano. SIMS analyses of ^{1}H and ^{12}C in samples of the Lower Pumice, Upper Pumice and co-magmatic xenoliths, provide the first depth estimates for these Nisyros magmas.

Analyses

The Nisyros samples contain abundant phenocryst-hosted glassy melt inclusions >30μm diameter, ideal for analysis by SIMS (Figure 1). Phenocrysts and glass fragments were hand-picked from crushed rock samples, and resin mounted. Samples were left uncoated for preliminary SEM work, to avoid carbon-coating affecting ^{12}C measurements. Polished thin sections were additionally used for analyses. Pumice samples were collected from a range of localities and different levels of the stratigraphic sequence.

55 analyses were carried out on melt inclusion and interstitial glasses. Melt inclusions in plagioclase phenocrysts were analysed in the rhyolitic Lower Pumice and Upper Pumice, and dacitic post-caldera domes. Melt inclusions in clinopyroxene and olivine phenocrysts were analysed in co-magmatic basaltic plutonic xenoliths, brought up during the Lower Pumice eruption. A key focus was on the dissolved volatiles (CO_2, H_2O) for determining volatile saturation pressure [4]. A range of trace elements were also measured. EMP analyses were carried out after the SIMS analyses.

Results and discussion

Melt inclusions and matrix glasses from the Lower Pumice samples display a range in H_2O from 2.0 to 5.3 wt%, and CO_2 between 49 and 368 ppm. The Upper Pumice samples have H_2O ranging 1.3 to 5.6 wt%, and CO_2 between <10 and 502 ppm. The interstitial glasses yield the lowest H_2O and CO_2 values, consistent with degassing. Trace elements for the Lower Pumice and Upper Pumice melt inclusions show significant overlap. Melt inclusions in the post-caldera domes display a range in H_2O from 0.01 to 0.7 wt%, and CO_2 between 86 and 186 ppm. Low H_2O and CO_2 values indicate the post-caldera dome magma was largely degassed at the time of melt inclusion entrapment. Phenocryst-hosted melt inclusions in co-magmatic basaltic xenoliths display a range in H_2O from 2.2 to 6.1 wt%. H_2O in interstitial glasses is lower, ranging from 0.3 to 0.9 wt%. CO_2 in melt inclusions and interstitial glasses is between <10 and 112 ppm.
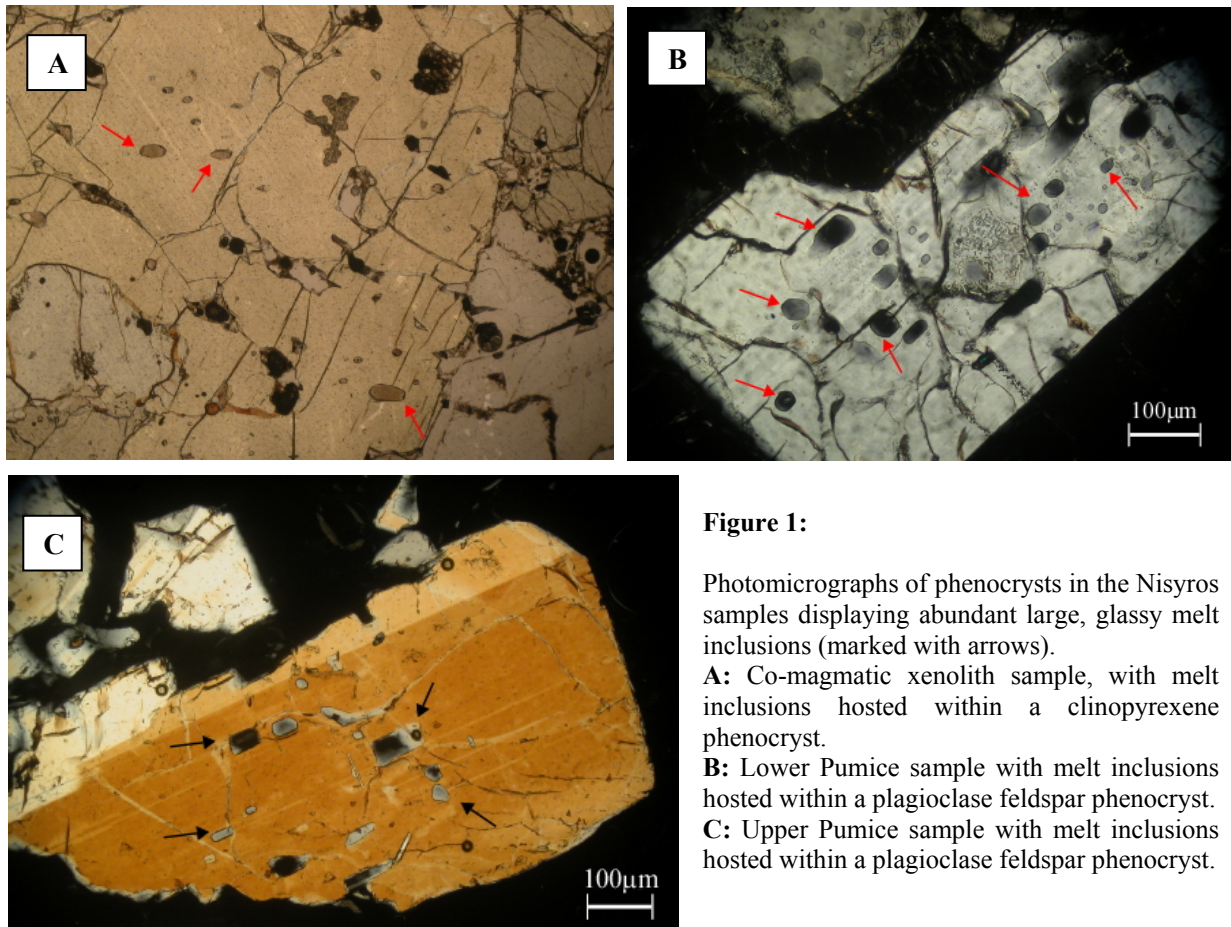
Figure 1:

Photomicrographs of phenocrysts in the Nisyros samples displaying abundant large, glassy melt inclusions (marked with arrows).
A: Co-magmatic xenolith sample, with melt inclusions hosted within a clinopyrexene phenocryst.
B: Lower Pumice sample with melt inclusions hosted within a plagioclase feldspar phenocryst.
C: Upper Pumice sample with melt inclusions hosted within a plagioclase feldspar phenocryst.

H_2O and CO_2 in the analysed glasses were used to constrain the equilibration pressure for the melts, using the technique of Newman and Lowenstern (2002) with VolatileCalc [4]. Volatile content in the Lower and Upper Pumices yield pressures < 200MPa, indicating storage at shallow crustal depths < 6 km. The Lower Pumice and Upper Pumice reveal overlapping depths, with the Upper Pumice samples extending to slightly shallower levels. Pressures calculated for the co-magmatic xenoliths are also consistent with their storage at shallow crustal depths. Volatile content indicates pressures from approximately 170 to 270 MPa, corresponding with a depth range of approximately 5 to 7 km. The overlap of pressures with the Pumice samples supports the storage of the xenoliths in a common magma reservoir prior to the Lower Pumice eruption.

Further Work

Processing of the SIMS analyses is ongoing. A paper is in preparation which uses the melt inclusion data collected by SIMS, together with other petrological investigations into the co-magmatic xenoliths, to examine mechanisms of magma differentiation and storage beneath Nisyros [5]. These additional investigations indicate that the shallow level storage and crystallisation of the xenoliths indicated by melt inclusions, is a late stage in their evolution, following derivation from a deeper magmatic system [5].

References

[1] S.C. Stiros et al. (2005) In: Fytikas, M., & Vougioukalakis, G.E, The South Aegean Volcanic Arc, Elsevier, 217-225
[2] A. Tibaldi et al. (2008) Journal of Structural Geology **30,** 1489-1506
[3] E. Lagios et al. (2005) Buliten of Volcanology **68**, 201-214
[4] P. Newman and J. Lowenstern (2002) Computers and Geosciences **28**, 597-604
[5] M.A. Loader (in prep) Mechanisms of Magma Differentiation beneath Nisyros, Greece, revealed by Cognate Xenoliths

Disentangling environmental and physiological influences on otolith growth: unlocking the potential use of otoliths as natural tags

A. Lewis-Sturrock[1, 2], C. Trueman[1], and E. Hunter[2]

[1] National Oceanography Centre, University of Southampton, Waterfront Campus, Southampton SO14 3ZH, UK
[2] Centre for the Environment, Fisheries & Aquaculture Science, Pakefield Road, Lowestoft NR33 0HT, UK

Background

Despite its potential value as a recorder of the environmental history of individual fish, the underlying mechanisms governing incorporation of elements into otoliths are poorly understood, with little *in situ* validation and the effects of physiology remaining largely unknown. The current project aimed to address both issues by 1) tracking otolith chemistry alongside blood chemistry and physiological variables in mature and immature fish maintained over an entire reproductive cycle and 2) coupling ground tracks of wild marine fish (*Pleuronectes platessa*) recorded by electronic Data Storage Tags (DSTs) with chemical profiles across otoliths of the same fish. At EIMF otolith δ^{18}O and Li, Mg, K, Ca, Sr, Ba concentrations were measured using the Cameca 1270 and 4f, respectively.

1) Results from the aquarium study

In order to retrospectively couple weekly to monthly blood and water samples with concomitant otolith material, an accurate identification of the timing of otolith deposition was crucial, as growth rates varied considerably over time. To provide a 'start check', fish were injected with oxytetracycline, leaving a fluorescent growth band (Fig. 1). Intra-annual growth was estimated using predicted vs. measured δ^{18}O profiles. Predicted δ^{18}O was calculated using weekly salinity and temperature measurements (*1*) and 'wiggle matching' was carried out in AnalySeries 2.0 (*2*) (Fig. 1). There was some noise in individual δ^{18}O measurements (Fig.2), but overall excellent agreement between predicted and measured profiles, with correlations generally >0.8. Some of the variation in absolute values can be explained by calibration and/or instrument error, but offsets generally did not preclude the use of the technique for picking out inflection points. Much of the noise can be explained by the attenuation of signals during periods of slowed growth and imperfections in the sample preparation. What was clear was that the timing of growth band deposition and intra-annual otolith growth rates varied considerably among individuals, and had a constant growth rate been assumed, blood, water and otolith samples could have been mismatched by more than three months (Fig. 2)
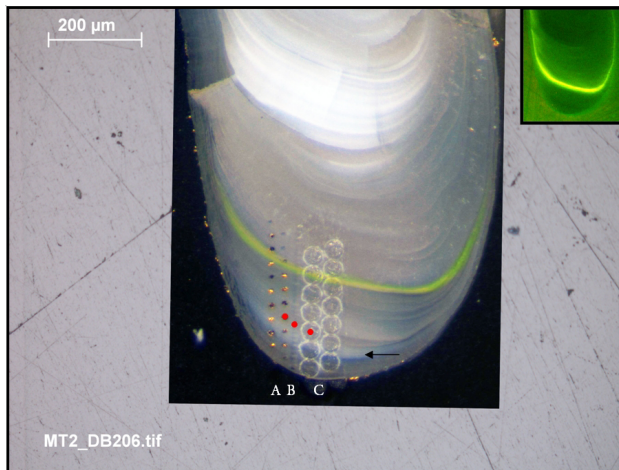
Fig. 1 (Left) Frontal otolith section under reflected and (inset) UV light showing pits left from the three types of analyses used in the current study:
(A) δ^{18}O (Cameca 1270, ~20µm spot size),
(B) Li, Mg, K, Ca, Sr, Ba (Cameca 4f, ~8 µm size)
(C) Mn, Cu, Zn, Sr, Ba (HR-LA-ICP-MS, 35 µm size). The red spots indicate an example of where a spot from each analysis type has been visually matched by following growth band axes. The opaque band is indicated by an arrow.

(Below) "Wiggle matching" carried out in AnalySeries 2.0. Predicted (red) and measured (green) δ^{18}O profiles. (A) Raw data, (B) wiggle matched. The blue lines indicate anchor points and right hand side plot shows the correlation between profiles. In this particular example, the correlation coefficient was 0.94.
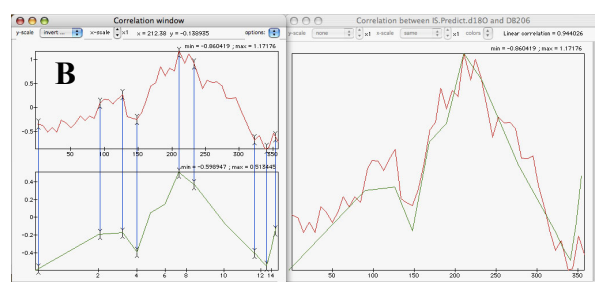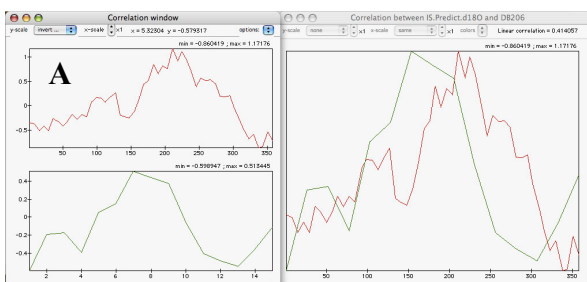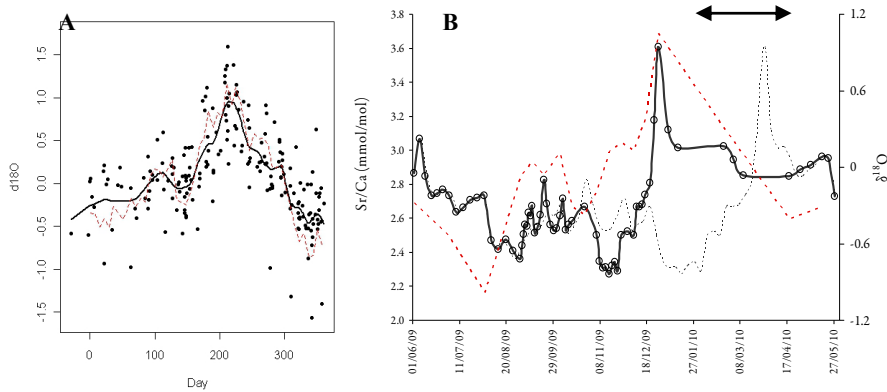
Fig. 2 (A) Measured (black spots & line) vs. predicted (red line) otolith $\delta^{18}O$ for 18 experimental plaice.
(B) Otolith Sr/Ca and $\delta^{18}O$ profiles for an experimental female. The $\delta^{18}O$ (red dashed line) corrected Sr/Ca profile (thick black line) peaked 3 months earlier than it would have done if constant growth been assumed (grey dashed line).

Linear mixed model analyses were used to examine which variables were most likely to be controlling otolith trace elemental concentrations. Most models indicated that a significant proportion of the variance could be explained by physiological processes such as growth rate and gonad development (Fig. 4). If a common phenomenon among marine fish, this potentially lessens the usefulness of otolith trace elements to retrospectively track individual movements, however, certain elements (e.g. Li) exhibited variations consistent with environmental control (Fig. 3).

Fig. 3 Some of the significant relationships highlighted by mixed model analyses examining controls on otolith elemental concentrations in experimental plaice. Otolith [Mg] was largely explained by otolith growth rate (GR); otolith [Sr] largely by blood [Sr/Ca] (in turn controlled by protein concentrations and gonadosomatic index) and otolith [Li] largely by the environment (ambient concentrations (Li.w) and/or temperature).
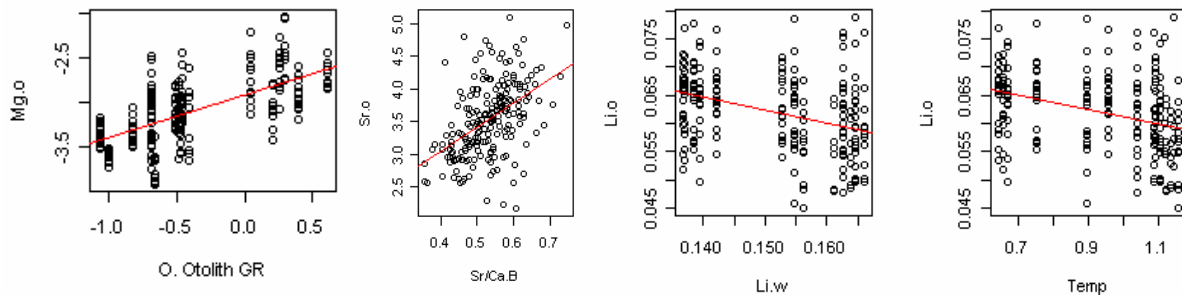
2) Wild DST tagged plaice

One of the chemical 'markers' considered to be the most promising for tracking movements of wild plaice was otolith $\delta^{18}O$. In two individuals exhibiting very different migration patterns (Fig.4), $\delta^{18}O$ patterns faithfully reflected the contrasting temperature and salinity regimes and appeared to indicate repeat migration in both fish, and long term changes in habitat use by the Central North Sea fish.
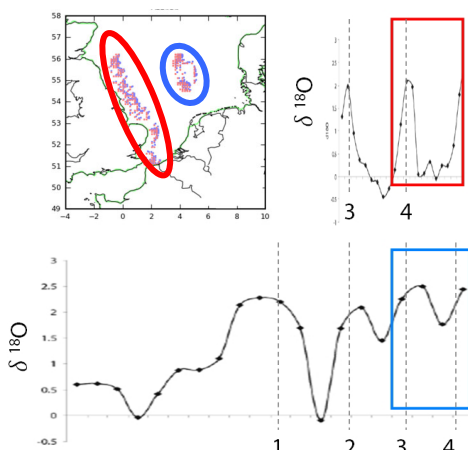
Fig. 4 Geolocations and $\delta^{18}O$ outputs for two fish tagged by DST, released October 2004. The central North Sea male (blue) undertook a shorter migration and encountered colder water with smaller salinity and temperature fluctuations. This was reflected in the higher, less variable otolith $\delta^{18}O$. The west North Sea female (red) migrated >500km between summer feeding grounds near the Scottish borders to spawning grounds at the mouth of the English Channel and encountered much larger physicochemical gradients, as reflected in the larger amplitude in $\delta^{18}O$. The minimum $\delta^{18}O$ values within each yearly cycle (ages indicated by vertical dashed lines) reflect otolith material deposited while on summer feeding grounds. These were clearly different among the population subunits and inferred a repeat migration in both individuals the year prior to tagging. In the male, the summers coinciding with ages 0-2 were clearly different. During these years the fish likely inhabited coastal nursery grounds, which, based on the $\delta^{18}O$ values, exhibited warmer and/or less saline summers than those encountered at the adult feeding grounds.

In summary, the superior spatial resolution of SIMS $\delta^{18}O$ analyses provided a new method to assign calendar dates to otolith sections and identify movements in wild fish. SIMS-measured elemental concentrations corresponded well with LA-ICPMS data, but allowed greater temporal resolution as well as measurement of K. Clear physiological effects on otolith composition were observed.

1. Hoie et al. (2004) ICES Journal of Marine Science **61**, 243. 2. Paillard et al., (1996) EOS Transactions, AGU Vol. 77, 379.

SIMS calibration of water concentration profiles surrounding vesicles in volcanic glass

E. Llewellin[1], I. McIntosh[1], M. Humphreys[2] & J. Larsen[3]

[1]Department of Earth Sciences, Durham University, Durham DH1 3LE, UK
[2]Department of Earth Sciences, University of Oxford, Oxford OX1 3AN, UK
[3]Department of Geology and Geophysics, University of Alaska Fairbanks, Fairbanks, AK 99775-7320, USA

Introduction

Volcanic eruptions are driven by the nucleation and growth of bubbles, the rate and extent of which are key controls on the explosivity of the eruption, and thus the volcanic hazard. Exsolution of magmatic volatiles and bubble growth can be modelled numerically by considering how the volatile concentration gradient surrounding the bubble changes through time; however these modelled profiles have not yet been tested by independent, direct measurements of volatile concentration.

Approach

Synthetic experimental samples of hydrated phonolite glass were decompressed under a range of known pressure and temperature conditions to create vesicular samples. H_2O was the only volatile phase present; thus bubble growth was governed by the exsolution and diffusion of H_2O through the melt. Secondary Ion Mass Spectrometry (SIMS) measurements were made of the H_2O concentration along radial profiles extending from bubble walls. These SIMS spot analyses were then used to calibrate greyscale variations in backscatter scanning electron microscope (BSEM) images of the sample using the technique of [1] (whose data were also acquired at Edinburgh IMF). Using this technique we extracted quantitative H_2O concentration profiles at a high spatial resolution (resolution of a pixel, ~0.5µm, cf ~10µm SIMS spot size). These concentration profiles were then compared with results from numerical modelling of the sample conditions.

Results and Preliminary Interpretations

SIMS-calibrated greyscale variations in BSEM images were used to extract quantitative H_2O concentration data for both SIMS-analysed profiles and other profiles selected in the same BSEM image. An example of the data acquired is shown below in Figure 1.
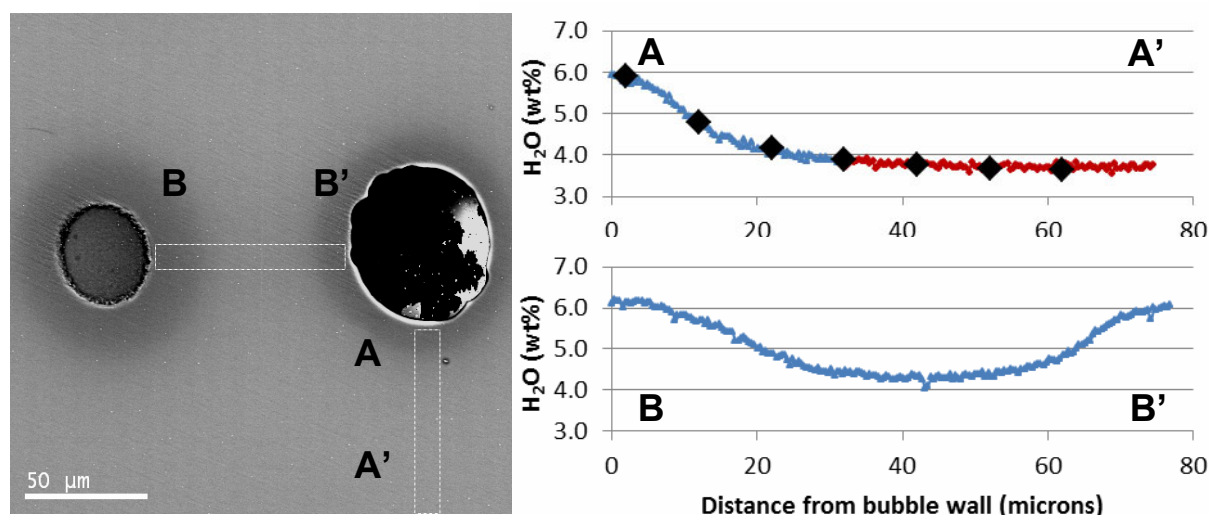
Figure 1. *Left*: BSEM image of bubbles in phonolite glass showing analysed profiles **A – A'** (SIMS and greyscale intensity) and **B – B'** (greyscale intensity only). Note bright white edge effect at bubble walls.
Right top: H_2O concentrations extracted from BSEM greyscale image (blue triangles) along profile A – A' with points measured by SIMS (black diamonds) for comparison.
Right bottom: H_2O concentrations extracted from BSEM greyscale image along profile B – B' using the SIMS-calibration of greyscale intensity derived from profile A. Blue sections highlight rehydration during bubble resorption; red sections result from syn-experimental bubble growth.

These data were compared to concentration profiles predicted by numerical modelling using the standard theory of bubble growth (e.g. [2]), where concentration at the bubble wall is governed by the solubility concentration for the experimental temperature and pressure. For slow decompression rates diffusion of H_2O into the bubble is sufficiently fast to keep the bubble in equilibrium with the surrounding melt, creating a flat concentration profile. Faster decompression rates lead to diffusion-limited disequilibrium degassing and the development of a super-saturated far field.

Figure 2 compares profile A – A' from Figure 1 with the modelled, expected, profile. Instead of being highest in the far field, H_2O concentration is instead greatest at the bubble wall, while the far field H_2O concentration (red triangles) rests at the calculated equilibrium solubility value. The far field concentration is interpreted as evidence of equilibrium degassing during the experiment. The higher H_2O concentrations (blue triangles) are interpreted as evidence of melt hydration and bubble resorption during the final quench to glass, since they must reflect an increase in equilibrium solubility and therefore pressure and/or temperature conditions. Since quench was isobaric, this solubility increase was caused by the temperature decrease.
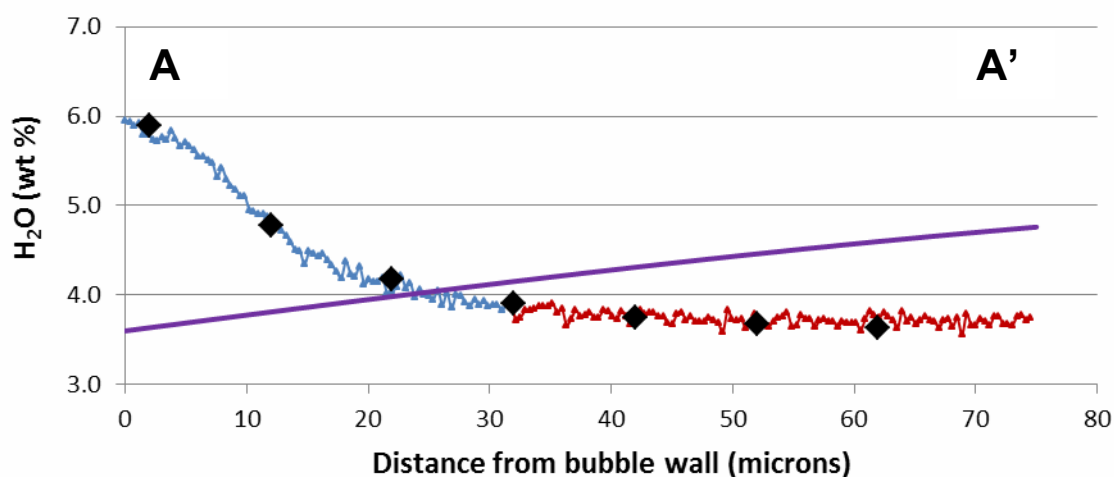
Figure 2. Comparison between expected H_2O concentration profile (purple line) and measured H_2O concentration profile A – A' from Figure 1 (SIMS spots, black diamonds; calibrated greyscale, blue/red triangles). Expected profile produced using standard theory of diffusive bubble growth (e.g. [2]).

Implications
Bubble resorption during quench has important implications for both experimental petrology studies and for the interpretation of natural samples. Final bubble size and porosity of experimental samples are widely used to study degassing processes yet may be significantly altered during quench, while concentration profiles altered by quench-resorption in natural samples may be misinterpreted as evidence of pressurisation prior to eruption.

Use of Results
Data from the Edinburgh IMF pilot project were used to prepare a full application for further analyses, to take place in 2012. In addition, preliminary data have been presented in the following presentations:

I.M. McIntosh et al. (2012) (Mis)understanding bubble growth in magma: Evidence from preserved volatile concentrations in glass *Volcanic and Magmatic Studies Group* (Jan 2012)

I.M. McIntosh et al. (2011) Reconstructing the growth history of bubbles in magma from preserved volatile concentrations in glass *Volcanic and Igneous Petrology meeting* (Nov 2011)

References
[1] M.C.S. Humphreys et al. (2008) Earth and Planetary Science Letters, 270, 25-40
[2] A.A. Proussevitch et al. (1993b) Journal of Geophysical Research, 98, 22,283-22,308

Hydrogen in nominally anhydrous minerals

E. Melekhova & J. Blundy

University of Bristol, Wills Memorial Building, Queen's road, BS8 1RJ

Introduction

Most of the water in the Earth's upper mantle is stored in nominally anhydrous minerals (NAMs), olivine, pyroxenes and garnet. Partitioning of hydrogen between NAM's and basaltic magma has a considerable influence on mantle properties such as; melting temperature, rheology, electrical conductivity, and seismic velocity. Therefore, partition coefficients (D) are very important for the modelling of mantle properties. At the moment, estimating the bulk D is limited due to technical challenges both in experiments, growing big enough crystals coexisting with melt, and analytical technique. Recently it was shown [1,2] that SIMS has by far and away the greatest potential for the routine measurement of H in high-pressure experiments.

In January 2011 we had our second session to complete the project started in 2010. In the report from 2010 we showed that new approach for measuring hydrogen by SIMS in NAM's minerals is robust and reliable.

During our last session we analysed water in olivines and coexisting melts in cumulate xenolith from St Vincent volcano, Lesser Antilles.

Analytical

Hydrogen is an abundant contaminant in mass spectrometer vacuums, in primary ion sources and easily absorbed onto the sample surfaces. All of this is a cause of high background hydrogen for standard analytical procedure, and it is why it has been so difficult to achieve accurate measurements of low concentrations of hydrogen by SIMS. Following earlier work (e.g. 1,2) we try to reduce hydrogen contamination and achieve relatively high vacuum during our analytical session. To improve vacuum conditions the instrument was baked for 6 hours at 130°C (outside measurements). After samples were introduced into the chamber the temperature was reduce to 80 °C and the instrument was baked for another 48 hours. The chamber was not opened again during the analytical session. To avoid the degrading of the vacuum we use epoxy-free samples. All samples including the standards were mounted in to indium. Samples were stored in the oven at 110-120 °C before gold coating. These steps allowed us to reach a total vacuum of 6×10^{-10} torr prior to measurement (by the end of the week the vacuum had improved to 9.29×10^{-10} torr). We use a primary beam of O^- ions measuring positive secondary ions. Every spot was prespattered for 2 minutes with a 11 nA beam. The analyses were performed using a 5nA primary beam 8-15mm in diameter. During this time we monitored ^1H, ^{26}Mg, and ^{30}Si. This setup allowed us to reach a hydrogen background of ~15 ppm in San Carlos Olivine.

Results

During the first session we analysed 7 olivines (45 to 190 ppm H_2O), 8 clinopyroxenes (700 to 900 ppm H_2O) and an orthopyroxene (1390 ppm H_2O) in four different samples from our experiments performed at upper mantle P-T conditions. Experimental melts have 3.9 to 9.3wt% of H_2O and average melt/mineral partition coefficients are $D^{ol/melt} = 0.0021$, $D^{cpx/melt} = 0.013$ and $D^{opx/melt} = 0.035$.
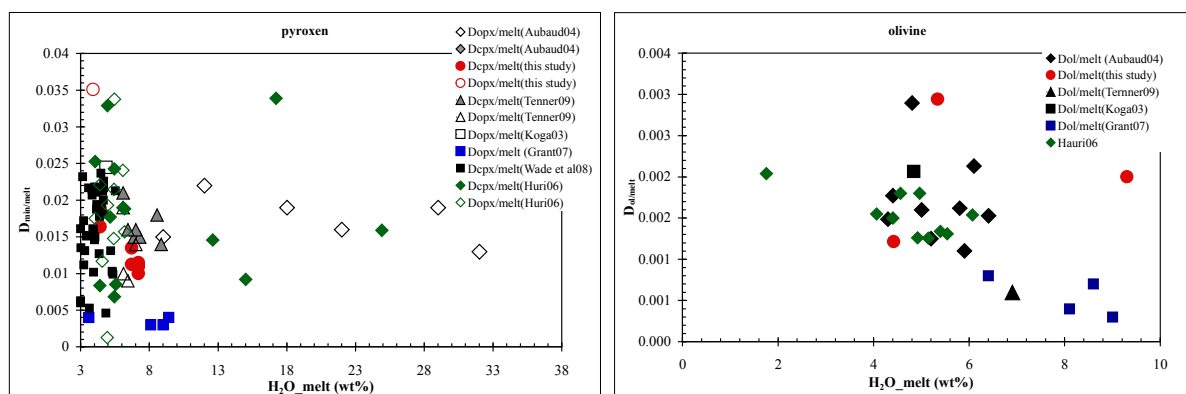

Figure 1. *Results showing partition coefficient verses H_2O contents of melt.*

Measured partition coefficients are presented in Figure 1 together with the data from other studies. We did not observe any correlation between D and P, T, oxygen fugacity. However, we showed very strong correlation between water content of olivine and coexisting melt. At the same time water content of clinopyroxene seems to be independent of water content of coexisting melt, which is quite controversial and might need more thinking and constrains to be explained.

During the second session water content of olivine and coexisting melt from cumulate xenolith were analysed. First striking result of the analyses is water content of melt inclusions itself. In 2008, Bouvier et al. [3] analysed water content of melt inclusion in primitive olivines from scoria. They conclude that St Vincent basaltic melt inclusions contain between 2.2 and 5wt% of H_2O. We analysed 7 melt inclusions coexisting with olivine in cumulate xenolith. The water content vary between 2 and 4.5 wt%. The freshness of cumulates (e.g. no zonation) and high water content of melt inclusions in them is indicators of very fast processes. It means that the magma did not spend long enough at the shallow level to lose all the water.

This analyses together with field observations and experimental constrains might allow us to build a model to predict how long magma store in the magma chamber prior an eruption. At the moment we are carrying out extra analyses of cumulate assemblages and performing experiments at low pressures in order to constrain the periodicity of a magma chamber filling and an eruption.

The partition coefficient for olivine melt is in the same range as for $D^{ol/melt}$ from experiments. It is between 0.002 and 0.003 wt% and correlate with the water content of coexisting melt inclusion. As we know water diffusion is very fast and it is reasonable that water in olivine increase with increasing water in the melt. It is what we see both from experimental results and natural rocks.

References
[1] K. Koga, E. Hauri, M. Hirschmann & D. Bell, G^3. 4 (2003) 1019.
[2] C. Aubaud, A.C. Withers, M.M. Hirschmann, et al., Am.Min.92 (2007) 811-828.
[3] A-S. Bouvier, N. Metrich & E. Deloule, J.of Petrol. 49 (2008) 1427-1448

Accessory mineral evidence for the preservation of different stages of magma evolution in silicic magmas

Andrew Miles[1], Colin Graham[1], Martin Gillespie[2], Chris Hawkesworth[3] and Richard Hinton[1]

[1]School of GeoSciences, West Mains Road, University of Edinburgh Edinburgh, EH9 3JW, UK
[2]British Geological Survey, Murchison House, West Mains Road, Edinburgh, EH9 3LA, UK
[3]School of Geography and Geosciences, University of St Andrews, North Street, St Andrews, KY16 9AL, UK

Introduction

Accessory minerals have provided valuable insights into the processes of crustal differentiation, particularly those involving silicic magmas. In addition to zircon, apatite is becoming an increasingly dependable geochemical tracer of the evolution of silicic magmas. The trace element compositions of apatite record the effects on melt compositions of the crystallization of different Rare Earth Element (REE)-rich accessory minerals that were present before and after initial apatite saturation [1]. We present Cameca ims-4f ion microprobe and Cameca SX 100 electron microprobe trace element analyses of apatite inclusions hosted by a range of minerals, including zircon, in the post Caledonian, zoned granitic pluton of Criffell, Scotland.

Results

Apatite inclusions from outer metaluminous zones (1 & 2) of the Criffell pluton reveal REE heterogeneity comparable in magnitude to that of the whole-rock suite throughout the pluton (Fig. 1). Most variability is seen in LREE concentrations, which vary from 2677 to 277 ppm. This marked depletion results from simultaneous crystallisation of small modal proportions of allanite and is supported by equally marked decreases in Th/U ratios in apatite. Differentiation in Criffell, as in most silicic magmas, is characterised by a reduction in REE concentrations due to their compatible behaviour during accessory mineral crystallisation. The earliest apatites to form are therefore those with the most elevated La concentrations. Ion probe data shows that the melts from which the earliest apatites formed strongly resemble their present-day whole-rock (WR) composition. The preservation of liquidus compositions by only the earliest apatite and the WR indicates that fractional crystallisation is unlikely to have occurred during the crystallisation of apatite and that the compositional variability seen in apatite results primarily from the competitive crystallisation of other REE-rich phases. Furthermore, despite evidence that intra-sample differentiation is dominated by allanite, WR La/Yb ratios correlate positively with increasing differentiation and not negatively as would be expected if allanite was also responsible for WR differentiation.

Apatites from peraluminous zones (4 & 5) define a second trend in La-Yb space, and are more depleted in La (mostly <1000 ppm) but more enriched in Yb (276 < Y > 3212 ppm) than those from metaluminous zones. All apatite in these zones is more depleted in La than their respective WRs; this requires that a La-rich phase pre-dated apatite saturation in these magmas. Monazite is know to be stabilised in peraluminous magmas and is highly effective at removing La from the melt. Monazite crystallisation in these zones is supported by Nd anomalies in apatite, reflecting preferential uptake of Nd. Crucially, however, this anomaly is not evident in the WR. Despite its presence in the inner three zones of the pluton, fractional crystallisation of monazite could not have been important in determining peraluminous WR compositions.

A model is therefore required where liquidus compositions are preserved by WR and where accessory phases like allanite and monazite exercise their effects only at the scale of other accessory minerals. In situ crystallisation [2] has been proposed to operate in large magma bodies and enables WR compositions to preserve liquidus compositions for elements that

behave compatibly. However, the model suggests that WR and mineral compositions are determined together. Crystallisation of accessory minerals such as allanite and monazite should therefore result in a lowering of La/Yb ratios in magmas that undergo allanite crystallisation and a marked Nd anomaly in magmas that undergo monazite crystallisation. Neither is observed in the WR suite. An alternative model is that WR compositions and those of individual phases are determined in spatially distinct regions of the magmatic system. The crustal hot zone model [3] proposes that WR compositions are determined in a deep crustal hot zone through open system processes such as fractional crystallisation and assimilation. Such processes are required to account for WR isotopic and elemental variability. Textural maturation is thought to operate following segregation of small melt volumes from the hot zone at higher crustal levels. If crystallisation occurs after melt separation and is largely in situ, it may be possible to reconcile evidence for open and largely closed system processes at different scales.
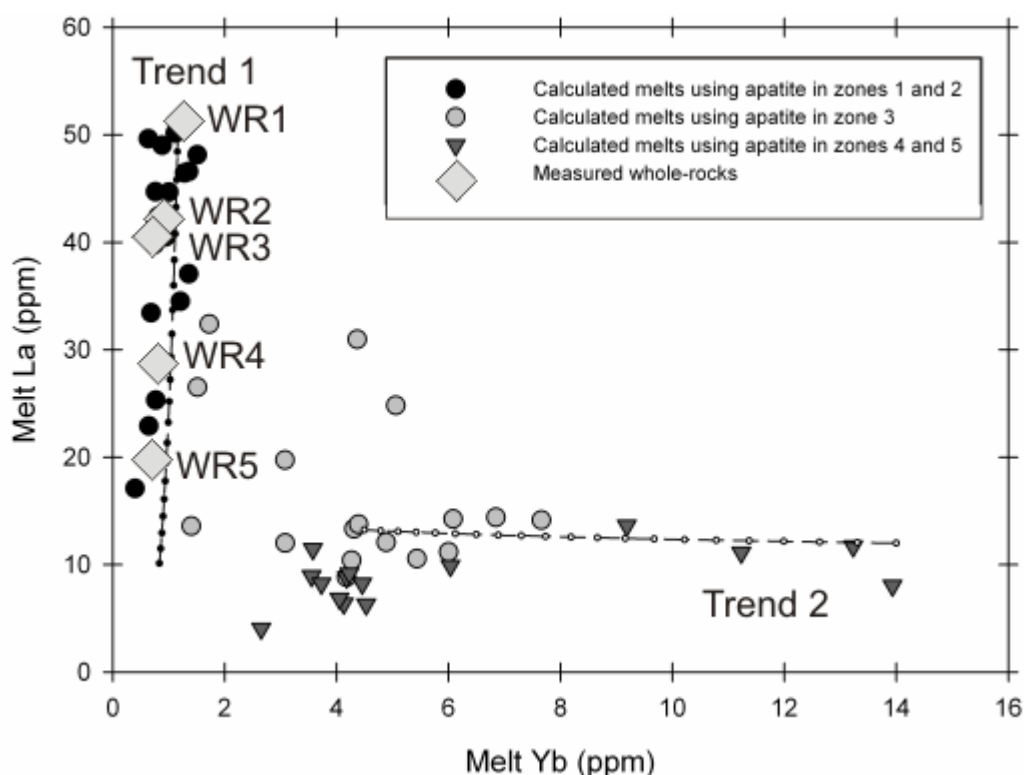
Figure 1 La and Yb compositions of melts from which apatites crystallized in all zones (small circles and triangles). Yb data are only available for ion probe analyses. Whole rock (WR) compositions for each zone are shown as larger symbols. Numbers next to WR symbols denote the zone. Crystallization models for trends 1 and 2 are shown. The trend 1 model used a starting composition similar to that of Zone 1 WR and is plotted in increments of 3% crystallization. Modal proportions of fractionating mineral assemblages for trend 1 are: 2 % sphene, 0.5 % zircon, 0.5 % apatite and 0.1 % allanite. The trend 2 model assumes a starting composition that post-dates monazite crystallization, with 12 ppm La and 14 ppm Y. The crystallizing mineral assemblages for trend 2 are: 2 % apatite and 2 % zircon.

References
[1] P.W. Hoskin et al. (2000) Journal of Petrology **41**, 1365-1396.
[2] C.H. Langmuir et al. (1989) Nature **340**, 199-205.
[3] C. Annen et al. (2006) Journal of Petrology **47**, 505-539.

The role of volatiles in the behaviour of subglacial rhyolitic eruptions in Iceland

J. Owen[1], H. Tuffen[1] & D.W. McGarvie[2]

[1]Lancaster Environment Centre, Lancaster University, Lancaster LA1 4YQ, UK
[2]Department of Earth and Environmental Sciences, The Open University, Milton Keynes MK7 6AA, UK

Aims of the project

To collect the first dataset of initial volatile concentrations in Icelandic rhyolites and determine what controls the explosivity of rhyolitic eruptions beneath ice. Volatiles are known to control the style of subaerial eruptions, with high initial volatile concentrations and closed system degassing favouring explosive activity. A transition from explosive to effusive eruptions is often attributed to a change between closed and open system degassing or to a volatile stratified magma chamber [1]. Whether these relationships extend to subglacial rhyolitic systems has never been investigated. In subglacial settings, explosivity is also influenced by magma-water interaction. A recent study [2] suggests that vesicular rhyolite magma may interact less violently with external water than vesicle-poor magma. This suggests that high volatile contents could stifle explosivity. We aim to investigate the role of volatiles in determining the behaviour of subglacial rhyolitic eruptions by analysing initial and final volatile contents in the products of effusive, transitional and explosive rhyolite eruptions beneath Icelandic glaciers.

Methods

We measured H_2O, Li, Be, B, CO_2, F and Cl in melt inclusions and matrix glasses from 16 samples collected from six subglacial (and one subaerial) rhyolitic edifices in Iceland that represent a variety of eruptive styles. In correspondence with R. Hinton, results were carefully sifted to exclude erroneous measurements, for example rejecting results with non-stable ion counts, low Si counts or points that intersected obvious cracks (103 of the 182 analyses were accepted). Calibration was achieved against standards of known concentrations which were measured each day.

Results

Robust results show that effusively produced samples display significantly lower pre-eruptive H_2O content than explosively produced samples (Fig. 1 and Fig. 2). In addition, the explosive and effusive samples show different H_2O-Cl relationships, with effusive samples requiring higher Cl distribution coefficients than explosive samples (Fig. 1). CO_2 results varied but were generally less than 2000 ppm. However, they were considered unreliable as they greatly exceeded results from FTIR (<30 ppm). Li concentrations were usefully measured (12-91 ppm) and these help shed light on degassing trends. F and Cl concentrations in melt inclusions are 1,045 - 5,608 ppm and 696 - 4,385 ppm respectively.
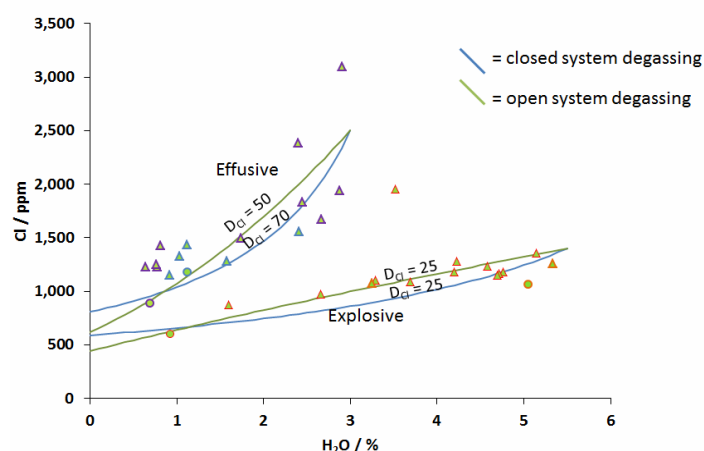
Figure 1. H_2O and Cl data for Dakalvísl samples. Circles represent matrix glass and triangles depict melt inclusions. The different colours represent different sampling locations of which the blue and purple were produced effusively and the red and orange explosively. The lines represent closed (blue) and open (green) system degassing, calculated using formulas from [3]. D_{Cl} refers to the distribution coefficient for Cl.
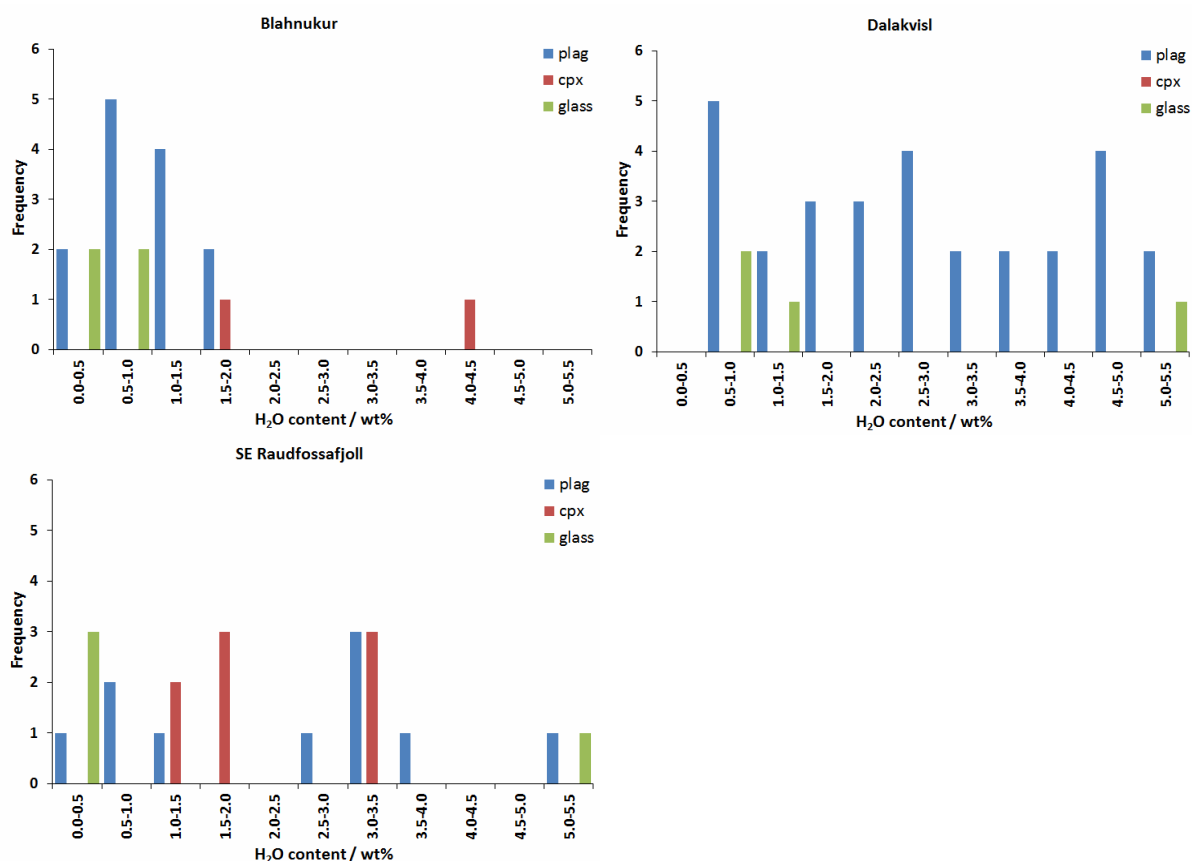
Figure 2. H$_2$O concentrations from melt inclusions within plagioclase (blue), melt inclusions within clinopyroxene (red) and matrix glass (green) for three contrasting subglacial rhyolitic edifices in Iceland (Blahnukur - effusive, Dalakvisl, transitional, SE Raudfossafjoll - highly explosive).

Discussion

High Cl distribution coefficients are associated with microlite growth, which in turn, is associated with open system degassing [4].Therefore, our results show that effusive activity correlates with low pre-eruptive H$_2$O content (Fig. 2) and open system degassing (Fig. 1), whereas explosive activity correlates with high pre-eruptive H$_2$O contents and closed system degassing. We are confident that the high pre-eruptive water contents of Dalakvísl and SE Rauðfossafjöll inclusions do not reflect hydration as high water content inclusions do not correspond spatially with domains of hydrated matrix glass. Results for plagioclase and clinopyroxene-hosted inclusions appear broadly similar. We are currently testing for post-entrapment effects such as crystallisation and diffusion; and constructing degassing models to explore how magma vesicularity evolved during eruptions beneath ice – was the confining pressure sufficient to prevent magma vesiculation? We have presented preliminary data in two conference abstracts[5,6] and two articles are in preparation[7,8].

Conclusion

Volatiles seem to play a strong controlling factor in determining the eruptive behaviour of subglacial rhyolitic eruptions. Furthermore, this is the same role as with subaerial eruptions, thus the presence of snow/ice appears to have little effect on the role of volatiles.

References

[1] C. Martel et al. (1998) Earth and Planetary Science Letters **156**, 89-99. **[2]** A. Austin-Erickson et al. (2008) Journal of Geophysical Research **113**, B11201. **[3]** M. Humphreys et al. (2009) Geochimica et Cosmochimica Acta **73**, 5693-5708. **[4]** B. Villemant et al. (2008) Earth and Planetary Science Letters **269**, 212-229. **[5]** J. Owen, H. Tuffen, D.W. McGarvie (2012) What controls the explosivity of subglacial rhyolitic eruptions in Iceland*?* Abstract, VMSG 2012, Durham. **[6]** J. Owen, H. Tuffen, D.W. McGarvie (2012) Geophysical Research Abstracts 14, EGU2012-10218. **[7]** J. Owen et al. (in prep for Geology) The role of volatiles in controlling subglacial rhyolite eruptions **[8]** J. Owen et al. (in prep) Pre-eruptive volatile content, degassing paths and depressurisation: explaining the transition in style at the subglacial rhyolite eruption of Dalakvísl, Torfajökull, Iceland.

Trace-metals in sedimentary diatom frustules as tracers for past micronutrient availability in the surface Ocean

Laetitia E. Pichevin, Walter Geibert, Raja S. Ganeshram, Kate Darling

School of GeoSciences, University of Edinburgh, Edinburgh EH9 3JW, UK

Background and Objectives

Dust input to the ocean and the associated micronutrient availability to primary producers are considered to have played an important modulating role on the marine carbon pump and global climate throughout the past [1,2]. However, attempts to accurately reconstruct past changes in micronutrient availability in the ocean and its effect on primary productivity have been hindered by the lack of an appropriate proxy for micronutrient concentration in the surface ocean and uptake by the phytoplankton.

Diatoms are amongst the most important marine primary producers. They require silicic acid to build their siliceous frustules. They also require micronutrients, of which iron and zinc have been shown to play a particularly important role in controlling diatom growth and macronutrient utilisation [3]. Recent calibration studies have shown that diatoms take up elements such as Fe, Al, Zn, etc proportionally to their biological availability in sea water and incorporate these metals into their frustules [4-6]. Hence, trace metals concentration in sedimentary diatom frustules can potentially be used to track past changes in micronutrient availability in the surface ocean [7]. However rigorous attempts to investigate in details whether the signal is altered during transit through the water column and sediment burial is lacking. We used the Ion Microprobe technique on clean suspended and sedimentary diatoms to measure the concentration in metallic elements in their opaline frustules.

The ultimate objective of this proxy development is to confirm whether past changes in micronutrient supply to the surface ocean have triggered changes in productivity and macronutrient (N, P, Si) cycling by biota as suggested in recent works [2,3,7,8]. Specifically, we propose to test whether trace metals concentration in **sedimentary** diatom frustules is a suitable proxy for past micronutrient availability, and the hitherto missing tool to address this major question. The project was organised in three progressive steps testing the following hypotheses:

1) Trace metal concentrations in sedimentary diatoms accurately reflect the signal formed in living diatoms.

2) The range of variations in micronutrients availability is fully recorded in sedimentary diatoms.

3) Change in micronutrient availability in the ocean triggers change in marine productivity and macronutrient utilisation

Diatom frustules present rough surfaces that can easily trap clays and other particles rich in metals, especially in sedimentary environment. Several mechanical and chemical cleaning steps are required to ensure that the frustules are free of terrigenous coating prior to measurement. However, with conventional methods (ICP-MS & OES) it is extremely difficult to guarantee that all the terrigenous material has been successfully eliminated. Unlike ICP-MS/OES techniques which involve dissolution of the sample, the Ion Microprobe method enables us to differentiate between the terrigenous coatings (potentially) remaining on the frustules surface from the biologically-fixed metals inside the siliceous matrix. This allows us to produce more accurate measurements of diatom-bound metals while bypassing the need to use more aggressive cleaning methods. We can also determine if exchange processes during early diagenesis in marine sediments affect the trace metal signal of the frustules.

Results

1) Is the signal accurately exported to the sea floor?

Culture experiments have shown that [Fe] (above a threshold value) and [Zn] in diatom frustules reflect the biological availability of these elements in the medium [4-6]. However, no test has been done to assess whether the signal is preserved in the sediment after the organisms' death. We analysed Si, Al, Fe, Mg, K, Ba, Na and Th in thoroughly cleaned diatoms (pressed on indium foil) from a sediment core and a sediment trap retrieved from the Gulf of California. The sediment trap samples consisted of settling

diatoms collected between March 1996 and February 1997. These samples are very well preserved and have not undergone diagenetic alteration. The comparison between the sedimentary and trap diatoms show that there is no increase in metal composition in the sediment and that in the gulf of California where diatom productivity and opal accumulation are high there is no noticeable diagenetic alteration of the trace metal signal in the diatoms (Fig. 1).

Figure 1: Average diatom-bound trace metal concentration (ppm) in sediment samples and trap samples from the Gulf of California. There is no enrichment in trace metal content in sedimentary diatoms.
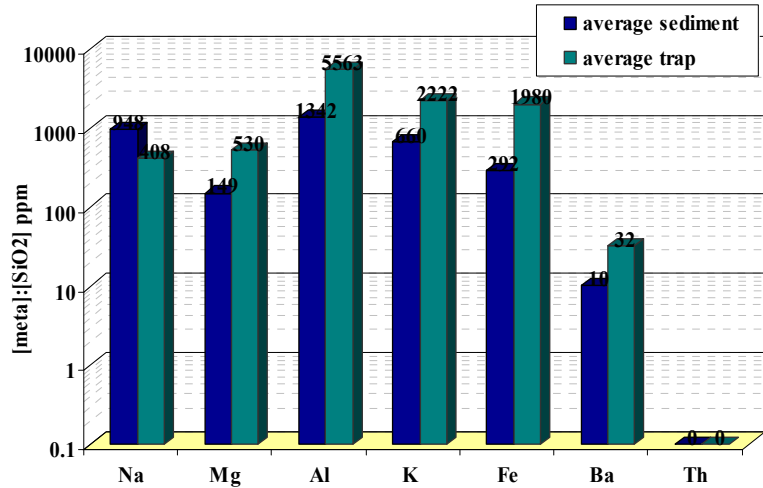
Diatom-bound trace metal signals from the trap show seasonal variations with higher levels of metals in summer during the stratified, low productivity season (Fig. 2). Overall trap diatoms have slightly higher diatom-bound trace metal concentrations than sedimentary diatoms. We attribute this to the fact that most diatom production and accumulation occurs in winter, when trace metal concentration is lower in the frustules.
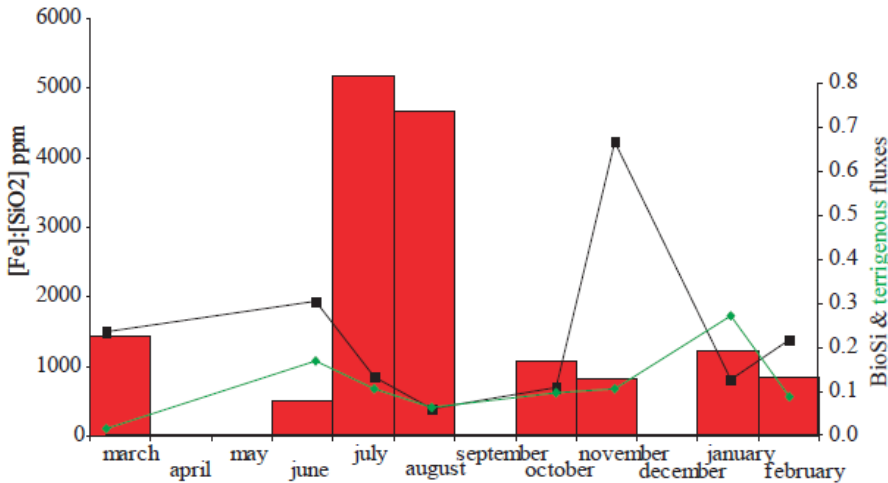
Figure 2: Seasonal variation in diatom-bound Fe concentrations (red bars) in the sediment trap samples compared to biogenic silica fluxes (black line) and terrigenous fluxes (green line) in the trap. Fe:SiO$_2$ increases sharply during the summer, when upwelling and biological demand of Fe decreases.

2)   Do diatoms record the full range of micronutrients concentration in the sea surface?
The range of micronutrients supply to different locations in the ocean can vary by several orders of magnitude [9,10]. We compared trace-metal signals in diatom frustules from the Gulf of California (trap samples) and the Weddell Sea, Southern Ocean (suspended diatoms). Models and data of dust deposition on the ocean surface show that the Gulf of California receives between 50 and 100 times more dust than the southern Ocean and hence much higher levels of iron for instance. We find that diatom bound trace metal concentration in the Gulf of California is 5 to 55 times higher than those from the Southern Ocean, depending on the metal (Fig. 3). While Mg and Na show the smallest increase, Fe, Al and Ba show the highest increase. Mg and Na are conservative elements in the ocean and their

average concentration in sea water is high. Therefore it is not surprising that their concentrations in surface water and in diatom frustules are less sensitive to (even large) spatial changes in dust/micronutrient inputs than those of iron and aluminium for instance. Therefore these results are strong indications that the diatom-bound trace metal signal adequately records the natural range of micronutrients availability in the sea surface, especially for iron.
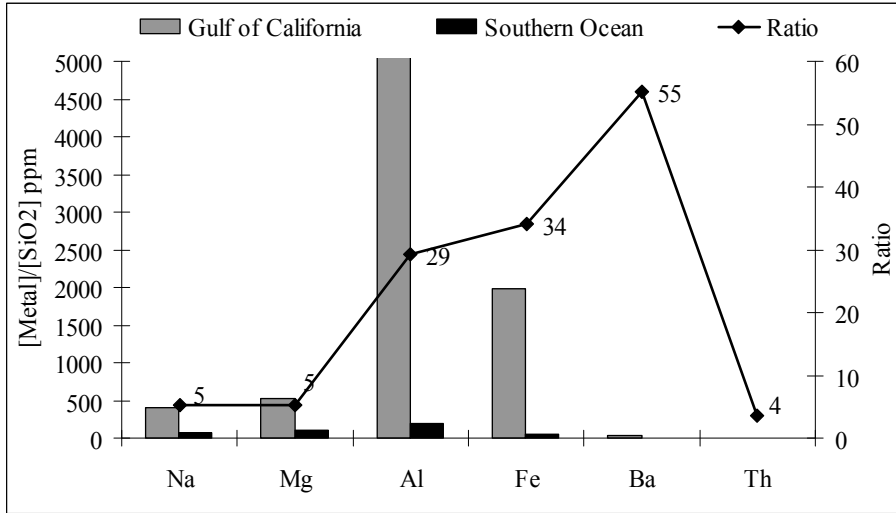

Figure 3: difference in diatom-bound trace metal concentration between the Southern Ocean and the Gulf of California.

3) *Temporal changes in micronutrient availability, macronutrient uptake and productivity:*
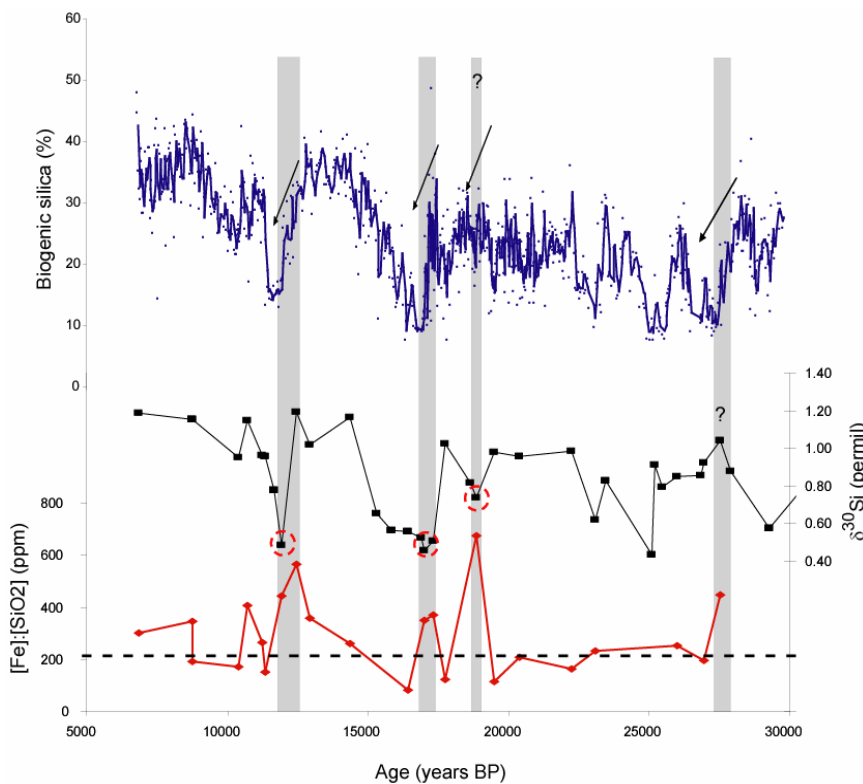
Figure 4: Down-core records of diatom-bound Fe concentration (red), silicon isotopes (black) and biogenic silica content (blue) in the sediment of the Gulf of California. Grey stripes and arrows highlight episodes of decreasing biogenic silica accumulation and silicic acid utilisation associated with increases in the Fe:SiO$_2$ ratio.

Seasonal variations in diatom-bound metal concentration in the Gulf of California (fig. 2) appear related to the biological demand: during intense, highly productive upwelling events in the winter, diatom-bound trace metal concentrations are low because micronutrients become limiting relative to macronutrient such as nitrate and silicic acid [11]. At the beginning of the less productive, stratified season, the biological demand for iron and other element decreases, resulting in higher metal content in the frustules (fig. 2). Therefore, the diatom-bound trace

metal signal appears to reflect changes in the biological demand for micronutrients. The down-core Fe:SiO$_2$ record from the Gulf of California is shown on figure 4. Values of around 200 ppm are measured for most of the record with occasional peaks up to 600 ppm. These peaks occur at times of decreasing biogenic silica accumulation (reduced productivity) and silicon isotope values (decreasing silicic acid relative utilisation by biota). Therefore, increases in diatom-bound Fe can be interpreted as indicators of decreasing biological demand for Fe by the phytoplankton. Conversely, low diatom-bound Fe concentration denotes conditions of iron limitation triggered by intense upwelling and biological demand for both micro and macronutrients.

Implications of the findings

1) Direct implications

Our results from the Gulf of California demonstrate for the first time that the trace metal signal recorded in diatom's hard part is transferred to the sediment without undergoing significant alteration during transport and burial, at least in areas where biogenic silica is well preserved in the sediment like in the Gulf of California. In order to apply the diatom-bound trace metal proxies to paleoceanographic studies it was imperative to test whether the signal recorded in the frustules was adequately preserved during transport and in the sediment. Therefore, our findings represent a crucial step towards the application of these new tools in sediment cores.

Existing studies of metal incorporation in diatom frustules so far were exclusively performed in culture experiments which generally fail to reproduce natural conditions adequately. Comparison of our results from the Southern Ocean and the Gulf of California suggests that in natural sea water diatoms are able to incorporate trace metals in proportion to their concentration/availability at the sea surface and can record a wide range of metal concentrations. Therefore our findings validate and strengthen the use of diatom-bound trace metal signals as tracers of micronutrient availability in the sea surface.

Our seasonal and down-core records of diatom-bound iron concentration from the Gulf of California reveal that Fe content in diatoms reflects the biological demand for iron at the sea surface rather than the flux of terrigenous iron and therefore has the ability to trace changes in the biological availability of the micronutrient.

2) Far reaching implications

Fe fertilisation of the ocean is proposed as a means to sequester carbon into the ocean as a mitigating strategy for atmospheric CO$_2$ increase and global warming. Large scale Fe fertilisation experiments have been conducted in the SO to understand biological response to such manipulations. Often these experiments produce variable results with large variations in carbon sequestration efficiencies and the long-term ecological impact of such manipulations remain uncertain. Such uncertainties are partly attributed to short time scales of these experiments. The use of diatom-bound trace metal signals in sediment cores will allow for the first time to document and understand how natural changes in Fe fertilisation in the past impacted biological productivity and CO$_2$ exchange in key regions of the ocean for carbon cycle changes.

In addition, the novel proxies have application well beyond paleoceanography. If diatom-bound trace metals reflect the bio-availability of metals during diatom growth then this can be directly applied to pollution studies in marine environments.

References

1   Martin, J. H. *et al.* (1994) *Nature* **371**, 123-129.
2   Falkowski, P. G. (1997) *Nature* **387**, 272-275.
3   Takeda, S. (1998) *Nature* **393**, 774-777.
4   Ellwood, M. J. & Hunter, K. A. (2000) *Limnology and Oceanography* **45**, 1517-1524.
5   Lal, D. *et al.* (2006) *Geochimica Et Cosmochimica Acta* **70**, 3275-3289.
6   Jaccard, T., Ariztegui, D. & Wilkinson, K. J. (2009) *Chemical Geology* **265**, 381-386.
7   Brzezinski, M. A. *et al.* (2002) *Research Letters* **29**.
8   Pichevin, L. E. *et al.* (2009**)** *Nature* **459**, 1114-U1198.
9   Jickells, T. D. *et al.* (2005) *Science* **308**, 67-71, doi:10.1126/science.1105959.
10   Mahowald, N. *et al.* (1999) *Journal of Geophysical Research-Atmospheres* **104**, 15895-15916.
11   Pichevin, L. *et al. Paleoceanography* (in press).

Geothermobarometery of coexisting garnet and clinopyroxene

Joe Pickles and Jon Blundy

School of Earth Sciences, University of Bristol, Bristol, BS8 1RJ

Introduction

Understanding deep earth processes, in the context of the prevailing pressure (P) and temperature (T) conditions, requires a knowledge of the phases present and the affinity of these phases to incorporate different elements at different conditions. This knowledge has an industrial application in the diamond exploration industry or can be used to enhance the understanding of the structure of the Earth and Earth's history through time.

Due to the scarcity of diamonds, even in diamond-rich sources, understanding the provenance of mantle minerals in relation to diamond/graphite stability is crucial. The primary source of diamonds at the Earth's surface are kimberlite volcanic pipes, which entrain parts of the surrounding mantle (xenoliths). Therefore, understanding the conditions at which the xenoliths and their constituent minerals last equilibrated is critical in predicting the presence or absence of diamond.

Garnet and clinopyroxene (cpx) are ubiquitous in the upper mantle and are the dominant xenoliths at a number of economically and scientifically important kimberlites. However, geobarometers which can be applied to garnet and cpx are incredibly limited. All geothermometers for the two minerals are limited to the exchange of Fe/Mg, any irregularities in the Fe will therefore give erroneous results from more than one thermometer.

Through high-pressure experiments this research investigates the potential for new geothermobarometers applicable to coexisting garnet and clinopyroxene. Trace elements were measured with the Cameca ims 4f and the affect of T and P on the partition coefficient investigated. The applicability of the lattice strain model [1] when applied to partitioning between garnet and cpx is also investigated.

Discussion

The data show that as pressure increases the partition coefficient (D=gnt/cpx) of Li increases with an increase in pressure. The trend has been identified previously, however, with the extra data generated it is possible to formulate a barometer applicable to eclogitic assemblages. The barometer can estimate experimental pressures to within 0.3 GPa and creates a valuable tool for mantle minerals.

The lattice strain model shows how the partitioning of elements between a mineral and its coexisting melt is a function of the ionic radius of the cation. The ease with which a crystal lattice will accommodate an element is dependent on the charge and size of the element and how stiff the lattice is. Work by [2] adapted the lattice strain model from mineral-melt to mineral-mineral to investigate the partitioning between olivine, opx and cpx. In this study the partitioning of trace elements between garnet and cpx is investigated with values calculated using the methods of [1] and [3]. The calculated values are compared to the experimental data. Figure 1 shows the data and the calculated fit. There is generally good agreement between the theory and the experiments.
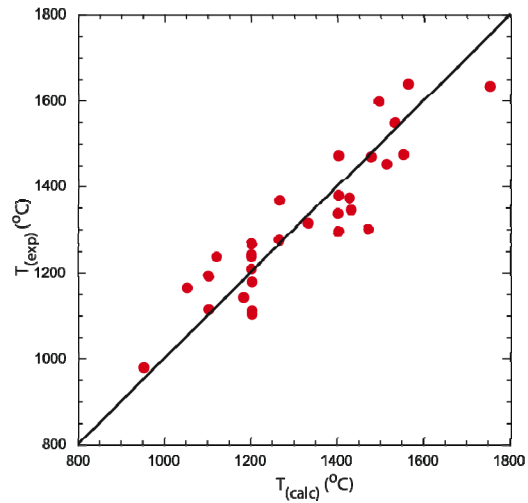
The slope of the rare earth elements against ionic radius has a temperature and composition dependence. This is calibrated to return a geothermometer. Figure 2 shows the calculated temperatures against the experimental temperatures. The model predicts the experimental temperatures to within 80 ^{o}C.

Summary

Through the data generated using the ion probe a new geothermometer and a new geothermometer have been developed. These models are applicable to coexisting garnet and cpx. The models have been calibrated on data from pressures above and below the diamond-graphite equilibrium and can be used in diamond exploration and to enhance the understanding of processes within the mantle.
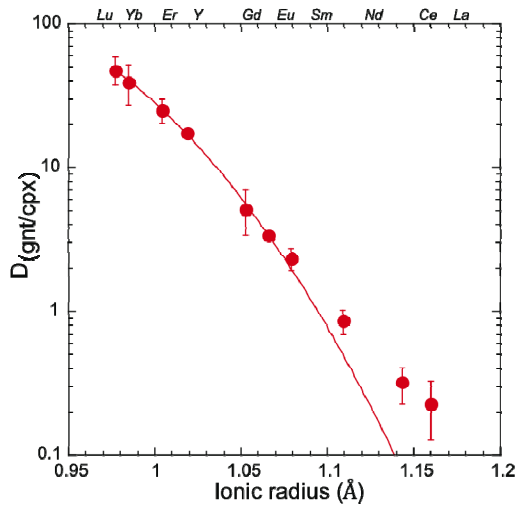
Figure 2. Partition coefficient of rare elements and Y partitioning between garnet and cpx. The red line shows the calculated fit based on values from [1] and [3].

Figure 1. Calculated temperature against experimental temperature. The calculated temperature uses the slope of the rare earth elements against ionic radius. The black line shows the 1:1 line.

References

[1] Wood and Blundy (1997) Contributions to Mineralogy and Petrology **129**, 166-181
[2] Lee et al. (2007) Geochimica et Cosmochimica Acta **71**, 481-496
[3] Van Westrenen and Draper (2007) Contributions to Mineralogy and Petrology **154**, 717-730

Degassing, and crystallisation of intermediate magmas at Volcan de Colima, Mexico

Olivier Reubi[1,2], Jonathan Blundy[1], Nicholas R. Varley[3]

[1] School of Earth Sciences, University of Bristol, BS8 1 RJ, Bristol, UK
[2] ETH Zurich, Institute of Geochemistry and Petrology, Switzerland
[3] Facultad de Ciencias, Universidad de Colima, Colima, Mexico

Introduction

In volatile-saturated magmas, degassing and crystallisation are interrelated processes which influence the eruption style. The causal relationship between these processes and their implications for short-term shifts in eruptive behaviour characteristic of intermediate subduction zone volcanoes are, however, still poorly understood. Phenocryst-hosted melt inclusions provide valuable information on the pre-eruptive volatile contents of arc magmas and on the degassing paths followed during their ascent through the upper crust. In addition, melt inclusions have been used to document the relationship between crystallisation and degassing. To establish the link between degassing, crystallisation, and eruption style, as well as the reliability of the volatile contents recorded by pyroxene hosted melt inclusions, we examined H_2O, CO_2, and selected trace element contents of melt inclusions from a suite of samples covering the 1998-2005 effusive and Vulcanian eruptions at Volcán de Colima, Mexico.
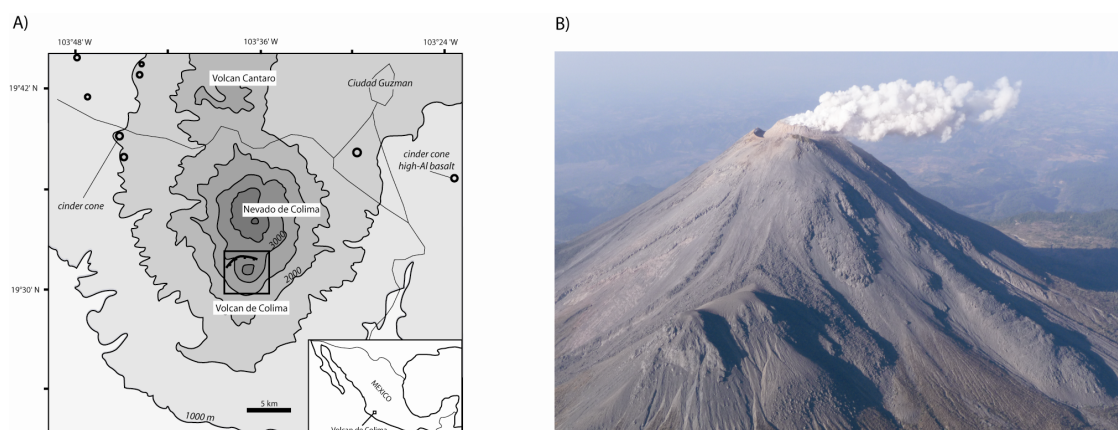

Figure 1. (a) Location map of Volcan de Colima. (b) Degassing event from the summit dome (Feb. 2011). Several of historical lava flows (from left to right 1961, 1975, and 1869) can be seen in the foreground.

Preliminary results & implications

All investigated magmas are andesitic in composition with 59.0-61.4 wt% SiO_2 (H_2O-free). The melt inclusions show a broad range of compositions and can be divided into two distinct chemical groups on the basis of their K_2O contents: termed "low-K" and "high-K" by [1]. Detailed investigation of the chemistry of low-K melt inclusions demonstrates that they effectively record the composition of the crystallizing melt and were not modified appreciably by post-entrapment crystallization processes (exception of H_2O in some cases). This group of inclusions can therefore be considered as representative of the evolution of the melt in the system prior to eruption and are used here to probe the relationship between degassing and crystallisation. The low-K melt inclusions have between 64.2 and 75.8 wt% SiO_2 (H_2O-free) and describe compositional trends consistent with crystallisation of the phenocryst assemblage. These inclusions have low H_2O contents (< 4.1 wt%) consistent with petrological estimates of magmatic H_2O contents. Their CO_2 contents range from 236 ppm to below detection limit (<12-28 ppm). Entrapment pressures calculated using the solubility model of Papale et al. (2006) [2] range from 160 to 3 MPa at 1000

°C, the average temperature obtained from two-pyroxene. This corresponds to entrapment depth between 9-0 km (below the summit level). This range closely matches the depths of volcano-tectonic seismic swarms recorded prior to the eruption of the 1998-99 lava flow [3]. This agreement is an additional indication that, overall, the melt inclusions efficiently record the ascent and crystallisation of the volatile-saturated magma column. Nevertheless, H_2O and CO_2 contents can not be ascribed to straightforward open or closed-system degassing. Systematic comparison with petrological H_2O contents estimates indicates that post-entrapment diffusive loss of H_2O affected some of the inclusions and overprinted the degassing trend. The implications of this in terms of time scales of magma ascent and degassing are currently investigated. The melt inclusions major elements, CO_2, and S contents indicate that decompression is driving crystallization, but this trend is superimposed on earlier, possibly vapour under saturated, crystallization that result in a range of melt composition reaching the vapour saturated liquidus. No systematic differences in volatile contents, degassing and crystallization trends, or ascent rates are observed between the Vulcanian explosive and effusive eruptions [4].

References
[1] Reubi, Blundy. Journal of Petrology, 2008. 49: p. 2221-2243.
[2] Papale, Moretti, Barbato. Chemical Geology, 2006. 229(1-3): p. 78-95.
[3] Zobin et al., Journal of Volcanology and Geothermal Research, 2002. 117(1-2): p. 47-60.
[4] Reubi, Blundy, Varley. Contribution to Mineralogy and Petrology, submitted.

# Preliminary view on radiolarian geochemistry using secondary ion mass-spectrometry (SIMS) microanalysis

Aleksey Sadekov[1,2], Kate Darling[1], Henry Elderfield[2]

[1]University of Edinburgh, School of GeoSciences, West Mains Road, Edinburgh EH9 3JW, UK.
[2]Department of Earth Sciences,University of Cambridge, Cambridge CB2 3EQ, UK

Geochemistry of radiolarian shells remains largely unknown compared with other marine protozoa such as foraminifera and diatoms, which are commonly-used proxies for paleoclimate reconstructions. This is primarily due to analytical difficulties in obtaining accurate measurements from the microscopic siliceous shells of radiolaria. In this pilot study, we employed a novel microanalytical approach to study radiolarian geochemistry with the primary aim of revaluating the potential use of radiolaria as paleoclimate proxy.

Preliminary results based on $\delta^{11}B$ composition of *Cenosphaera* sp. suggest that biogenic silica is prone to diagenesis, altering the outer shell surface and significantly modifying its geochemistry. However, our results also demonstrate that using microanalytical techniques, such as SIMS, it is possible to accurately analyse the unaltered parts of radiolarian shells and potentially use them for paleoclimate reconstructions.
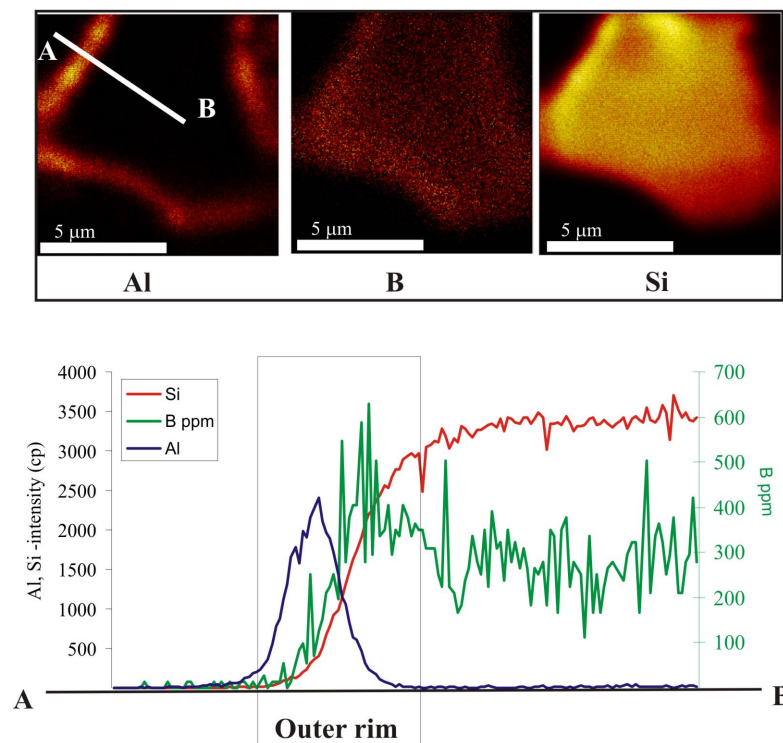
Fig. 1 Alteration/contamination of radiolarian shells as revealed by SIMS microanalysis. Top: Element maps showing distribution of Al, B and Si (in arbitrary units). Bottom: Plot displaying changes in element concentrations across the surface of radiolarian shells. Note presence of enrichment in aluminium and boron on the surface of the shell.

Carbon recycling in subduction zones

J. Blundy[1], S. Skora[1] & R. Brooker[1]

[1]Department of Earth Sciences, University of Bristol, Bristol BS8 1RJ, UK

Introduction: The planetary carbon cycle has important consequences for a range of important subjects such as planetary accretion, Earth's climate, diamond formation, carbonatite volcanism and mantle metasomatism. Subduction zones provide the major geotectonic settings where surface carbon can enter the Earth, and potentially return via arc volcanism. To date, experimental phase equilibria studies as well as thermodynamic calculations suggest that carbonates behave refractory in subducting slab lithologies during dehydration. Moreover, partial melting does not seem to liberate any carbon either from basaltic crust or pelitic sediments at fluid-absent conditions, mostly owing to a (apparent) solidus temperature that is significantly higher than any common subduction zone geotherm. This contrasts to observations from nature, where CO_2 is clearly emitted by arc volcanoes. Stable isotopic characteristics further suggest that most of this arc carbon is sediment-derived. The challenge is to relate the release of CO_2 at sub-arc depths to explain the high arc-flux of CO_2. This study aims to test the hypothesis that calcareous lithologies melt more readily at sub-arc conditions in the presence of external water, similarly to melting of non-calcareous lithologies (e.g. [1]).

Experiments and results: Two different calcareous lithologies were picked from the southern Lesser Antilles arc – one containing approx. 5% ("low C" lithology) and one with approx. 35% carbonate ("high C" lithology). Experiments were conducted at 3 GPa over a range of temperatures (800-1200°C), with 15 wt% of water added on top of structurally-bound water (total water content $\approx$ 24 wt%; fluid/rock ratios $\approx$ 1.3). The high H_2O content is designed to simulate fluxing by serpentine-derived fluids in the slab. The sub solidus phase assemblage is quartz + phengite + carbonate + epidote/clinozoisite + clinopyroxene ± garnet (+ ilmenite/rutile). A glass phase appears at 800-850°C, exhausting quartz, clinopyroxene and phengite. The solidus temperature is hence constrained to be at around 800°C. This is in contrast to previous studies who have placed the solidus at T > 900°C at 3 GPa at fluid-absent conditions. At 1100-1200°C, silicate glass coexists with carbonatite melt in the high C lithology, whereas glass is the only phase present in the low C lithology. We also have abundant textural evidences for an additional vapour phase being present in all experiments at run conditions. Quenched glasses are vesicular, evidencing that some degassing has occurred upon quench. H_2O and CO_2 measurements revealed that around 5-12 wt% H_2O and 1-5 wt% CO_2 are quenched into the glasses (Fig. 1). The total volatile content is approximately constant at around 10-12 wt%, suggesting that this is the maximum amount of volatiles that can be quenched into hydrous granitic glasses. Note that H_2O and CO_2 correlate negatively, suggesting quench modification (Fig. 1).

Discussion: Our results have very important implications for the recycling of CO_2 in subduction zones. Firstly it is immediately clear from our experiments that calcareous lithologies melt readily at sub-arc conditions (approx. 800°C, 3 GPa) in the presence of external water, thereby carrying considerable amounts of dissolved carbon into the overlying mantle wedge. The actual CO_2 solubility is not well constrained by our experiments because we have evidences that CO_2 degassing has occurred upon quench. However, highest CO2 measurements still constrain minimum CO_2 solubility in hydrous granitic melts. CO_2 measurements as high as 5-7 wt% are considerable higher compared to high pressure CO_2 data determined in dry granitic melts (Fig. 2, note that CO_2 solubility is mostly independent of temperature, but strongly dependant on melt composition, water content and pressure). We speculate that the addition of water has changed the speciation from molecular CO_2 only in dry granitic melts to molecular CO_2 and CO_3^{2-}, accompanied by an increase in its solubility (similar to what has been found by King & Holloway [2] for andesitic melts at lower pressures). We hence suggest that 5-7 wt% of CO_2 (or more) dissolved in large amounts of hydrous melts (e.g. at 850°C, low C lithology, over 60% melt is present) explains the return flux of CO_2 to the surface in arc volcanoes!

In addition, our experiments demonstrated for the first time that CO_2 has a dramatic effect for the location of the second critical endpoint – the PT conditions above which silicate melts and siliceous fluids are fully miscible. In carbon-free systems, supercritical conditions might be reached (or almost

reached) at 2.5-3 GPa and 800°C (e.g. Klimm et al. 2008, Skora and Blundy 2010). Hydrous melts of the latter two studies, for example, were estimated to have contained around 30-50 wt% H_2O in hydrous glasses at 800°C. In this study, for example, we have found that at 1100°C, 3 GPa (low C lithology), a silicate glass is coexisting with a vapour phase, where the total water content of the experiments was only around 24 wt%.
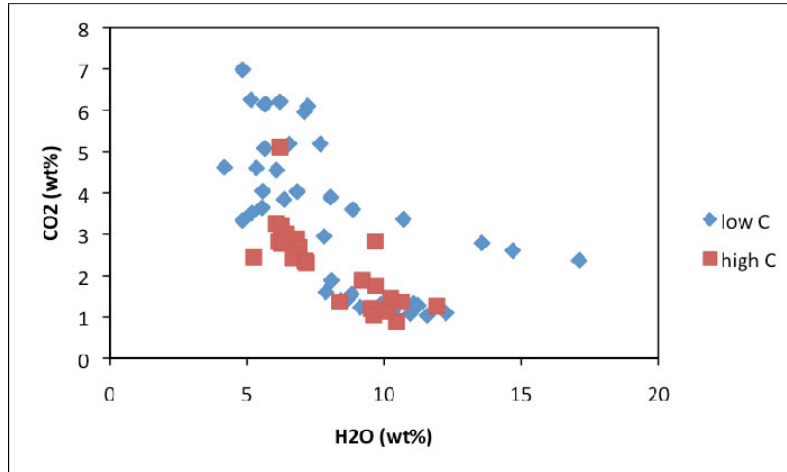
Figure 1. Plot of measured CO_2 versus H_2O data of this study. The data resembles a degassing trend, in concordance with textural evidences for degassing (vesicular glasses). Note that the total volatile content is always around 10-12 wt%, which appears to be the maximum volatile content that can be quenched into hydrous granitic glasses. However, highest CO_2 data still constrain minimum CO_2 solubility into hydrous granitic melts at high-pressure conditions.
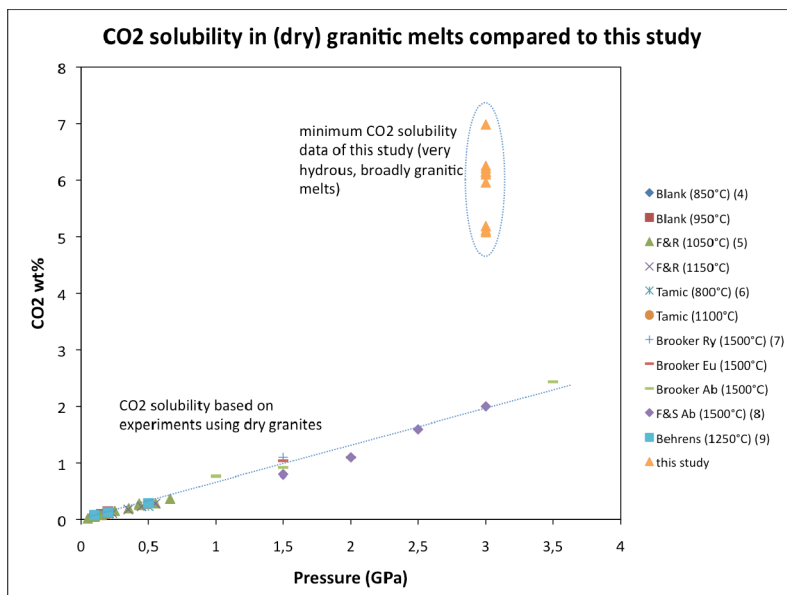
Figure 2. Plot of highest measured CO_2 data of this study compared to CO_2 solubility data of dry granites. CO_2 measurements as high as 5-7 wt% are considerable higher when compared to high pressure CO_2 data determined in dry granitic melts. We speculate that the addition of water has changed the speciation from molecular CO_2 only in dry granitic melts to molecular CO_2 and CO_3^{2-}, accompanied by an increase in its solubility.

References

[1] S. Skora & J.D. Blundy, J. Petrol. **51** (2010), 2211-2243.
[2] P.L. King & J.R. Holloway, GCA **359** (2002), 117-122.
[3] K. Klimm, J.D. Blundy & T.H. Green, J. Petrol. **49** (2008), 523-553.
[4] J.G. Blank, E.M. Stolper & M.R. Carrroll, EPSL **119** (1993), 27-36.
[5] R.A. Fogel & M.J. Rutherford, Am. Min. **75** (1990), 1311-1326.
[6] N. Tamic, H. Behrens & F. Holtz, Chem. Geol. **174** (2001) 333-347.
[7] R.A. Brooker, S.C. Kohn, J.R. Holloway, P.F. McMillan & M.R. Carroll, GCA **63** (1999) 3549-3565.
[8] G. Fine & E. Stolper, CMP **91** (1985), 105-121.
[9] H. Behrens, S. Ohlhorst, F. Holtz & M. Champenois, GCA **68** (2004), 4687-4703.

Magma storage and differentiation beneath Grenada (Lesser Antilles)

C.C.Stamper[1], J.D.Blundy[1], E.Melekhova[1] & R.J.Arculus[2]

[1]Department of Earth Sciences, University of Bristol, Bristol, BS8 1RJ, UK
[2]Research School of Earth Sciences, The Australian National University, Canberra 0200, Australia

Background

The igneous cumulate suite of the volcanic island of Grenada, Lesser Antilles is notable for its petrologic diversity, comprising wehrlites, hornblendites, clinopyroxenites and a variety of gabbros. Whilst the textures testify to a relatively simple crystallisation history, the impressive array of assemblages from this island arc volcano reflects a wide range of magmatic storage conditions. The ultimate goal of this project is to replicate the various cumulate assemblages by conducting equilibrium experiments on parental basalts under a range of volatile (H_2O, CO_2) contents, temperatures, pressures and fO_2, and so elucidate the conditions of magma storage and differentiation beneath Grenada. Initial experiments have focussed on determining the topology of the parental basalt liquidus and the near-liquidus phase relations. Experiments were carried out in the pressure range 0.0001-1.7 GPa using 1 atm furnace, TZM pressure vessel and piston cylinder apparatus employing a double capsule technique[1]; run products were ubiquitously glassy and contained a high melt fraction (f>0.60).

Purpose of SIMS analysis

The purpose of SIMS analysis in this project was twofold. Firstly, it was used to accurately determine the H_2O and CO_2 content of parental Grenadan melts by analysing the dissolved volatile contents of glassy melt inclusions from lava phenocrysts. These values were used to inform the nature of future experiments. Secondly, it allowed measurement of dissolved volatiles in experimental run products. Equilibrium experiments have been carried out using two different water contents, so it was important to verify that these conditions had been maintained throughout experimental runs. In addition, other volatiles species such as CO_2 (as carbon) and boron have the potential to diffuse into the noble metal capsules and can influence phase relations. If they were present, it was essential to quantity the amount present and modify the design of future experiments.
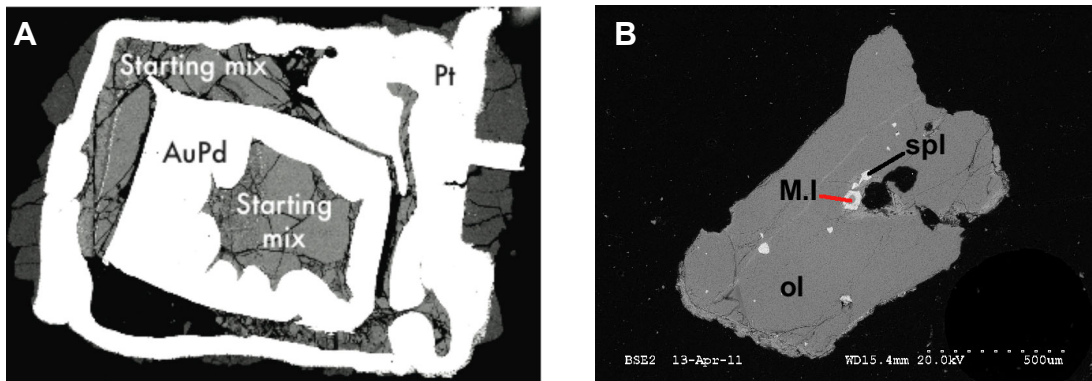
Figure 1. (a) BSE image of a piston cylinder run product comprising inner and outer capsule. White areas are noble metal, greyscale gives position of glass and crystals. Horizontal scale = 6mm. **(b)** BSE image of olivine phenocryst (0.5mm in size) containing a glassy melt inclusion (M.I) trapped within a spinel.

Results

a) Melt inclusions

Several hundred olivines were picked from scoria sampled from Queen's Park, Grenada. The paucity of vitreous melt inclusions from Grenadan samples has been noted by other studies[2] and very few melt inclusions in the olivines were suitable for SIMS analysis. In addition, their small size (<25μm) increased the likelihood of the analysis being contaminated by the surrounding mineral host. Ultimately, four olivine-hosted melt inclusions were successfully analysed for dissolved CO_2 and

H₂O. H$_2$O ranged from 0.43-0.93 wt %, falling well below the maximum measured water contents for Grenada[2,3]. This corroborates previous studies that have shown there is significant variation in H_2O content of parental melt batches[2]. CO_2 in melt inclusions has not previously been investigated at Grenada and the four analysed in this study yielded values between 40-3100ppm. Whilst displaying a large range, the non-negligible analyses hint that primitive arc magmas may have a significant CO_2 content[4].

b) Experiments

   The inner and outer capsule glasses of seventeen experimental run products were analysed for H_2O, CO_2 and B. Starting materials contained two different water contents (0.0 and 3.0 wt %) and were nominally free of CO_2 and B. The double capsule design was proven to be effective at preventing B flux into the inner capsule regardless of whether boron nitride was included in the assembly design: the maximum outer capsule B content was 2640ppm but did not exceed 200ppm in inner capsule glasses. However, the same was not found to hold for CO_2. The piston cylinder experiments contained <1.38 wt% CO_2 in the inner capsule, showing that carbon ingress was a significant problem. In contrast the TZM glasses contained only <365ppm CO_2. This information allowed us to isolate the source of carbon to be the graphite furnace and modify the design of future experiments. H_2O content of the water-bearing experiments was constant at 3.0 ± 0.4 wt %; anhydrous experiments yielded glasses with <0.28 wt % H_2O. That the appropriate H_2O content was maintained throughout the duration of the experimental run facilitated the quantification of the effect of pressure and temperature on the topology of the basalt liquidus and delineation of the near-liquidus phase relations.

References
[1] LJ Hall et al. (2004) Mineral. Mag, **68**, 75-81.
[2] JD Devine (1995) J. Volcanol. Geotherm. Res, **63**, 1-33.
[3] A-S Bouvier et al. (2010) Geochem. Geophys. Geosystem., **11**, Q09004.
[4] JD Blundy et al. (2010) EPSL, **290**, 289-301.

Trace element composition of 'superdeep' diamond inclusions

A.R. Thomson[1], M.J. Walter[1], S.C. Kohn[1], B.C. Russell[1], G.P. Bulanova[1], C.B. Smith[1] and D.J. Araujo[2]

[1]School of Earth Sciences, University of Bristol, Bristol, BS8 1RJ, UK
[2]Instituto de Geociências, Universidade de Brasília, CEP 70910-900 Brasília, DF, Brazil

Introduction & Background

Over the past 30 years, multiple studies of inclusions hosted in naturally occurring diamonds have identified minerals that are sub-lithospheric in origin [1]. Recently, a suite of inclusions from Brazilian diamonds was discovered that contains the entire experimentally determined lower mantle phase assemblage for basaltic composition [2]. The discovery of these stones, from the Juina-5 kimberlite pipe, implies the subduction of ocean-floor material into the lower mantle and subsequent diamond growth from carbon-bearing fluids or melts.
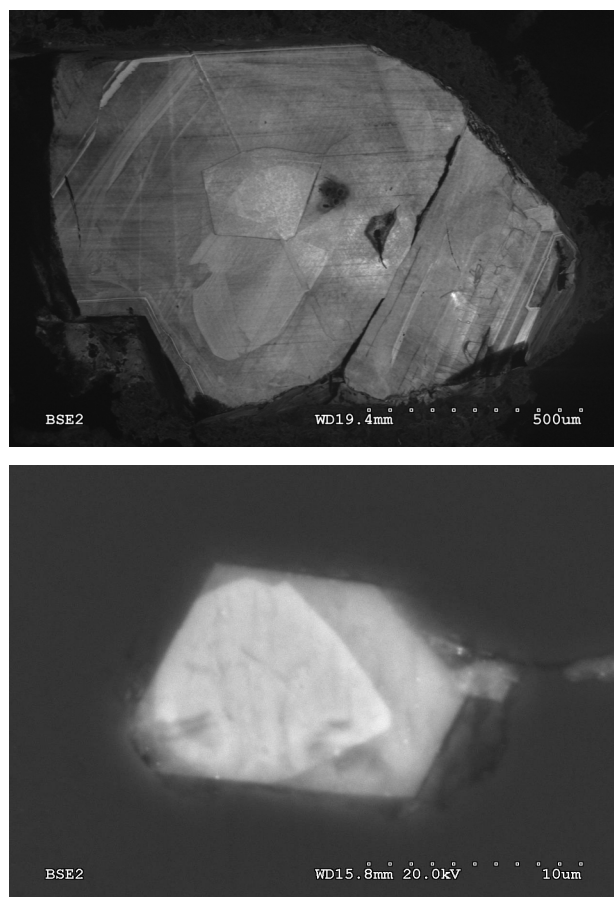
The aim of this study is to determine the trace element characteristics of sub-lithospheric diamond inclusions from Brazilian kimberlite pipes. This suite includes the basaltic, lower mantle, inclusions previously reported [2] along with supplementary samples of similar composition. Many of the inclusions have undergone retrograde reactions and/or unmixing during ascent to the surface, transforming the original lower mantle minerals into composite multi-phase inclusions (e.g. Fig 1). Inclusions analysed include several examples of unmixed NAL ("new aluminous") phase, iron-rich phases with stoichiometry similar to TAPP (tetragonal almandine-pyrope phase), possible magnesium silicate perovskite inclusions, and multiple calcium- and titanium-rich phases with a perovskite composition amongst other sub-lithospheric minerals.

Figure 1. (above) A CL image of one diamond, showing it has undergone a complicated history of nucleation and growth. (below) Backscattered electron image of an NAL phase inclusion which has unmixed on ascent.

Determination of the trace element signature preserved in 'superdeep' inclusions has the potential to elucidate a much greater understanding of the transition zone and lower mantle. By attempting to model trace element data, current hypotheses regarding sub-lithospheric mantle melts and diamond growth may be tested.
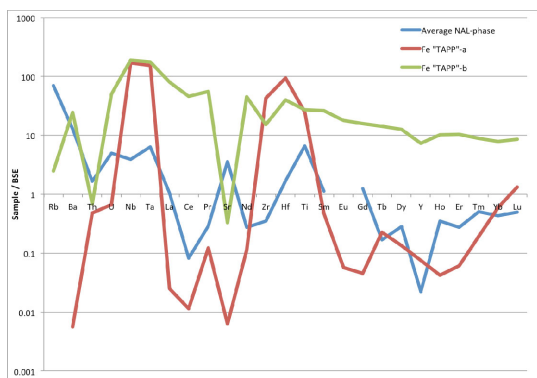
Results

SIMS analyses have allowed characterisation of the trace element composition of natural NAL and CF (calcium ferrite structure) phases for the first time. It is observed that NAL phase is a compatible host for the LILE and HFSE, as they are enriched by 1-10 times relative to bulk silicate earth (BSE). In contrast the REE are incompatible in NAL (Fig. 2).

Analysis of the iron-rich TAPP-like minerals has found two contrasting trace element patterns (Fig. 2). The first is similar to that previously documented from the Collier-4 kimberlite pipe [3], showing strong enrichment (up to 100 times BSE) in Nb, Ta, Zr, Hf and Ti with the concentration of all other elements a fraction of BSE. The second type of trace element pattern shows enrichment in all elements, except the LILE, relative to BSE.

Figure 2. Normalised trace element patterns of an averaged NAL composition (blue line), and examples of iron-rich TAPP-like minerals (green and red line).

Initial modelling has been undertaken using data gathered from analyses of calcium- and titanium-perovskite phases (with a Ca(Si,Ti)O₃ stoichiometry). These phases, as with previously reported samples [3], are very highly enriched in the REE (up to 70,000 times BSE) and show relative depletions in the HFSE and strong depletions in LILE (fig. 3). Partition coefficients determined experimentally in CO_2 bearing systems [4] have been utilised to calculate the melt that would have crystallised the analysed inclusions. The source rock capable of generating such a melt, by transition zone partial melting, has been computed by employing a melting reaction [5] and suitable partition coefficients. This calculated source is found to be very comparable with MORB (fig. 3). It may be suggested that the difference between MORB and the model output could be accounted for by fluid interaction with the slab in a relatively shallow subduction zone setting, allowing Sr to be removed and Nb, Zr and Hf retained preferentially in accessory phases. This would also allow a small enrichment of the HREE signature.
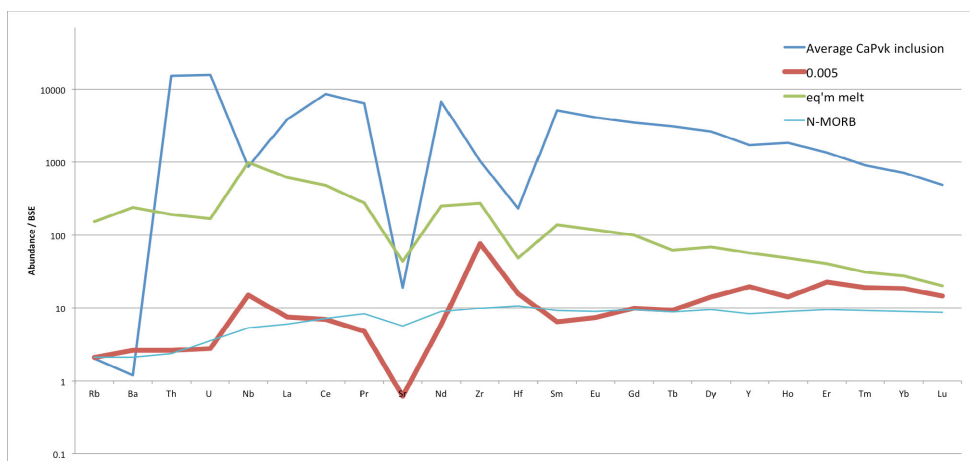
Figure 3. Results of initial trace element modelling for calcium-rich perovskite inclusions. Dark-blue line is an average of inclusion compositions. Green line is the calculated melt that crystallised the inclusion. The red line is the calculated source rock, from which 0.5% fractional melting creates the melt. The light blue line is N-MORB.

Conclusions & Further Work

This study has successfully quantified the trace element composition of sub-lithospheric minerals found in diamond-hosted inclusions, including the trace element characterisation of natural NAL and CF phases for the first time. It has also been possible to demonstrate that the chemistry of some of the inclusions can be explained by crystallisation of a melt generated from subducting oceanic-floor material.

Analysis and interpretation of data is currently in an early stage, and is on-going. It is anticipated the current model can be extended to incorporate data from further phases. This will potentially provide an explanation that reveals details of the geochemical, and perhaps geophysical, processes occurring in the deep diamond formation regions. Future carbon isotope analyses on the same 'superdeep' diamond samples studied here will allow identification of the carbon source for diamond growth.

References

[1] B. Harte (2010) Mineralogical Magazine **74**, 189-215, [2] M.J. Walter et al. (2011) Science **334**, 54-57, [3] G.P. Bulanova et al. (2010) Contributions to Mineralogy and Petrology **160,** 489-510, [4] C. Dalou et al. (2009) Geochimica et Cosmochimica Acta **73,** 239–255, [5] S. Keshav and G. H. Gudfinnsson (2010) Journal of Geophysical Research **115**

Major, trace and volatile chemistry of the March to May 2010 basaltic flank and benmorite summit eruptions at Eyjafjöll volcano, Iceland

T. Thordarson, M.E. Hartley, C. Hayward & J.G. Fitton

School of GeoSciences, University of Edinburgh, Edinburgh EH9 3JW, UK

Background

The 14th April-22 May eruption at Eyjafjallajökull volcano (Iceland), caused significant social and economic disruption in the UK and Europe, because of its ash-rich nature and the state of atmospheric flow. This explosive benmorite summit eruption, together with its predecessor, the 20 March to 12 April alkali (FeTi) basalt flank eruption at Fimmvörðuháls, has provided an opportunity to study and quantify a set of interlinked magmatic and volcanic processes extending from the source to place of deposition of the erupted magma [1,2,3]. Researchers at the University of Edinburgh have, together with colleagues in Iceland, France, Italy, Norway and United Kingdom have formed an informal multidisciplinary collaborative research alliance. This alliance is engaged in a multifaceted study integrating volcanological, petrochemical, and geophysical aspects of these eruptions.

Objectives

This two-day ion probe session was a follow up on the work done under the two one-day scoping studies undertaken in 2010 to further underpin the findings reported on in our 2011 report. Part of the results obtained from the 2011 session were published in our recent JGR paper [1], while the whole data set will be published in the forthcoming manuscripts [2,3].

Results

The primitive flank magmas of Eyjafjallajökull volcano, erupted at the Fimmvörðuháls Pass and recorded in MIs in olivines with Fo > 80, have an average volatile content of 1058 ppm S, 273 ppm Cl, 542 ppm F and 0.98 wt% H_2O. Melt inclusions trapped in early formed minerals, such as magnesian olivine phenocrysts, are potentially undegassed and therefore could hold clues to the primitive volatile composition of the erupted magma. However, MIs may form in minerals crystallizing from partially degassed magma, MIs may leak if fractures are present, hydrogen may diffuse out of the inclusion and fast-diffusion species may enter from the melt around the host crystals into the MIs. In this study, only MIs with no visible fracture or dislocation boundaries were chosen for analyses (Figure 1). Hydrogen diffusion out of the olivine during natural cooling of the sample cannot be excluded and such diffusion might explain the low water content of B2.

Alternatively, this MI represents a partially H_2O degassed melt. The facts that the average Cl/K_2O of all inclusions is close to the value of 0.06 ± 0.02, typical for Icelandic basalts ($Cl/K_2O = 0.04$), the H_2O, F and Cl concentrations and S/Cl are close to those from other mantle-plume related magmas (e.g., $S/K_2O = 0.05-0.4$, S/Cl = 0.5–6) implies negligible degassing of the MIs.
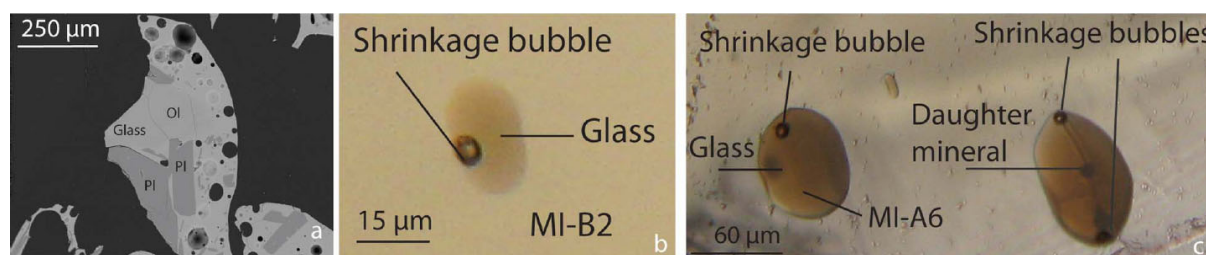

Figure 1. (a) Backscattered-electron images of individual tephra grain from Fimmvörðuháls eruption showing glass and homogeneous crystals (Ol: olivine, Pl: plagioclase). (b) Melt inclusion in olivine Fo < 80 showing only glass and a shrinkage bubble. (c) Melt inclusions in olivine Fo ≥ 80: The inclusion to the left contains only glass and a shrinkage bubble, whereas that to the right MI contains two shrinkage bubbles and visible daughter minerals. Only MIs without daughter minerals were analyzed in this study.

In addition, their water concentration and H_2O/K_2O (except for B2) are also consistent with those measured in subglacial basaltic glasses from Iceland (Figure 2), which are likely to reflect the juvenile water concentrations ($H_2O/K_2O = 0.1–2$). These arguments allow us to assume that most of the MIs represent undegassed melts with juvenile S, Cl, F and H_2O concentrations.
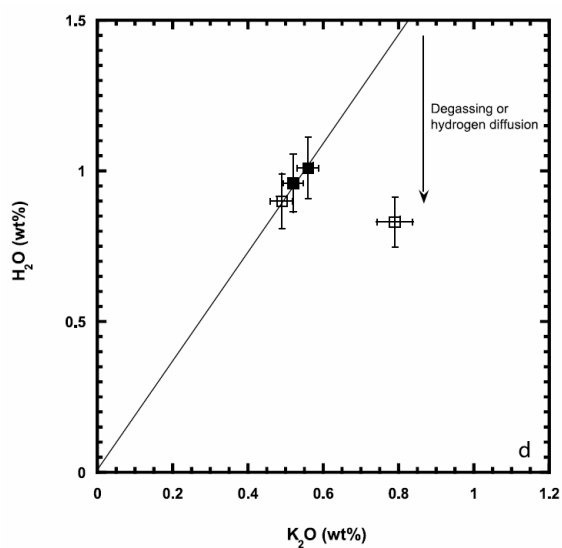

Figure 2. Evolution of the dissolved volatile concentrations in Fimmvörðuháls melt inclusions (MIs) as a function of K_2O concentration. A few of the more evolved MIs seem to have trapped a melt already degassed in water and sulfur.

References

[1] S. Moune, O. Sigmarsson, P. Schiano, T. Thordarson and J. K. Keiding (2012) Melt inclusion constraints on the magma source of Eyjafjallajökull 2010 flank eruption. Journal of Geophysical Research 117, B00C07, doi:10.1029/2011JB008718.

[2] Thordarson, T. et al., Volatile contents and degassing history of the 14 April–22 May 2010 summit eruption at Eyjafjallajökull volcano, Iceland, in prep for JGR Joint Atmosphere and Solid Earth Special Issue on the 2010 Eyjafjallajökull eruptions. Haywood J., S. Loughlin, T. Thordarson [Guest Editors]

[3] Hayward C., Volatiles and magma degassing in the 20 March–12 April 2010 Fimmvörðuháls eruption, Eyjafjallajökull volcano, Iceland, in prep for JGR Joint Atmosphere and Solid Earth Special Issue on the 2010 Eyjafjallajökull eruptions. Haywood J., S. Loughlin, T. Thordarson [Guest Editors]

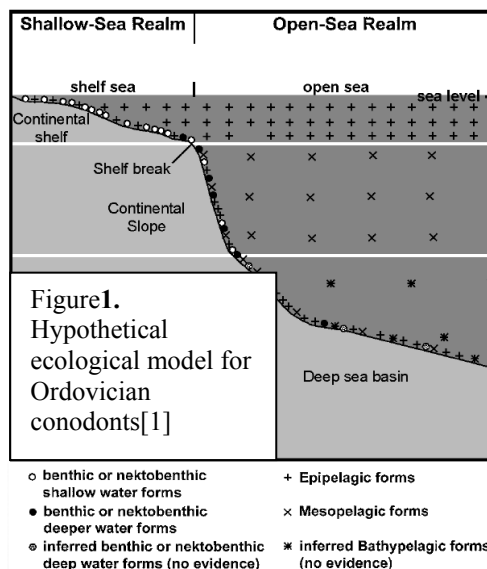# Constraining conodont δ^{18}O for marine Palaeozoic palaeothermometry

J.R. Wheeley[1], M.P. Smith[2] & I. Boomer[1]

[1]School of Geography, Earth and Environmental Sciences, University of Birmingham, Birmingham EH9 3JW, UK

[2]Oxford University Museum of Natural History, Parks Road, Oxford OX1 3PW, UK

Introduction

A number of models and variants have been proposed for conodont palaeoecology across different time intervals based on the distribution patterns of taxa within sediments. Most models invoke the presence of both pelagic and nektobenthic lifestyles and the recognition of bathymetrically based assemblages (e.g. **Figure 1**). However, research into conodont δ^{18}O via traditional bulk trisilverphosphate methods suggests that for a range of Ordovician taxa predicted to have lived at different depths, and thus potentially in water masses with different temperatures and isotopic composition, there is no significant difference in δ^{18}O between taxa [2]. Our previous ion microprobe investigations on Ordovician conodonts have, however, identified variation in δ^{18}O between taxa assigned to differing life habits, which potentially result from their occupation of different water masses with contrasting temperatures [3].

Figure **1**. Hypothetical ecological model for Ordovician conodonts[1]

○ benthic or nektobenthic shallow water forms
● benthic or nektobenthic deeper water forms
◉ inferred benthic or nektobenthic deep water forms (no evidence)
+ Epipelagic forms
× Mesopelagic forms
✳ inferred Bathypelagic forms (no evidence)

Figure 2. Lower Ordovician, Point of Head section, Cow Head Peninsula, Newfoundland, Canada, being sampled for conodonts.

2011 analyses

Our latest ion microprobe analyses have been aimed at building the isotopic dataset for testing models of conodont palaeoecology and particularly to see if taxa with different life habits record the thermal structure of Ordovician and Carboniferous oceans. This line of enquiry has immense potential for reconstructing oceanic thermal structures and testing models of upwelling for example. With material from the Ordovician of Canada (**Figure 2**), from a unique shelf-edge setting that contains both pelagic and nektobenthic conodonts of significantly different bathymetries and the Carboniferous of Iowa, we have begun to investigate how conodonts archive temperature and/or water mass differences in oxygen isotope composition.

Multiple individual elements of a range of taxa from Ordovician and Carboniferous samples have been analysed to test for both inter- and intra-species variability. The focus in the initial stage of this study has been to target taxa with contrasting morphologies (e.g. **Figure 3**) as these may be indicative of variable palaeoecologies.
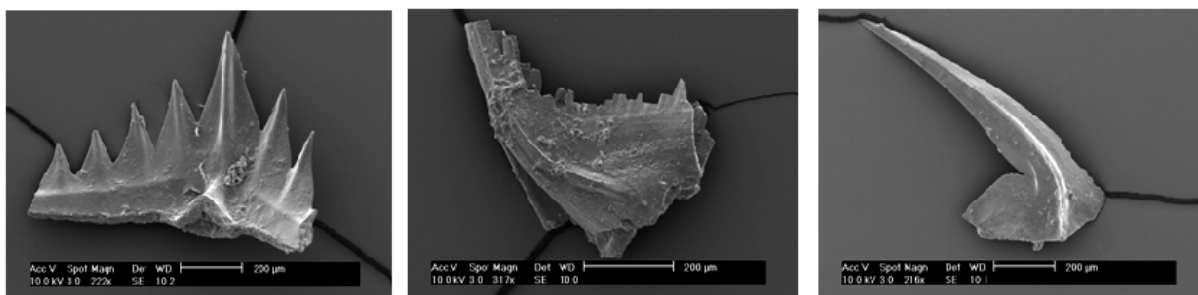
Figure 3. Examples of conodonts from the Lower Ordovician, Point of Head section, Newfoundland, Canada. From left to right: *Bergstromognathus extensus*; *Oepikodus evae* and *Oistodus aff. O. lanceolatus.*

Analyses of conodonts were undertaken on the Cameca 1270 in December 2011 following the protocols for ion microprobe analysis of conodonts set out by [3]. Results of spot analyses for oxygen isotopes yield generally consistent species signals for Carboniferous and Ordovician material but there is some significant (~1.5‰) inter-species variability between several of the Ordovician taxa investigated (**Figure 4**).
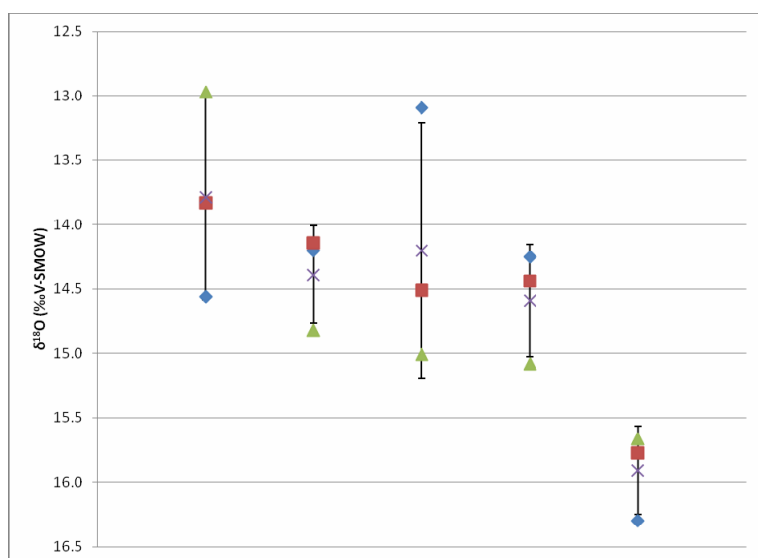
Figure 4. δ^{18}O (‰V-SMOW) values for 5 species of Ordovician conodont. Three conodont 'elements' were analysed for each species; mean is shown with x along with standard deviation error bars. Note that the y-axis is reversed – potentially warmer surface waters at top of plot, cooler deeper water towards the lower part.

The inter-species variability of ~1.5‰ in the Ordovician sample is comparable with the magnitude reported between some species of a mid-Ordovician (Darriwilian) sample analysed previously [3]. This latest finding suggests that such isotopic offsets between taxa may be 'real' and this has implications for choosing taxa for seawater temperature profile curves. It is possible that the isotopic range present in the Ordovician sample analysed represents species occupying a range of depths in the water column. The intra-species consistency in δ^{18}O is within 1‰ in three out of the five taxa investigated from this sample, which is consistent with previous analyses of multiple representatives of sample species [3].

Future work

Incorporation of further analyses of species to this initial data set will help to determine the extent of oxygen isotopic offset between conodont taxa. Additionally, comparing a range of conodont 'element' types from the same species will help build up a picture of how consistent oxygen isotopes are within species.

References
[1] Zhen, Y.Y. & Percival, I.G. (2003) Lethaia **36**,357–370.
[2] Buggisch, W. et al. (2010) Geology **38**, 327–330.
[3] J.R. Wheeley et al. (2012) Journal of the Geological Society London **169** (in press).

Quantifying the dynamics of calcite cement growth with oil emplacement

Thorpe, D.T.[1] & Wood, R.A.[1]

[1]School of GeoSciences, University of Edinburgh, Edinburgh EH9 3JW, UK

Introduction

Pore space in sedimentary rocks is known to decrease regularly with increasing burial depth but subsurface oil reservoirs are a notable exception to this pattern. Oil reservoirs have greater porosity than their depth would indicate because they contain less cement than the surrounding rocks [1]. When oil fills pores in sediments, water is partially displaced, and, as water is the medium for diagenetic reactions, cementation is inhibited or retarded [2].

Cementation and oil migration are thought to occur synchronously, but the oil-filling of reservoirs is a gradual process where pores in the crest are filled first [3]. Cement growth will therefore cease or slow initially in the crest and continue down structure until the final oil/water contact is reached. Below the oil/water contact cementation can continue as long as conditions are right for precipitation in the water-saturated pores and space exists into which cement can grow. In both quartz-cemented sandstone reservoirs [1] and calcite-cemented carbonate reservoirs [4], cements within the oil leg contain inclusions of oil, indicating that they grew in pores that contained both water and oil.

The notion that cement growth and oil charge occur synchronously over millions of years during burial means that the conditions under which the cements grow change. Temperature will rise and formation waters evolve through reactions with the rocks during burial and with the passage of time. These changes should be reflected in the chemistry of the cement. Calcite precipitated during burial will experience rising temperatures with increasing depth, leading to progressively lower $\delta^{18}O$ $_{VPDB}$ values. The ^{18}O evolution of formation waters is variable but commonly becomes greater due to calcite dissolution/re-precipitation reactions. Although these effects may cancel one another out, many analyzed late calcites show decreasing ^{18}O $_{VPDB}$ values related to increasing temperature during burial.

Here we have generated $\delta^{18}O$ data derived from *in situ* ion microprobe measurements to explore the dynamic relationship between cement growth and oil emplacement in a giant Lower Cretaceous carbonate reservoir from Abu Dhabi.

Objectives, aims and methods

Calcite cements precipitated from both marine and meteoric waters are found in these rocks but only macrocements (>10 μm diameter) that crystallized from formation waters during burial will be analysed. The workflow to quantify the dynamics of cementation in oil vs. water leg samples is given below:

1. A Catholuminescence Cold cathode CITL 8200 MK3A was used to identify cement zones separated by differing luminescence. This will form the basis for establishing cement stratigraphies in the water and oil legs.

2. Syntaxial cements growing upon echinoid fragments were selected to gain in-situ ion probe $\delta^{18}O$ measurements as these contain both the earliest cement zones and final zones abutting against pore space, indicating preservation of the final, youngest cement growth. For each syntaxial overgrowth a single transect was undertaken at regular spacing (~100 μm, with a beam width of 20-30 μm) from the oldest, innermost cement adjacent to the echinoderm fragment, to the youngest outermost cement abutting an open pore (Figure 1). This allowed $\delta^{18}O$ values and trends through the macrocements to be compared regardless of zone colour and luminescence characteristics. Previous one-day pilot studies have shown that the internal precision for each spot ranges between 0.009 and 0.015 (% Standard Error) [5]. External precision was estimated to be 0.4‰ as determined by consecutive analysis of a UWC (University of Wisconsin Calcite) standard that was assessed to be homogenous.
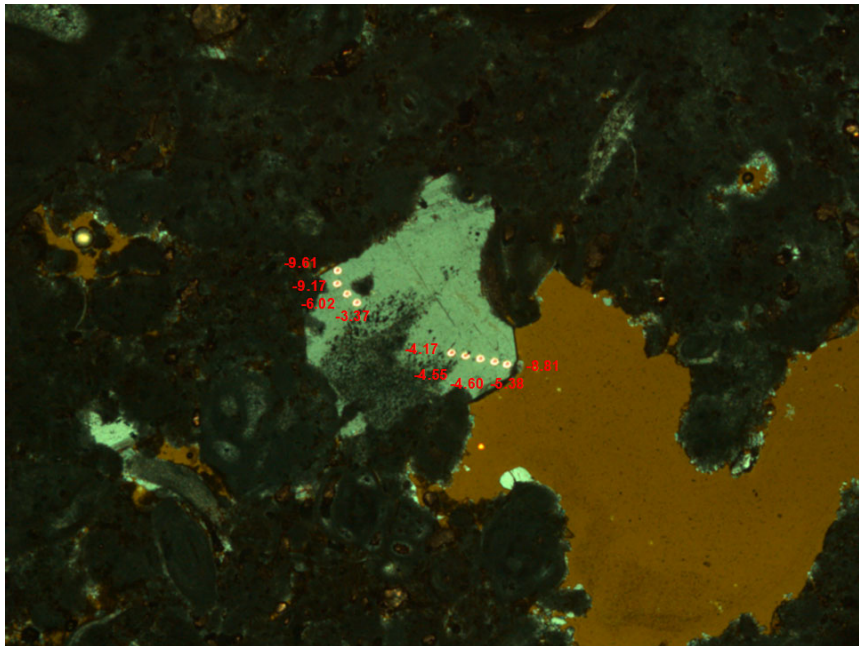
Figure 1: Location of targets and $\delta^{18}O$ data in syntaxial cement in the oil leg

Results

Results from one-day pilot studies show $\delta^{18}O$ _VPDB_ data from the oil leg cements that range from -1.2‰ in the oldest zone decreasing to -10.3‰ in zone 11, returning to -7.7‰ in the final zone (Figure 2A). The oldest distinguishable cement zone in the water leg shows highly variable $\delta^{18}O$ from -3.6‰ to -9.3‰ with a mean of -7.3‰, with subsequent zones decreasing to a mean value of -9.4‰ for the youngest cement zone (Fig. 2B). We have interpreted these decreasing $\delta^{18}O$ values as indicating increasing temperature with burial and the evolution of pore water composition: broadly similar trends in the oil and water legs suggest precipitation under the same general conditions [5]. Unlike the oil leg cements, the final zone in the water leg occludes nearly all remaining pore space. We have previously inferred therefore that burial cementation slowed in the presence of oil due to a reduction of potential nucleation sites as well as porewater and solute movement within weakly oil-wet pores, whereas continued flow and solute movement through all pores, including the micropores (<10 μm diameter) enabled extensive cementation in the water leg [5].
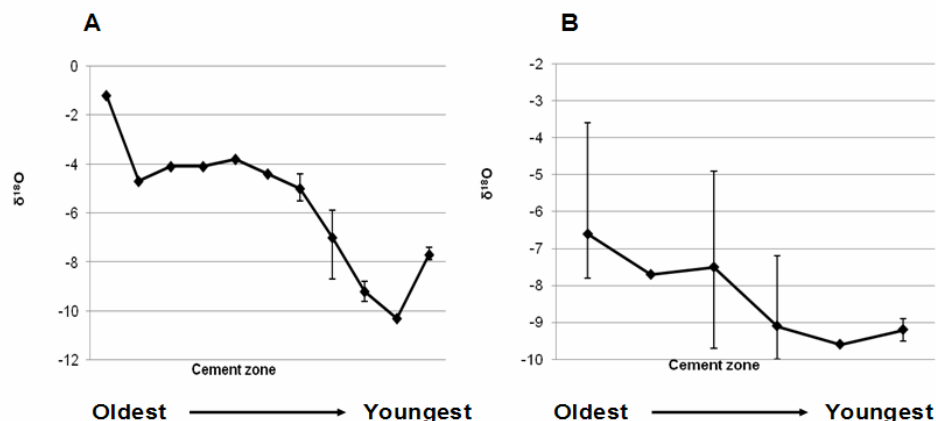
Figure 2: Mean in situ $\delta^{18}O$ data for successive zones within syntaxial burial cements from A) Oil leg, B) Water leg. Vertical bars show the data range for each

References

[1] Emery, D., et al., 1993. Phil. Trans. Roy Soc. London A, 344, 115–125.
[2] Heasley, E.C. et al., 2000. Marine and Petroleum Geology 17, 639-654.
[3] Marchand, A.M.E. et al., 2001.Geology 29, 915-918.
[4] Neilson, J.E. et al., 1998. Marine and Petroleum Geology 15, 57-72.
[5] Cox et al, 2010. Sedimentary Geology, 228, p.p. 246-254.

Interrogating trees as archives of environmental sulphur variability

P.M. Wynn[1], N.J. Loader[2] & I.J. Fairchild[3]

[1]Lancaster Environment Centre, Lancaster University, Lancaster, LA1 4YQ, UK
[2]Department of Geography, College of Science, Swansea University, Swansea, SA2 8PP, UK
[3]School of Geography, Earth and Environmental Science, Birmingham University, Birmingham, B15 2TT, UK

Background and rationale (NERC grant NE/H012257/1): A principal driver of climatic variability over the past 1,000 years is caused by changes in atmospheric composition resulting from sulphur aerosols. Understanding the impact of sulphur emissions upon climate beyond the last few hundred years however is not straightforward. Problems with analytical resolution and dating uncertainties in the ice core records hinder climate-volcanic correlations; and archives are frequently distal from points of emission. We believe tree rings constitute an archive which can overcome these difficulties. However, until recently the sulphur contained within tree rings has largely remained beyond the reach of environmental scientists and climate modellers owing to difficulties associated with the extraction of a robust signal. Such a precisely dated and ice-independent record can be used to locate the source of past volcanic eruptions, resolve dating uncertainties in the ice-core volcanic records and provide an independent mid-latitude continental dataset of sulphur forcing for climate modelling. We believe combining tree ring width with replicated sulphur concentration and isotopic analysis at sub-annual resolution provides the best possibility of building a reliable record of sulphur forcing and its impact upon climate during the past millennium.

Overall Aim: To develop methods required to extract the stable sulphur isotopic composition of woody tissues at (sub)annual resolution, with the long-term goal of developing new Holocene palaeorecords of sulphur isotopic variability from tree rings.

The detailed objectives for access to the ionprobe are:

Objective 1: Undertake method development to establish the optimum sample preparation protocol, including extraction of labile resins, precision cutting of laths (2-0.5mm thick) to obtain a surface sufficiently smooth for ion probe analysis and evaluation of resin impregnation to avoid sample de-gassing under vacuum. We propose to develop and test the following materials as analytical standards of constant concentration and isotopic composition:

1. Cellulose 'paper' discs soaked in sulphate solution
2. Pure cellulose slurry infused with sodium sulphate
3. "Doped" cellulose prepared from dissolved tree-ring cellulose solution,
4. Natural wood surface from single growth years
5. Compressed pellet of wood powder

Objective 2: will generate high resolution data in European Abies alba (S ≈100 ppm) to provide isotopic evidence for an industrial pollution record; and across selected periods identified by narrow growth rings in Bristlecone pine trees known to coincide with and be sensitive to volcanic events identified in the Greenland ice core (S ≈200 ppm).

Results: Objective 1: Establishing the optimum sample preparation protocol

Resin impregnation: Small blocks of tree ring series were cut and impregnated in resin prior to surface polishing / ion milling (Figure 1). Ion milling was unsuitable as a finishing technique. Surface polishing allowed preparation of a flat, smooth surface and elimination of cell vacuoles. Analysis of polished sections demonstrated a sulphur content great enough for isotopic analysis, albeit only marginally above the background signal from the resin (Figure 2).

Fig. 1: Resin impregnation followed by surface polishing and ion milling

Further tests on the sulphur content of 'low sulphur resins' were undertaken, but all were found to contain substantial quantities of S.

Dry surface preparation: Wood samples were prepared to a flat surface using a variety of techniques. These included cutting using a double bladed saw, microtome, modeling drill dissection, sanding to a high polish, and core-microtome (courtesy of collaboration with Holger Gärtner, Swiss Federal Institute for Forest, Snow and Landscape Reseach (WSL)). Each of these preparation protocols was unsuccessful, either due to uneven surfaces or smearing of cellular structure. The most successful microtome preparation was achieved via the core-microtome, although this surface still did not appear perfectly flat.

Fig. 2: Ionprobe S and O signals of wood, epoxy and glue

Indium mounting: Each of the above surface preparations were mounted in indium. However, sample deformation post mounting influenced surface relief and large cellular cavities prevented consistent count rates. Despite gold coating, few reflective surfaces could be observed and high Field x/y values showed variability greater than expected.
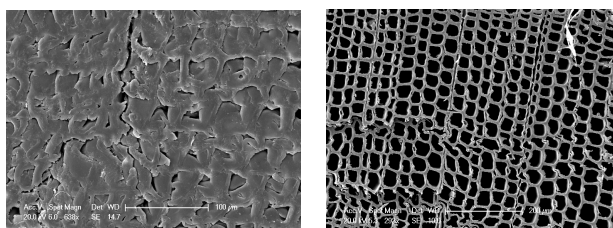

Fig. 3. SEM image of the Larix deciduas sample pressed into Indium.

SEM image of the Larix deciduas sample before pressing.

Development of analytical standards: Due to the lack of success in developing a protocol for tree core surface preparation, natural wood surfaces and compressed pellets of wood powder have yet to be tested as suitable standard materials. Cellulose powders have been obtained from a variety of sources (Sigma, IAEA, Whatman) and tested for sulphur content by EA analysis. None contained sulphur. Natural sources of cellulose are now being tested, including tea leaves, which actually contain 0.3 % S. This cellulose has been compressed into a disc and will form the next test for surface quality and homogeneity.

Objective 2: Due to the lack of success in developing a suitable preparation protocol, objective 2 has not yet been attempted.

Conclusion and ways forward: High resolution sulphur isotope analysis on tree ring material can be undertaken, providing a suitable sulphur free impregnating material can be found. There are several lines of research still to pursue here. We would like to take the opportunity to thank the ion probe staff for their hard work and determination in pioneering these analyses.